HYDROGEN ISOTOPE RATIOS OF INDIVIDUAL ORGANIC COMPOUNDS

Alex L. Sessions

Submitted to the faculty of the University Graduate School
in partial fulfillment of the requirements
for the degree
Doctor of Philosophy
in the Department of Geological Sciences
Indiana University
August, 2001

Acknowledgements

The completion of this thesis is due to the patient advice and kind help of many, many people. Foremost among them is Dr. John Hayes, who has worked tirelessly to teach me not only the fundamentals, but the art of conducting scientific research. The depth and breadth of my education under him has been remarkable, and I am deeply grateful. I can think of no better compliment than the fact that I am eagerly staying on as a post-doc under his direction.

My advising committee, Drs. Simon Brassell, Tim Eglinton, Gary Hieftje, and Arndt Schimmelmann, also deserve a hearty thank-you. They have been encouraging and supportive as I progressed through the Ph.D. program, and each one has answered more than his share of ridiculous questions (Why does D_2O kill bugs?) My parents – who also deserve a great deal of credit for encouraging an inquistive mind and love of science – sympathize with you all.

Two people in particular are responsible for teaching me the nuts and bolts of isotope geochemistry. Dr. Tom Burgoyne, a post-doc at Bloomington, coached me in the fine points of using, fixing, and understanding mass spectrometers. Dr. Chris Reddy, a post-doc and later assistant scientist at WHOI, showed me how to work in an organic geochemistry laboratory. It is a rare day that I do not use some technique, trick, or rule of thumb that they taught me.

Many other folks have helped me with this thesis in countless ways. Arndt Schimmelmann performed offline δD measurements of all our organic standards, and of the culture media and gases used in Chapter 5. Peter Sauer helped collect specimens for our first D/H analyses (Chapter 1), and Great Pond sediment for exchange experiments. Sean Sylva helped prepare, extract, and analyze the hydrogen exchange experiments (Chapter 4). Linda Jahnke grew *Methylococcus capsulatus*, and Kathleen Londry grew sulfate-reducing bacteria, which together comprise Chapter 5. Roger Summons provided numerous consultations over mass spectra. Other helpful folks include: Steve Studley, Julie Primack, Kristen Leckrone, Lisa Pratt, Jennifer Villinski, and Jon Fong at Indiana University; Daniel Montlucon, Jeff Seewald, Kai-Uwe Hinrichs, Paul Fucile, Carl Johnson, Leah Houghton, and the entire staff of NOSAMS at WHOI.

Financial support during the past five years has been provided by a fellowship from the University Graduate School at Indiana University; by grants to John Hayes from NASA and the National Science Foundation; through John Hayes' WHOI research funds; and by a generous grant from Royal Dutch Shell, arranged by Dr. Olaf Podlaha.

Last and most importantly, I would not have made it this far without my wife, Karen. She has supported and encouraged me in every way possible. Many thanks to all of you.

Preface

When I first met John Hayes in February, 1996, he suggested that the development of continuous-flow hydrogen-isotopic analyses might be a good thesis project. While I scarcely understood what 'continuous-flow' meant at the time, the project sounded exciting and I accepted. Thus began a five-year project involving myself, John Hayes, Tom Burgoyne, and Arndt Schimmelmann. By the spring of 1997 work was underway. Tom quickly developed high-temperature pyrolysis as an efficient means for converting organic hydrogen to H_2, work that was later published in Analytical Chemistry (1998, 70:5136-5141). Meanwhile, Arndt and I struggled to perfect a Pd filter for separating H_2 from He. That approach quickly fizzled, and I began to systematically study the problem of H_3 correction in continuous flow hydrogen analyses. In preparation for improvements to come, I began to develop the Excel macros that Tom would eventually dub 'AlexDAT' after the Finnigan software of a similar name.

By the spring of 1998, we were testing our second prototype of the 'ED,' an energy-discriminating lens that Tom designed and built to suppress low-energy He^+. In June, I moved my family and the partially-developed hydrogen system to Woods Hole to continue work in John's new labs. A discouraging summer of testing and rebuilding the ED followed, but by the fall the ED had evolved enough to allow us to make our first crude D/H measurements of real samples.

We quickly discovered that many, if not all, organic geochemical laboratories are rife with the perdeuterated compounds used as internal standards for GC. To facilitate more rapid progress, John and I scoured the WHOI biology department in search of suitable phytoplankton cultures, and in February, 1999, Peter Sauer and I collected the plants from Woods Hole Harbor that eventually formed the basis for our 1999 Organic Geochemistry paper (Chapter 1). With an initial publication under our belt, in the summer of 1999 we turned back to refining analytical techniques, working both on perfecting H_3 corrections and on eliminating the GC peak-tailing that had plagued us from the earliest days. Work on H_3 corrections eventually culminated in the publication of back-to-back papers in Analytical Chemistry in December, 2000 (Chapters 2 and 3). But despite the helpful suggestions from many gurus of gas chromatography, we never solved the peak-tailing problems, though (much to our chagrin) Andreas Hilkert in Bremen did.

By the fall of 1999 Tom had moved to Oklahoma State, the hydrogen system was largely functional, and our research interests diverged. I began dabbling with hydrogen exchange experiments, and travelled to Moffett Field to learn how to grow *Methylococcus capsulatus* from the master, Linda Jahnke. The period from fall, 1999, to spring, 2001 was spent producing the data that appears in Chapters 4 and 5.

The purposes of this rambling preface are twofold. The first is to provide a historical perspective for the D/H project. This thesis chronicles only the parts of the project for which I was primarily responsible. The chapters of the thesis are presented as they were written, in chronological order, rather than in some logical progression of topics. Chapters 1–3 have been reproduced in the form they appeared in publication, complete with abstract and references. For consistency, chapters 4 and 5 follow this format, though they have not yet been submitted for publication. The second purpose of this preface is to emphasize that this project has been a team effort in every sense, and while each of us was responsible for different aspects of it, none of the work reported here (or elsewhere) would have been possible without the individual contributions of all four scientists.

Table of Contents

List of Tables

List of Figures

Chapter 1 — Fractionation of hydrogen isotopes in lipid biosynthesis[*]

ABSTRACT

Isotopic compositions of carbon-bound hydrogen in individual compounds from eight different organisms were measured using isotope-ratio-monitoring gas chromatography-mass spectrometry. This technique is capable of measuring D/H ratios at natural abundance in individual lipids yielding as little as 20 nmol of H_2, and is applicable to a wide range of compounds including hydrocarbons, sterols, and fatty acids. The hydrogen isotopic compositions of lipids are controlled by three factors: isotopic compositions of biosynthetic precursors, fractionation and exchange accompanying biosynthesis, and hydrogenation during biosynthesis. δD values of lipids from the eight organisms examined here suggest that all three processes are important for controlling natural variations in isotopic abundance. *n*-Alkyl lipids are depleted in D relative to growth water by 113 to 262‰, while polyisoprenoid lipids are depleted in D relative to growth water by 142 to 376‰. Isotopic variations within compound classes (*e.g.*, *n*-alkanes) are usually less than ~50‰, but variations as large as 150‰ are observed among isoprenoid lipids from a single organism. Phytol is consistently depleted in D by up to 50‰ relative to other isoprenoid lipids. Inferred isotopic fractionations between cellular water and lipids are greater than those indicated by previous studies.

INTRODUCTION

We have developed an analytical system capable of measuring the D/H ratio of nanogram quantities of individual organic compounds with a precision of 5‰ or better. Variations in the natural abundance of D in C-bound hydrogen clearly record both environmental (Yapp and Epstein, 1982; Sternberg, 1988) and biochemical effects (Estep and Hoering, 1980; Yakir and DeNiro, 1990). Furthermore, isotope effects for hydrogen are commonly large (Bigeleisen, 1965). Therefore, the ability to examine hydrogen isotopic variation at the natural abundance level in individual organic compounds should prove to be quite useful. At present, with the exception of specific analyses of cellulose, almost nothing is known about hydrogen isotopic variability in individual compounds. As an initial examination, therefore, we extracted lipids from eight separate organisms and measured the D/H ratio of individual components in those extracts.

The purpose of this study was to examine the natural range of fractionations between cellular water and lipids, among lipids of similar and disparate biosynthetic origin, and among lipids from different organisms. To this end, we examined two cultures of unicellular marine algae (*Alexandrium fundyense*, a dinoflagellate, and *Isochrysis galbana*, a haptophyte), two species of multicellular marine algae (*Fucus vesiculosis* and *Ascophyllum sp.*, both brown algae), a submergent higher plant (*Zostera marina*, a sea grass) and an emergent higher plant (*Spartina alterniflora*, a marsh grass), a bacterial culture (*Methylococcus capsulatus*, a methanotroph), and the leaves of a carrot plant (*Daucus carota*). Aquatic organisms were selected preferentially to minimize isotopic differences between cellular and growth water due to evapotranspiration (Edwards, 1993). *Daucus* was selected to examine isotopic characteristics related to a recently discovered biosynthetic pathway (Schwender *et al.*, 1996).

EXPERIMENTAL

Isotopic Measurements

Hydrogen isotopic compositions of individual compounds were measured using an isotope-ratio-monitoring gas chromatography-mass spectrometry (irmGCMS) system developed in our laboratory. The system is similar to that described by Scrimgeour *et al*. (1999) and Tobias and Brenna (1997), but with several important improvements. The effluent from a conventional GC using He carrier gas is fed into a graphite-lined alumina tube held at 1400°C, at which temperature organic compounds are quantitatively pyrolyzed to graphite, H_2, and CO (Burgoyne and Hayes, 1998). An open split transmits 200 µL/min of the resulting gas stream to a Finnigan MAT 252 mass spectrometer. An electrostatic filter in front of the mass-3 Faraday cup reduces scattered $^4He^+$ reaching that collector to <75 femtoamps at 200 µL/min He.

Mass-2 and -3 ion currents are recorded at 4 Hz and all data are processed using Visual Basic computer codes that we have developed. Raw mass-3 ion currents are corrected for contributions from H_3^+ on a point-by-point basis: each mass-3 data point is corrected based on the corresponding mass-2 data point using the equation $i_{HD} = i_3 - K(i_2)^2$, where i_2 and i_3 are the raw mass-2 and -3 ion currents, i_{HD} is the corrected ion current, and K is the H_3^+ factor. We have tested this correction scheme extensively, and find that it reliably corrects for H_3^+ currents for a wide variety of peak shapes and sizes, retention times, and sample compositions. Following correction for H_3^+, ion currents are integrated, ion-current ratios are calculated, and isotope ratios are computed and standardized using techniques similar to those used in carbon irmGCMS (Ricci *et al*., 1994). The working concentration range for this system (to obtain ~5‰ precision) is 20-100 nmoles H_2 injected on-column per sample component.

All values for δD reported here are relative to VSMOW. A laboratory standard containing 15 homologous *n*-alkanes, varying in concentration over a five-fold range and varying in δD over a 210‰ range, was analyzed daily. Values of δD for these alkanes were determined by offline combustion to a precision of ±1.6‰. The alkane standard was used to (1) determine the H_3 factor for the day, (2) normalize δD values to the VSMOW scale, and (3) monitor the stability of the system.

The H_3 factor is determined as the value of K that minimizes the mean absolute error for the fifteen peaks of varying size. Values of K determined using this method are generally within 5% of those determined conventionally (*i.e.,* by observation of i_3/i_2 at varying values of i_2; Friedman, 1953). Regression of δD (irmGCMS) on δD (offline) for these standards provides a normalization line analogous to that used in batchwise analyses (*i.e.*, so that δD values for VSMOW and SLAP are 0 and $-428‰$, respectively; Coplen, 1988). Values of r^2 for this regression always exceeded 0.99, and normalization results in corrections of $<10‰$ (commonly $<5‰$) to any δD value. The mean precision of measurement of δD for these alkanes over the three-month period of this study was $\pm 4.2‰$ ($n = 33$ injections) and the root-mean-square error ($\equiv \sqrt{\sum d^2 / n}$, where $d = \delta D_{measured} - \delta D_{known}$ and $n =$ number of values for d) was 5.3‰ ($n = 491$ measurements) with no systematic bias due to peak size or retention time.

Values of δD for sample compounds were determined by reference to coinjected n-alkane standards. Where possible, four to six n-alkanes were coinjected with each sample; two of these were used as isotopic reference peaks, with the remaining alkanes providing tests of analytical accuracy. To avoid analyzing isotopically exchangeable H from carboxyl and hydroxyl positions, and to improve chromatography, alcohols and fatty acids were derivatized as trimethylsilyl ethers and esters using bis-(trimethylsilyl)-trifluoroacetamide (BSTFA). BSTFA is an attractive derivatizing reagent because (1) it can be used for both alcohols and acids; (2) hot, acidic conditions which might promote hydrogen isotopic exchange are avoided; and (3) all hydrogens in the derivatizing reagent are in the trimethylsilyl (TMS) groups, so that the δD of the derivatizing H can be measured directly by irmGCMS analysis of the BSTFA peak. To test this procedure, we measured the δD of non-exchangeable H in a cholestanol standard by first measuring the acetate, ketone, and trifluoroacetate derivatives using conventional, offline techniques, then measuring the TMS derivative using irmGCMS. The three offline measurements produced derivative-corrected δD values of -247, -250, and $-253‰$ (all $\pm 1.5‰$), and the irmGCMS measurements produced a corrected δD of $-256 \pm 3‰$.

Sample Collection and Preparation

Alexandrium clone #GTCA28 was grown in a 1-L culture on f/2 medium at 15°C with a 14:10 hour light:dark cycle. *Isochrysis* clone T-ISO was grown in a 20-L culture on f/2 medium at 20ºC under continuous illumination. The f/2 medium for both cultures was prepared from sterile-filtered Vineyard Sound seawater, which has a salinity of 31.5 to 32.0‰. Both cultures were filtered onto precombusted 0.7-µm glass-fiber filters (Whatman GF/F) prior to extraction. *Ascophyllum* and *Fucus* were collected from Quisset Harbor, Woods Hole, MA. *Spartina* was collected from a salt marsh on Penzance Point, Woods Hole, and *Zostera* was collected from Woods Hole Harbor. *Daucus* with attached leaves was obtained from a local grocery, and only the leaves were analyzed. The *Methylococcus* culture analyzed here was the same as that described by Summons *et al*. (1994) and was obtained in dried form. All native specimens were collected in February 1999.

Samples were extracted with an Accelerated Solvent Extractor (Dionex) using dichloromethane (DCM)/methanol (90:10 v/v) with three five-minute extraction cycles at 100°C and 1000 psi. Total lipid extracts from *Ascophyllum*, *Spartina*, and *Daucus* were saponified by reacting with methanolic NaOH at 75°C for 6 hours, then neutral and acid fractions were extracted into hexane and combined. Lipids were separated into classes by elution from disposable, solid-phase extraction cartridges containing 500 mg of an aminopropyl stationary phase (Supelclean LC-NH$_2$). Fractions collected were: hydrocarbons (4 mL hexane), ketones (6 mL hexane/DCM 3:1), alcohols (5 mL DCM/acetone 9:1), and fatty acids (8 mL DCM/formic acid 4:1). Each fraction was analyzed by GCMS to identify compounds of interest.

RESULTS AND DISCUSSION

Results are summarized in Table 1-1. Standard deviations of replicate analyses typically ranged from 3 to 12‰. Worse precision (up to 24‰) was obtained for some compounds where coeluting or especially small peaks were measured. When these were included in order to provide a conservative overview of the results, the pooled estimate of the standard deviation of a single analysis was 9.2‰ (375 degrees of freedom in 155 sets of replicates). The arithmetic mean error for the

Table 1-1. δD measurements for individual lipids

Species/compound	δD (‰)[a]	σ (‰)[b]	Species/compound	δD (‰)[a]	σ (‰)[b]
Cultured Specimens			*Spartina alterniflora* (marsh grass)		
Alexandrium fundyense (dinoflagellate)			Hydrocarbons		
Hydrocarbons			n-C_{25} alkane	−150	10
C_{22} alkadiene[d]	−204	10	n-C_{26} alkane	−170	11
Fatty acids			n-C_{27} alkane	−166	1
14:0 + 14:1	−232	NA[c]	n-C_{28} alkane	−164	4
16:0	−227	NA[c]	n-C_{29} alkane	−169	3
22:4	−218	NA[c]	n-C_{30} alkane	−161	19
Sterols[e]			n-C_{31} alkane	−160	7
$27\Delta^5$	−323	8	n-C_{32} alkane	−145	NA[c]
$30(4\alpha,23,24)\Delta^{22}$	−295	9	n-C_{33} alkane	−155	15
$29(4\alpha,24)\Delta^{22}$	−311	1	Ketones		
Other isoprenoids			C_{33} alkanone	−178	16
phytol	−357	13	Triterpenoids		
			lupenone	−142	6
Isochrysis galbana (haptophyte)			pentacyclic triterpenone[d]	−144	5
Hydrocarbons			lupenol	−171	1
C_{31} alkadiene[d]	−113	6	pentacyclic triterpenol[d]	−165	3
Fatty acids			pentacyclic triterpenol[d]	−151	8
14:0 + 14:1	−216	18	Other isoprenoids		
16:0	−209	10	phytol	−278	4
18:1 (2 isomers)	−181	7			
Sterols[e]			*Daucus carota* (carrot)		
$28\Delta^{5,22}$	−258	11	Hydrocarbons		
			n-C_{23} alkane	−141	4
Methylococcus capsulatus (methanotroph)			n-C_{24} alkane	−135	18
Fatty acids			n-C_{25} alkane	−158	6
14:0	−144	8	n-C_{26} alkane	−139	7
16:0 + 16:1	−161	5	n-C_{27} alkane	−166	3
Sterols[e]			n-C_{29} alkane	−162	2
$28(4\alpha)\Delta^{8(14)}$	−234	6	n-C_{30} alkane	−134	15
$29(4,4)\Delta^{8(14)}$	−234	6	n-C_{31} alkane	−113	21
			n-C_{32} alkane	−117	11
Native Specimens			Alcohols		
Ascophyllum sp. (brown alga)			n-C_{22} alkanol	−186	11
Fatty acids			n-C_{24} alkanol	−192	12
14:0	−208	7	n-C_{26} alkanol	−192	6
16:0	−210	6	n-C_{28} alkanol	−197	7
16:1	−213	8	n-C_{30} alkanol	−180	15
18:1	−189	4	Fatty acids		
Sterols[e]			12:0	−262	8
$29\Delta^5$	−219	11	14:0	−217	7
			16:0	−172	6
Fucus vesiculosis (brown alga)			16:1	−204	17
Fatty acids			18:0, 18:1, 18:2, 18:3	−190	7
14:0	−187	8	C_{24} hydroxy-fatty acid	−193	12
16:0	−167	4	Sterols[e]		
18:1	−157	10	$29\Delta^{5,22}$	−283	7
Sterols[e]			$29\Delta^5$	−292	7
$29\Delta^{5,24(28)}$	−208	4	Triterpenoids		
			Δ-amyrin + β-amyrin	−252	10
Zostera marina (sea grass)			pentacyclic triterpenols[f]	−239	6
Hydrocarbons			pentacyclic triterpenol[d]	−226	16
n-C_{17} alkane	−167	6	pentacyclic triterpenol[d]	−231	16
n-C_{19} alkane	−159	3	Other isoprenoids		
n-C_{21} alkane	−147	6	caryophyllene ($C_{15}H_{24}$)	−308	6
squalene	−241	8	sesquiterpene[d] ($C_{15}H_{24}$)	−320	7
Sterols[e]			phytadiene	−345	2
$27\Delta^5$	−253	1	phytol	−376	4
$27\Delta^{5,24}$	−205	24			
$29\Delta^5$	−194	6			

[a] Corrected for TMS derivatization.
[b] Standard deviation of 3 to 5 replicate analyses.
[c] Only 1 analysis available.
[d] Specific identity could not be determined.
[e] Leading number indicates total C and parenthesized numbers indicate positions of methyl substituents (where known).
[f] Three coeluting triterpenol peaks.
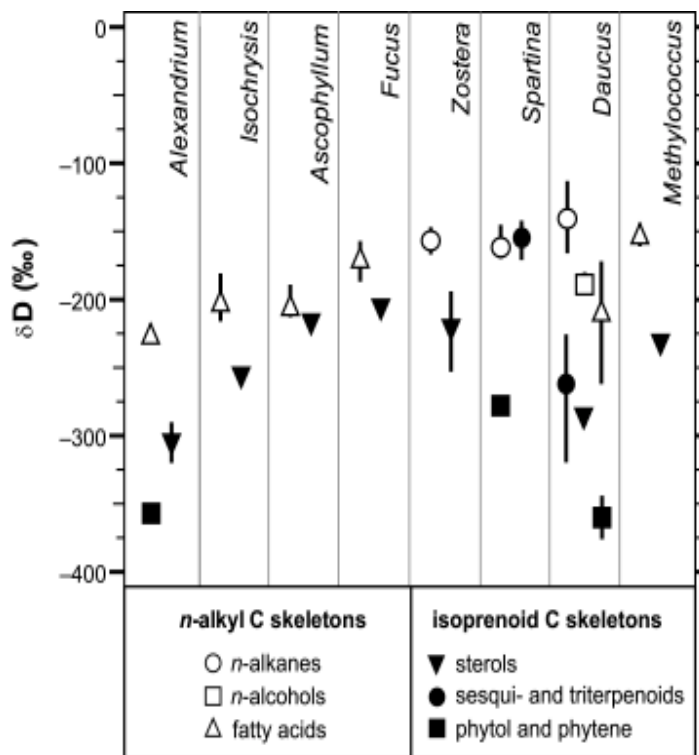
Figure 1-1. Summary of δD measurements for compound classes. Each symbol represents the mean for that class, and the bars represent the range of measured values.

coinjected alkanes that served as test compounds in these analyses was 0.3‰, and the root-mean-square error was 7.6‰. Considering all possible sources of error in the measurement of unknown compounds, we estimate that the δD value measured for each compound is accurate to within ±15‰. However, relative differences between compounds in the same chromatogram are probably accurate to within ±5‰.

Results are summarized graphically in Figure 1-1. Several points emerge. First, for any of the eight organisms examined, the differences between compound classes (*e.g.*, *n*-alkanes, sterols, fatty acids, etc.) are greater than those within any one class. Second, where isotopic compositions of growth water are known, all lipids are depleted in D relative to growth water by 150‰ or more. Third, compounds from a given class (*e.g.*, sterols) can have substantially different δD values in different organisms, despite growing in water with the same hydrogen isotopic composition.

Variations of δD Within Organisms

Compound classes exhibit restricted ranges in δD, with individual lipids in each class generally falling within a range of <50‰. Variations between classes are much larger, with differences of 50 to 150‰ being common. Polyisoprenoid lipids are generally depleted relative to acetogenic (*n*-alkyl) lipids (compare filled and open symbols, Figure 1-1), but there are also differences between compound classes with biosynthetically equivalent carbon skeletons (*e.g.*, *n*-alcohols versus *n*-alkanes in *Daucus*). Based on compounds examined in *Daucus*, the range of variability appears to be somewhat greater within the polyisoprenoid lipids than within the acetogenic lipids.

Three potential sources of isotopic variability in lipid hydrogen can be identified: (1) the isotopic composition of biosynthetic precursors, (2) isotope effects (including exchange of organic H with H_2O) associated with biosynthetic reactions (Martin *et al*., 1986), and (3) the isotopic composition of hydrogen added, commonly from NADPH, during biosynthesis (Smith and Epstein, 1970; Luo *et al*., 1991). This third control, which is not related to the flow of substrates used in assembly of the carbon skeleton, is notably different from those encountered in carbon-isotopic studies (Hayes, 1993). Below we discuss evidence that isotopically different pools of NADPH may exist within cells; this suggests that compound-specific hydrogen isotopic analyses will provide information about compartmentalization of biosynthesis in cells, as well as about biosynthetic pathways.

The depletion of D in isoprenoid lipids relative to acetogenic lipids was first described by Estep and Hoering (1980). Our results confirm and extend, but do not explain, this finding. Acetogenic lipids, sterols, and pentacyclic triterpenols all use acetyl-CoA — either directly or via the formation of mevalonic acid (MVA) — as the biosynthetic precursor (Abeles *et al*., 1992). Slightly more hydrogen in acetogenic lipids derives from NADPH (~50%) as compared to isoprenoid lipids derived from the MVA pathway (~37%). If the acetogenic-versus-isoprenoid contrast (roughly –200‰ versus –250‰) were attributed to this difference alone, it would require that NADPH-derived hydrogen is substantially enriched (δD≈0) and acetate-derived hydrogen is highly depleted (δD≈–400). More plausibly, as noted by Estep and Hoering (1980), the depletion of D in polyisoprenoids relative to *n*-alkyl lipids is due to isotope effects associated with the two pathways.

In *Daucus*, fatty acids and *n*-alcohols have similar δD values, but are depleted in D by ~50‰ relative to *n*-alkanes. Estep and Hoering (1980) also found substantial hydrogen isotopic differences (up to 54‰) between fatty acids and hydrocarbons separated from three higher plants and from *Trichodesmium.* In that case, however, the pattern was reversed from that observed here, with fatty acids in the higher plants D-enriched relative to the hydrocarbons. Given that the carbon skeletons of fatty acids, *n*-alcohols, and *n*-alkanes are all formed via the same biosynthetic pathway, these differences must be due to changes in the isotopic composition of acetate starting material, or of NADPH, or both. These changes could occur through time (*e.g.,* as growth rate changes), or could exist spatially within the cell or plant at any given time. There appears to be a slight trend toward D-enrichment with longer chain length in the fatty acids. If real, this may also reflect synthesis in different parts of the plant.

Substantial hydrogen isotopic variations occur between classes of polyisoprenoid lipids. In particular, phytol is consistently depleted relative to sterols and pentacyclic triterpenoids by 50 to 140‰. Part of this large variability may be due to isotopically different pools of NADPH in the cytosol, where triterpenols are synthesized, and the chloroplasts, where phytol is synthesized. In plants, NADP$^+$ is reduced to NADPH by two processes: electron-transport chains associated with photosynthesis in the chloroplasts, and during oxidation of sugars in the pentose-phosphate pathway in the cytosol (Abeles *et al*., 1992). The sources of hydrogen for NADPH are very different in these two cases (H_2O in photosynthesis, and C-bound H from sugars in the pentose-phosphate pathway), so it is plausible that isotopically distinct pools of NADPH might exist within these different cellular compartments.

Isotopic differences between phytol and triterpenols may also be due in part to different biosynthetic pathways. Schwender *et al*. (1996) have recently described a novel pathway for polyisoprenoid synthesis, in which glyceraldehyde phosphate and pyruvate — rather than three molecules of acetyl-CoA — condense to form I-deoxy-D-xylulose phosphate (DOXP), the immediate precursor of isopentenyl phosphate. The phylogenetic distribution of this novel pathway is still under investigation. Of the species included here, only *Daucus* has been examined. *Daucus* uses the well-known MVA pathway to synthesize cytosolic isoprenoids, including sterols, while using

the novel DOXP pathway to synthesize plastidic isoprenoids, such as phytol (Lichtenthaler, 1999). In general, the DOXP pathway appears to be closely related to chloroplasts, and it is presumed to be a relict biochemical pathway preserved from the endosymbiotic origin of chloroplasts (Disch *et al*., 1998). If differences between the DOXP and MVA pathways are responsible for the observed depletion of phytol relative to triterpenols, this would require either that glyceraldehyde phosphate and pyruvate are D-depleted relative to acetate, or that there is a larger isotope effect associated with the DOXP pathway.

Based on the data presented here, we cannot distinguish the source of isotopic variability in isoprenoid lipids. Differing biosynthetic precursors, isotope effects and exchange associated with biosynthesis, isotopically distinct pools of NADPH, or all three may be responsible for the observed pattern. If different isotope effects can be positively associated with the DOXP and MVA pathways, compound-specific D/H measurements would become a valuable tool for studying the distribution and importance of this novel biosynthetic pathway.

Isotopic Fractionation

We calculate values for ε (isotopic fractionation) by estimating that the δD value of the cellular water for all samples except *Daucus* and *Methylococcus* was close to 0‰. For those organisms that were submerged in ocean water (*Alexandrium*, *Isochrysis*, *Ascophyllum*, *Fucus*, and *Zostera*) this is straightforward. Cellular water in *Spartina* may have been enriched relative to the growth water by evaporation, but the nearly identical δD values for alkanes from *Zostera* and *Spartina* suggest that this was minimal. The isotopic compositions of water in the *Daucus* and *Methylococcus* cultures are unknown.

Fractionation factors are defined and summarized in Table 1-2. Values for $\varepsilon_{\text{fatty acid/water}}$ range from –170 to –226‰ (mean = –200‰), values for $\varepsilon_{\text{alkane/water}}$ range from –158 to –162‰ (mean = –160‰), and values for $\varepsilon_{\text{sterol/water}}$ range from –208 to –310 (mean = –244‰). By comparison, fractionations between bulk lipids and water measured by offline techniques range from –125 to –178‰ (mean = –150‰). The observed fractionation between water and alkanes is indistinguishable from that previously observed between water and bulk lipids, but fractionations between fatty acids and

Table 1-2. Hydrogen isotopic fractionation between lipids and water

Compound-specific measurements, this study[a]				Bulk lipid measurements, previous studies				
Sample	$\varepsilon_{fa/w}$	$\varepsilon_{ak/w}$	$\varepsilon_{st/w}$	$\varepsilon_{ph/w}$	Sample	$\varepsilon_{l/w}$	$\varepsilon_{sl/w}$	$\varepsilon_{nsl/w}$	ref.[b]
Alexandrium	−226		−310	−357	Cyanobacteria	−175			1
Isochrysis	−202		−258		Macrophytes		−152	−232	1
Ascophyllum	−205		−219		Red algae	−139			2
Fucus	−170		−208		Brown algae	−178			2
Zostera		−158	−223		Green algae	−132			2
Spartina		−162		−278	Macrophytes	−125			3

Abbreviations: water (w), alkanes (ak), fatty acids (fa), sterols (st), phytol (ph), bulk lipids (l), saponifiable lipids (sl), non-saponifiable lipids (nsl); $\varepsilon_{a/b} = 1000\,[(\delta_a + 1000)\,/\,(\delta_b + 1000) - 1]$.
[a] Calculated using the mean δD for each compound class, and assuming $\delta D_w = 0$‰.
[b] (1) Estep and Hoering, 1980; (2) Sternberg *et al.,* 1986; (3) Sternberg, 1988.

water are nearly 50‰ larger on average. *n*-Alkanes were the most D-enriched lipid compounds observed in this study and fatty acids were in most cases the most abundant lipid components; it therefore appears unlikely that the smaller fractionations measured by previous studies are due solely to differences in the relative abundance of these components. A possible explanation is that components of the bulk extracts which do not appear in GC analyses (*e.g.,* lipoproteins) are D-enriched relative to the lipids we examined. In addition, bulk lipid measurements may incorporate hydrogen from H_2O or exchangeable oxygen-bound positions, which would be expected to produce anomalously large δD values (Schimmelmann, 1991).

Variations of δD Between Organisms

Differences in δD of up to 80‰ that cannot be reconciled as stemming from differences in cellular water exist between the same compounds in different organisms (*e.g.,* compare $\varepsilon_{phytol/water}$ in *Spartina* and *Alexandrium* in Table 1-2). These differences appear to be most pronounced between the cultured organisms (*Alexandrium*, *Isochrysis*, and *Methylococcus*) and *Daucus* versus the native specimens (*Ascophyllum*, *Fucus*, *Spartina*, and *Zostera*). Values of $\varepsilon_{sterol/fatty\ acid}$ range from –70 to –118‰ in the former group, and from –18 to –46‰ in the latter. $\varepsilon_{triterpenol/alkane}$ is –112‰ in *Daucus* and +8‰ in *Spartina*, and $\varepsilon_{phytol/alkane}$ is –274‰ in *Daucus* and –138‰ in *Spartina*. Thus, the depletion of D in isoprenoid relative to acetogenic lipids is greater in the actively growing cultures and in *Daucus* than in the native specimens collected in winter. If the differing extents of

isotopic fractionation observed here represent a more general pattern, they should be useful for understanding the underlying mechanisms, which could involve differences in photosynthetic activity, growth rate, water temperature, light intensity, nutrient supply, or other parameters.

A correlation between D-depletion in lipids and photosynthetic activity would not be surprising, as a similar situation is observed for carbohydrate metabolism. Photosynthesis produces C-bound H in carbohydrates that is D-depleted relative to tissue water by 100 to 170‰ (Estep and Hoering, 1981; Yakir and DeNiro, 1990). In contrast, "heterotrophic processing" of carbohydrates within plants (such as isomerization of triose phosphates and interconversion of fructose-6-phosphate and glucose-6-phosphate) results in the exchange of up to 50% of C-bound H with tissue water, with those exchanged positions becoming D-enriched by up to 158‰ relative to the tissue water (Yakir and DeNiro, 1990). Luo and Sternberg (1991) found that starch from chloroplasts was highly depleted relative to cytoplasmic cellulose in the same plant, due probably to this effect. Thus, the δD value of carbohydrates in plants is thought to represent a balance between autotrophic and heterotrophic metabolism, and can potentially be used as an indicator of photosynthetic status in plants (Yakir, 1992). Our results suggest that a similar pattern may exist in lipids.

CONCLUSIONS

We have measured δD values of 80 individual lipids from eight separate organisms using a newly-developed analytical system. This system is flexible, robust, and accurate, and provides a means for measuring D/H ratios in many geochemically important organic compounds, including hydrocarbons, sterols, and fatty acids.

Although the data presented here are limited in scope, they suggest several generalizations: (1) There is little isotopic variability within specific compound classes in individual organisms, but there is significant variability between compound classes, even among those that share common biosynthetic origins. Part of this variability may be due to isotopically distinct pools of NADPH used for hydrogenation during biosynthesis. (2) Phytol is significantly and consistently depleted in

D relative to sterols and other triterpenols. This difference suggests that the hydrogen-isotopic characteristics of the MVA and DOXP pathways for synthesis of isoprenoid lipids may differ significantly. If so, this contrast may facilitate further study of the occurrence of the DOXP pathway. (3) The estimated isotopic fractionation between cellular water and individual lipids is larger than previous estimates using bulk lipid measurements.

REFERENCES

Abeles, R. H., Frey, P. A. and Jencks, W. P. (1992) *Biochemistry*. Jones and Bartlett, Boston.

Bigeleisen, J. (1965) Chemistry of Isotopes. *Science* **147**, 463–471.

Burgoyne, T. W. and Hayes, J. M. (1998) Quantitative production of H_2 by pyrolysis of gas chromatographic effluents. *Analytical Chemistry* **70**, 5136–5141.

Coplen, T. B. (1988) Normalization of oxygen and hydrogen isotope data. *Chemical Geology* **72**, 293–297.

Disch, A., Schwender, J., Müller, C., Lichtenthaler, H. K. and Rohmer, M. (1998) Distribution of the mevalonate and glyceraldehyde phosphate/pyruvate pathways for isoprenoid biosynthesis in unicellular algae and the cyanobacterium *Synechocystis* PCC 6714. *Biochemical Journal* **333**, 381–388.

Edwards, T. W. D. (1993) Interpreting past climate from stable isotopes in continental organic matter. In: Swart, P.K., Lohmann, K.C., McKenzie, J., Savin, S. (Eds.), *Climate Change in Continental Isotopic Records*. American Geophysical Union, Washington, D.C., pp. 333–341.

Estep, M. F. and Hoering, T. C. (1980) Biogeochemistry of the stable hydrogen isotopes. *Geochimica et Cosmochimica Acta* **44**, 1197–1206.

Estep, M. F. and Hoering, T. C. (1981) Stable hydrogen isotope fractionations during autotrophic and mixotrophic growth of microalgae. *Plant Physiology* **67**, 474–477.

Friedman, I. (1953) Deuterium content of natural water and other substances. *Geochimica et Cosmochimica Acta* **4**, 89–103.

Hayes, J. M. (1993) Factors controlling ^{13}C contents of sedimentary organic compounds: Principles and evidence. *Marine Geology* **113**, 111–125.

Lichtenthaler, H. K.. (1999) The I-deoxy-D-xylulose-5-phosphate pathway of isoprenoid biosynthesis in plants. *Annual Reviews of Plant Physiology* **50**, 47–65.

Luo, Y. -H., Sternberg, L. dS. L., Suda, S., Kumazawa, S. and Mitsui, A. (1991) Extremely low D/H ratios of photoproduced hydrogen by cyanobacteria. *Plant and Cell Physiology* **32**, 897–900.

Luo, Y. -H. and Sternberg, L. dS. L. (1991) Deuterium heterogeneity in starch and cellulose nitrate of CAM and C3 plants. *Phytochemistry* **30**, 1095–1098.

Martin, G. J., Zhang, B. L., Naulet, N. and Martin, M. L. (1986) Deuterium transfer in the bioconversion of glucose to ethanol studied by specific isotope labeling at the natural abundance level. *Journal of the American Chemical Society* **108**, 5116–5122.

Ricci, M. P., Merritt, D. A., Freeman, K. H. and Hayes, J. M. (1994) Acquisition and processing of data for isotope-ratio-monitoring mass spectrometry. *Organic Geochemistry* **21**, 561-571.

Schimmelmann, A. (1991) Determination of the concentration and stable isotopic composition of non-exchangeable hydrogen in organic matter. *Analytical Chemistry* **63**, 2456–2459.

Schwender, J., Seemann, M., Lichtenthaler, H. K. and Rohmer, M. (1996) Biosynthesis of isoprenoids (carotenoids, sterols, prenyl side-chains of chlorophylls and plastoquinone) via a novel pyruvate/glyceraldehyde 3-phosphate non-mevalonate pathway in the green alga *Scenedesmus obliquus*. *Biochemical Journal* **316**, 73–80.

Scrimgeour, C. M., Begley, I. S. and Thomason, M. L. (1999) Measurement of deuterium incorporation into fatty acids by gas chromatography/isotope ratio mass spectrometry. *Rapid Communications in Mass Spectrometry* **13**, 271–274.

Smith, B. N. and Epstein, S. (1970) Biogeochemistry of the stable isotopes of hydrogen and carbon in salt marsh biota. *Plant Physiology* **46**, 738–742.

Sternberg, L. dS. L. (1988) D/H ratios of environmental water recorded by D/H ratios of plant lipids. *Nature* **333**, 59–61.

Sternberg, L. dS. L., DeNiro, M. J. and Ajie, H. O. (1986) Isotopic relationships between saponifiable lipids and cellulose nitrate prepared from red, brown, and green algae. *Planta* **169**, 320–324.

Summons, R. E., Jahnke, L. L. and Roksandic, Z. (1994) Carbon isotopic fractionation in lipids from methanotrophic bacteria: Relevance for interpretation of the geochemical record of biomarkers. *Geochimica et Cosmochimica Acta* **58**, 2853–2863.

Tobias, H. J. and Brenna, J. T. (1997) On-line pyrolysis as a limitless reduction source for high-precision isotopic analysis of organic-derived hydrogen. *Analytical Chemistry* **69**, 3148–3152.

Yakir, D. (1992) Variations in the natural abundance of oxygen-18 and deuterium in plant carbohydrates. *Plant, Cell and Environment* **15**, 1005–1020.

Yakir, D. and DeNiro, M. J. (1990) Oxygen and hydrogen isotope fractionation during cellulose metabolism in *Lemna gibba L. Plant Physiology* **93**, 325–332.

Yapp, C. J. and Epstein, S. (1982) Climatic significance of the hydrogen isotope ratios in tree cellulose. *Nature* **297**, 636–639.

Chapter 2 — Correction of H_3^+ contributions in hydrogen isotope-ratio-monitoring mass spectrometry*

ABSTRACT

Two fundamentally different approaches, termed "pointwise" and "peakwise," are currently used to correct hydrogen isotope-ratio-monitoring data for the presence of H_3^+ ion contributions. Consideration of the underlying assumptions shows that the peakwise approach is valid only for peaks with the same functional shape, and only when background signals do not vary. The pointwise correction is much more versatile, and can be used even when peak shapes and sizes, as well as background signals, vary significantly. It is not exact, and is limited in accuracy by 1) the signal-broadening effects of electronic time constants, 2) the analog-to-digital conversion frequency, and 3) the highest frequency of the sample signal. To minimize errors for typical gas chromatographic signals, time constants of < 500 ms and analog-to-digital sampling intervals of ≤ 250 ms are needed. Errors are further minimized by matching sample and standard peaks in both amplitude and D/H ratio. Using the pointwise algorithm, we demonstrate that a series of 14 homologous n-alkanes varying in concentration over a 5-fold range can be analyzed with a mean precision of 2.3‰ and no systematic errors.

INTRODUCTION

Several methods have recently been described for measuring the $^2H/^1H$ (D/H) ratio of materials using isotope-ratio-monitoring mass-spectrometry (irmMS). These methods utilize elemental analyzers (Kelly *et al.*, 1998) or gas chromatographs (Scrimgeour *et al.*, 1999; Hilkert *et al.*, 1999; Sessions *et al.*, 1999; Tobias and Brenna, 1997) to produce H_2 peaks in a continuous stream of carrier gas. Hydrogen in samples is converted to H_2 via pyrolysis or coupled oxidation/reduction and flows into an isotope-ratio mass spectrometer. In all cases, mass-2 (H_2) and mass-3 (HD) ion beams are monitored continuously, and D/H ratios are based on integration of the mass-2 and mass-3 ion-current signals.

Data-processing procedures are similar to those used for carbon-isotopic analyses: sample peaks and background signals are defined, peak areas are integrated and ratios are calculated, and δD values are obtained by comparing the D/H ratios of samples to those from reference peaks of known isotopic abundance (Ricci *et al.*, 1994). For hydrogen-isotopic analyses, however, the mass-3 ion current must be corrected for the presence of H_3^+ ions (Friedman, 1953).

Two basic approaches, termed "pointwise" (Tobias *et al.*, 1995) and "peakwise," (Tobias and Brenna, 1996a) have been proposed to correct for the presence of H_3^+. While some successes have been reported with both of these approaches, neither has yet been shown to be universally applicable. To overcome such limitations, we report here a general method for processing hydrogen irmMS data, including the correction for H_3^+. These algorithms can be used with all types of isotope-ratio-monitoring analytical systems, including elemental analyzers and gas chromatographs.

THEORY

H_3^+ is formed in the ion source of the mass spectrometer by the reaction

$$H_2^+ + H_2 \rightarrow H_3^+ + H \cdot \tag{1}$$

Table 2-1. Definition of symbols and typical values of instrumental parameters

i_2	total ion current at mass 2, ~5 nA
i_{H_2}	ion current due to H_2^+, ~5 nA
i_3	total ion current at mass 3, ~300 fA
i_{H_3}	ion current due to H_3^+, ~40 fA
i_{HD}	ion current due to HD^+, ~260 fA
K	H_3^+ factor, ~20 ppm mV^{-1}
R	ratio of mass-3 to mass-2 ion currents
R^*	R corrected for H_3^+ contribution
R^+	R^* incorporating errors in H_3^+ correction
P_{H_2}	partial pressure of H_2 in MS ion source, ~10^{-7} mbar
$f(t)$	any continuous function describing a peak-shaped curve
A	integrated area under $f(t)$, A×s
A_2	integrated area under $[f(t)]^2$, A^2×s
c	proportionality constant relating H and A_2/A
h	amplitude scaling factor in Gaussian-shaped peak
μ	mean value for Gaussian-shaped peak, s
σ	standard deviation for Gaussian-shaped peak, s
δD	isotopic composition of a sample relative to SMOW, ‰
ε	relative error in integrated i_{H_3}, %
ξ	error in calculated δD value, ‰

(Friedman, 1953). The abundance of H_2^+ is proportional to the partial pressure of H_2, hence the production of H_3^+ is proportional to the second power of the partial pressure of H_2. In practice, it is convenient to substitute measured ion currents (i) for partial pressures, such that

$$i_{H_3} = K(i_{H_2})^2 \qquad (2)$$

where K is an experimentally determined proportionality constant (Friedman, 1953). The true isotope ratio of the sample (= D/H = $R^*/2$) is then calculated from

$$R = \frac{i_3}{i_2} = \frac{(i_{HD} + i_{H_3})}{i_{H_2}} = \frac{i_{HD}}{i_{H_2}} + Ki_{H_2} = R^* + Ki_{H_2} \qquad (3)$$

where i_2 and i_3 are the observed mass-2 and mass-3 ion currents, and R and R^* represent the measured and corrected ion current ratios, respectively.

In hydrogen-isotopic analyses, the proportionality constant K is commonly referred to as the 'H$_3$ factor,' and is determined by measuring R at multiple values of i_2 for a single sample. Equation 3 has the form $y = b + mx$, so that regression of R on i_2 ($\approx i_{H_2}$) yields the value of K as the slope of the regression. Typical units for K, which expresses a change in the i_3/i_2 ratio per unit increase in i_2, are $10^{-6}\,\mathrm{mV^{-1}}$ or $10^{-3}\,\mathrm{nA^{-1}}$. Under typical operating conditions, 5–30% of i_3 can be due to H_3^+. The correction for H_3^+ is therefore a significant one, and in 'conventional' hydrogen isotopic analyses (*i.e.*, repeated comparison of sample and reference gases introduced from dual viscous-leak inlets) it can be the limiting factor in the precision of the analyses (Schoeller *et al.*, 1983). It remains to be seen whether precision in irmMS techniques will also be limited by correction for H_3^+.

H_3^+ Correction Algorithms

Equation 3, as written, is strictly true only for instantaneous ion currents and is subject to the assumption that i_{H_2} is proportional to P_{H_2}. In conventional analyses, isotope ratios are measured at constant P_{H_2}, so that *integrated* ion currents can be substituted for *instantaneous* ion currents. Small deviations in i_2 across an integration interval will produce little error in the correction for H_3^+ as long as variations are symmetrically distributed about the mean value (Schoeller *et al.*, 1983). In isotope-ratio-monitoring analyses, however, the partial pressure of H_2 in the ion source is changing rapidly and continuously as each sample peak passes through the mass spectrometer. Therefore, the ion current will often change significantly across a single 125-ms integration interval. Under these conditions, application of equation 3 is no longer straightforward.

Two strategies for H_3^+ correction of irmMS data have been proposed. Tobias *et al.* (1995) first used a "pointwise" scheme in which, prior to peak integration, each measured value of i_3 was corrected based on the corresponding value of i_2. However, they observed a nonlinear dependence of R on i_2, perhaps due to fractionation of hydrogen isotopes by the Pd membrane they used to eliminate He from the mass spectrometer. They later abandoned this approach in favor of a "peakwise" correction (Tobias and Brenna, 1996a), which was based on the amplitude of the chromatographic peak, rather than on individual measurements of i_2. The relationship between R and peak height in the peakwise correction was also nonlinear. A similar approach was used by

Scrimgeour *et al.* (1999) who also used a peakwise correction based on peak height, but who (in a system not including a Pd membrane) found a linear relationship between *R* and peak height.

While these corrections have apparently been used successfully, there has not yet been any theoretical examination of their basis and characteristics. The first applications (Kelly *et al.*, 1998; Scrimgeour *et al.*, 1999; Tobias *et al.*, 1995; Tobias and Brenna, 1996a) investigated simple chromatograms with few analytes, constant peak shapes, and negligible chromatographic column bleed. It remains unclear whether the correction schemes can be applied accurately to peaks with different shapes, to partially coeluting peaks, to peaks superimposed on changing H_2 backgrounds, or under other conditions which are frequently encountered in the analysis of real samples.

Peakwise Corrections

For irmMS applications, the measured ratio of ion currents for any given peak is

$$R = \frac{\int i_3(t)\,dt}{\int i_2(t)\,dt} = \frac{\int i_{HD} + \int K i_{H_2}^2}{\int i_{H_2}} = R^* + K\frac{\int i_{H_2}^2}{\int i_{H_2}} \tag{4}$$

where $i_2(t)$ and $i_3(t)$ are time-variable ion currents and each ion current is integrated with respect to time. We make the distinction between integrated ion currents in equation 4 and instantaneous ion currents in equation 3 to emphasize that ion currents are changing continuously in irmMS systems, and that values of i_2 which have been averaged over some finite time *cannot* be used in equation 3.

From equation 4, any property of an integrated peak that is functionally related to the quantity $\int i_{H_2}^2 \big/ \int i_{H_2}$ could in theory be used as the basis for a peakwise correction (*i.e.,* to establish a useful relationship between *R* and *R**). To explore this idea, we first examine the relationship between peak height and integrated areas in peaks having a Gaussian shape. Any such peak can be described by

$$f(t) = h \exp\left[-\frac{1}{2}\left(\frac{t-\mu}{\sigma}\right)^2\right] \tag{5}$$

where μ is the mean value, σ is the standard deviation, and *h* is an amplitude-scaling factor. The overall height (amplitude) of a Gaussian peak is simply *h*, and the areas under $f(t)$ and $[f(t)]^2$ are

$$A \equiv \int_{-\infty}^{\infty} f(t)dt = h\sigma\sqrt{2\pi} \tag{6}$$

$$A_2 \equiv \int_{-\infty}^{\infty} [f(t)]^2 dt = h^2\sigma\sqrt{\pi} \tag{7}$$

Comparing integrated peak areas (equations 6 and 7) gives

$$\frac{A_2}{A} = \frac{h^2\sigma\sqrt{\pi}}{h\sigma\sqrt{2\pi}} = \frac{h}{\sqrt{2}} \tag{8}$$

Since A_2/A is analogous to $\int i_{H_2}^2 / \int i_{H_2}$, equation 8 shows that the peak height of any Gaussian-shaped chromatographic peak is directly proportional to $\int i_{H_2}^2 / \int i_{H_2}$ regardless of the size or width of the peak.

Values for c, a proportionality constant relating peak height and A_2/A, are tabulated for several other functions in Table 2-2. While each function has a characteristic value of c, these vary significantly between functions so that no single, peakwise calibration could be used to compare peaks with different functional shapes. For example, Gaussian peaks cannot be compared with rectangu-

Table 2-2. Heights and integrated areas for several peak-shape functions

Defining Function	peak height	A[a]	A_2[a]	c[a]
Gaussian $f(t) = h\exp[-\frac{1}{2}(t/\sigma)^2], \quad -\infty \le t \le \infty$	h	$h\sigma\sqrt{2\pi}$	$h^2\sigma\sqrt{\pi}$	$\sqrt{2}$
rectangle $f(t) = h, \quad 0 \le t \le w$	h	hw	$h^2 w$	1
triangle[b] $f(t) = -mt + h, \quad 0 \le t \le h/m$	h	h^2/m	$5h^3/3m$	5/3
parabola $f(t) = -at^2 + h, \quad -\sqrt{h/a} \le t \le \sqrt{h/a}$	h	$\frac{4}{3}h\sqrt{h/a}$	$\frac{11}{15}h^2\sqrt{h/a}$	20/11
Lorentzian $f(t) = \dfrac{h(\Gamma/2)}{(t-\mu)^2 + (\Gamma/2)^2}, \quad -\infty \le t \le \infty$	$2h/\Gamma$	$h\pi$	$h^2\pi/\Gamma$	2
sine $f(t) = h\sin(t), \quad 0 \le t \le \pi$	h	$2h$	$h^2\pi/2$	$4/\pi$

[a]See text for definitions.
[b]Given function is for half of a triangle. Values of A, A_2, and c are for the full (symmetric) triangle.

lar reference peaks. This is in agreement with the observation of Tobias and Brenna (1996a) that the peakwise correction is dependent on constancy of peak shape.

Further complications arise when background H$_2$ currents are present. The abundance of H$_3^+$ is proportional to the second power of the entire H$_2$ ion current, and contributions from sample H$_2$ and background H$_2$ cannot be added linearly. Stated mathematically,

$$i_{H_3} = K\left(i_{H_2(samp)} + i_{H_2(bkgnd)}\right)^2 \neq Ki^2_{H_2(samp)} + Ki^2_{H_2(bkgnd)} \tag{9}$$

Accordingly, correction for contributions of H$_3^+$ must take place *before* subtraction of background ion currents due to H$_2$. In cases where background currents change substantially, a straightforward application of the peakwise correction will not be possible.

Pointwise Corrections

The pointwise algorithm represents a fundamentally different approach to H$_3^+$ correction (Tobias *et al.*, 1995). In essence, the instantaneous ion currents required by equation 3 are approximated by integrating ion currents over very short intervals. Errors result when ion currents change significantly during a single measurement interval, and the precision of the pointwise correction is therefore limited in part by the frequency at which ion currents are digitized. On the other hand, the only data needed to compute a pointwise correction are the values of K, i_2, and i_3. The size and shape of the peaks, and the separation of sample and background components, do not influence the correction.

In practice, the pointwise algorithm is implemented by correcting each measurement of i_3 based on the i_2 measurement from the same time interval using the equation $i_{HD} = i_3 - K(i_{H_2})^2$. The value for K used in this equation should, to the extent possible, represent only the effects of H$_3^+$ formation on the measured ratio. Incorporation of other mass-discrimination effects, such as those originating in inlet systems, the mass spectrometer, etc., is theoretically possible (for example see Tobias *et al.*, 1995) but the correction becomes increasingly nonlinear and instrument-specific. The equations and error analysis developed here are not applicable to a nonlinear H$_3^+$ correction. With only the effects of H$_3^+$ formation accounted for by K, the pointwise H$_3^+$ correction can be applied to virtually

any hydrogen irmMS system. In an accompanying paper (Chapter 3), we describe several methods for measuring values of K and show that the value obtained for pointwise correction of irmGCMS data is approximately the same as that used for conventional analyses.

To summarize, the peakwise approach to H_3^+ correction does have a firm theoretical basis. Provided that peak shapes and background H_2 currents are constant, the peakwise correction is exact and can succeed (Scrimgeour *et al.*, 1999; Tobias and Brenna, 1997, 1996a, 1996b). However, the required consistent peak shapes and background signals are seldom encountered in isotope-ratio-monitoring experiments and the potential for significant errors is great. In contrast, the pointwise approach to H_3^+ correction is approximate in all cases but is not significantly influenced by changes in peak shape or background signals. This flexibility provides a significant advantage over the peakwise approach, provided that the approximation embodied in the pointwise correction (*i.e.,* that ion currents are constant over each integration interval) is sufficiently accurate. Below, we examine quantitatively the sources of error in the pointwise correction, and show that for most isotope-ratio-monitoring measurements the error introduced by this method should not be precision-limiting.

EXPERIMENTAL SECTION

Hydrogen-isotopic compositions of *n*-alkanes were measured using a conventional GC coupled to an isotope-ratio mass spectrometer via a 1400ºC pyrolysis furnace. The flow of He carrier gas into the mass spectrometer was 200 µL/min, and an electrostatic lens was used to prevent scattered $^4He^+$ ions from reaching the mass-3 detector. Details of this analytical system are provided in Chapter 3.

Samples

A standard solution containing a homologous series of 15 *n*-alkanes (from *n*-C_{16} to *n*-C_{30}) was prepared and used to test H_3^+ correction algorithms. The δD values of the individual alkanes, which ranged from −42 to −256‰, were determined by Dr. Arndt Schimmelmann at Indiana University following the method described by Schimmelmann *et al.* (1999). As recommended by Coplen

(1988) the results of the off-line analyses were normalized to yield $\delta D(SLAP) = -428‰$. Concentrations of the compounds in the standard solution yielded between 20 and 100 nmol $H_2/\mu L$ and were chosen so that they did not correlate with either carbon number or hydrogen isotopic composition. δD measurements for the first analyte in each chromatogram (n-C_{16}) were found to be significantly less precise ($\sigma = 10‰$) than for subsequent peaks ($2.1 \leq \sigma \leq 5.2‰$), and were excluded from all subsequent calculations. We have no precise explanation for this "first-peak" effect.

Data Processing

Ion currents at masses 2 and 3 were digitized and recorded at intervals of 62, 125, or 250 ms using Isodat v7.2-00 software (Finnigan MAT, Bremen, Germany). Raw ion-current measurements and times were transferred into Excel (Microsoft, Redmond, WA), and further data processing was managed by Visual Basic codes that we have developed. These codes are available at http://www.nosams.whoi.edu/jmh. First, background ion currents not related to H_2 are subtracted. Components include offset currents added to each signal to provide a more stable background ratio (Merritt and Hayes, 1994) as well as contributions from $^3He^+$, $^4He^{2+}$ and scattered $^4He^+$ ions. Next, the data stream is corrected for the presence of H_3^+ on a point-by-point basis using the equation $i_{HD} = i_3 - i_{H_3} = i_3 - K(i_{H_2})^2$. Peaks are then identified and defined by examining the first and second derivatives of the i_2 signal over ~1-s intervals. Typically, slopes of 1.0 and –0.1 mV/s are used to define the beginning and end of the peak, respectively.

Next, the difference in time between the maxima of the H_2 and HD peaks is calculated as described — for the case of $^{12}CO_2$ and $^{13}CO_2$ — by Ricci $et\ al.$ (1994). As with carbon isotopic measurements, this difference results from partial chromatographic separation of isotopically substituted molecules. For hydrogen-isotopic measurements, the differences in retention time (for peaks containing a natural abundance of D) can be as large as 1 s, compared to ~100 ms for typical separations between carbon isotopic peaks. The data-processing algorithms used in this work adjust the peak-start and -stop times for the mass-2 and -3 peaks by whole numbers of data points ($i.e.$, increments of 62, 125, or 250 ms) so that equivalent portions of each peak are integrated.

Background ion currents (including H_2-related components) for the n-alkane standard described above are assumed to be constant across the width of each peak, and are determined by averaging i_2 and i_3 across ~5-s intervals prior to each peak. Background currents for masses 2 and 3 in this system are typically 40 pA and 50 fA respectively with the GC column at 50°C, and 200 pA and 133 fA at 320°C. Finally, peak areas are integrated, isotope ratios are calculated, and values of δD are calculated by reference to standards (Coplen, 1988).

No organic standards are currently available with δD near that of SLAP (–428 ‰). We therefore calibrated the irmGCMS data relative to the dual-inlet values to produce the desired normalization to the SMOW-SLAP scale, as follows. For each n-alkane analysis, the slope and intercept of the regression of irmGCMS δD values on dual-inlet δD values was calculated. As will be shown, this consistently yields a linear relationship with $r^2 > 0.99$. The average slope and intercept of all n-alkane analyses for a given day were then taken as the normalization line which was applied to all analyses on that day.

Estimation of Errors and Uncertainties

To test the sensitivity of results to errors introduced during data collection and processing, we constructed a numerical simulation that describes all ion currents produced during measurement of a sample peak. These include H_2^+, HD^+, and H_3^+ produced by both sample and background components, plus non-hydrogen background at masses 2 and 3. The simulation allows the use of different functions to define peak shape, including rectangular and Gaussian peaks of variable size. The effects of amplifier time constants are also calculated (Sternberg, 1966). The resulting model data are then 'digitized' at any desired frequency to produce a stream of simulated i_2 and i_3 data points which mimics the actual data obtained from the mass spectrometer (Figure 2-1).

These simulated data, for which the accurate D/H ratios are known, can then be processed using various peak-definition and H_3^+-correction algorithms. Comparison of the D/H ratios obtained to the true ratios then provides a quantitative estimate of error. This approach supplements the direct observation of results from test samples by separating and quantifying the individual effects of frequency response, analog-to-digital conversion, and H_3^+ correction on the overall analytical uncertainty.
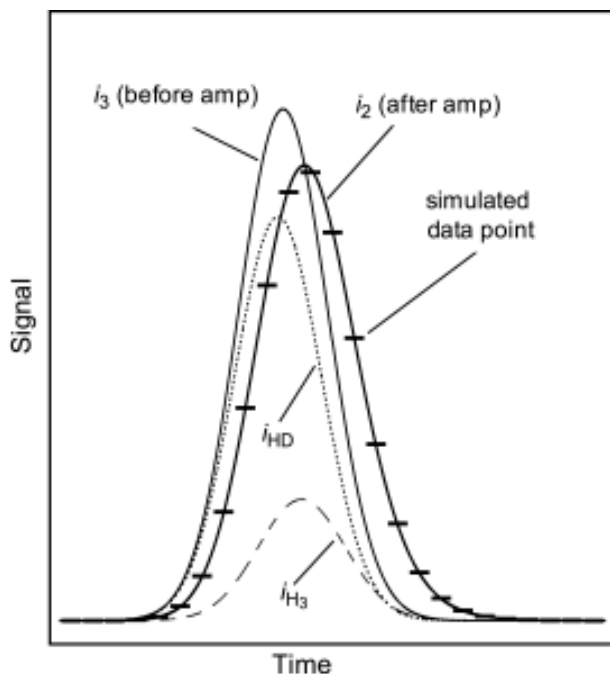
Figure 2-1. Typical output from the simulation of a Gaussian peak. H_3^+ and HD peaks are offset due to isotope chromatography. The sample peak is broadened by the existence of a 1.3-s time constant in the signal amplification circuit.

RESULTS AND DISCUSSION

Propagation of Errors

Errors in H_3^+ correction will cause errors in calculated values of δD. The magnitude of the errors in δD will depend on 1) the mismatch in size between sample and standard peaks; 2) the magnitude of K; and 3) the difference in D/H ratio of the sample and standard. To consider these factors both efficiently and quantitatively, we examine errors in δD as a function of the relative error in K. Relative errors in K and H_3^+ are equal, so that a 5% error in K will cause a 5% error in the magnitude of the integrated H_3^+ ion current. Below we report errors in integrated H_3^+ due to signal collection and processing (*i.e.,* which are not due to errors in the value of K). In a companion paper (Chapter 3) we report errors in the value of K obtained by several methods. Both sources of error are readily incorporated in the analysis provided here.

As a representative example, we consider the comparison of a sample-standard pair of Gaussian-shaped peaks. The δD value of a sample peak is calculated relative to the isotopic ratio of standard mean ocean water (SMOW) from

$$\delta D_{samp} = \left[\frac{R^*_{samp}}{R^*_{SMOW}} - 1 \right] \times 1000 \tag{10}$$

where R^* is the H$_3$-corrected HD/H$_2$ ratio. Since the isotopic standard in use rarely has an HD/H$_2$ ratio equal to that of SMOW, equation 10 can be modified for use with a standard peak having any δD value

$$\delta D_{samp} = \left[\frac{R^*_{samp}}{R^*_{std}} \left(\frac{\delta D_{std}}{1000} + 1 \right) - 1 \right] \times 1000 \tag{11}$$

For any Gaussian function, the value of R^* can be obtained by combining equations 4 and 8 to give

$$R^* = R - K \frac{\int i_2^2}{\int i_2} = R - K \frac{h}{\sqrt{2}} \tag{12}$$

where h is the height of the peak. If K has a relative error ε, the resulting, erroneously corrected HD/H$_2$ ratio of the peak becomes

$$R^+ = R - (K + \varepsilon K) \frac{\int i_2^2}{\int i_2} = R - (1 + \varepsilon) K \frac{h}{\sqrt{2}} \tag{13}$$

The resulting error in δD, ξ, will then be given by

$$\xi = \delta D_{meas} - \delta D_{true} = (\delta D_{std} + 1000) \left[\frac{R^+_{samp}}{R^+_{std}} - \frac{R^*_{samp}}{R^*_{std}} \right] \tag{14}$$

Values of R^* and R^+ can be evaluated directly from equations 12 and 13. The error in δD can, therefore, be determined using representative values of ε, K, R, and h for both sample and standard peaks (this approach assumes the magnitude of ε is identical in both sample and standard peaks). Values of K, R, and h are readily obtained from experimental data.
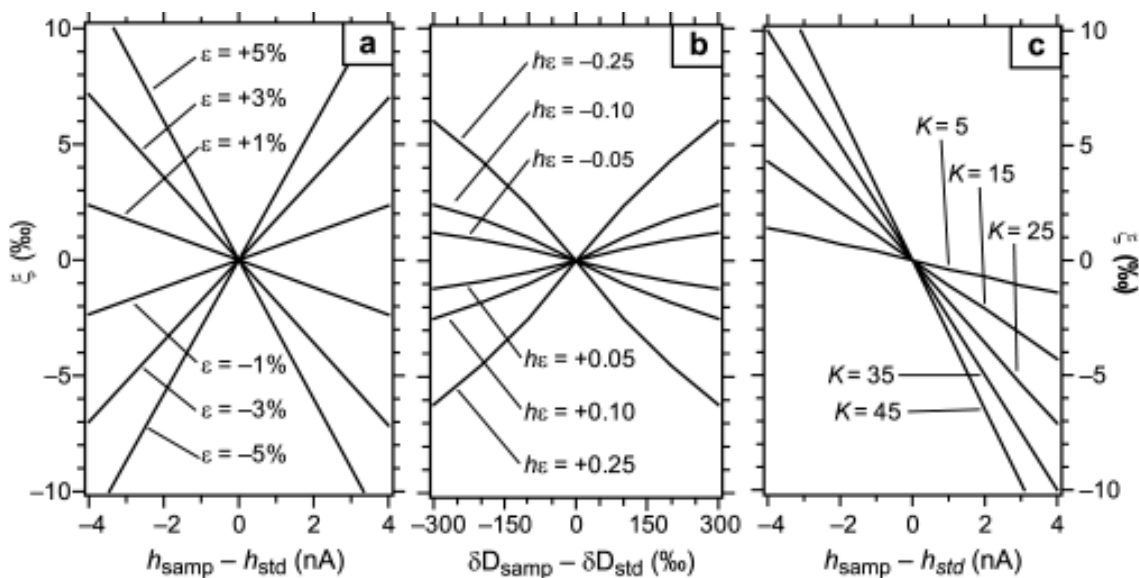
Figure 2-2. Errors in δD ($\equiv \xi$) as a function of pertinent variables: (a) as a function of error in integrated i_{H_3} ($\equiv \varepsilon$) and mismatched peak height (h), with matched δD values and with $K = 25$; (b) as a function of ε and mismatched δD values with matched peak heights and $K = 25$; (c) as a function of K and mismatched peak heights with matched δD values and $\varepsilon = 3\%$. Units for h are nA, and for K are ppm mV^{-1}.

Typical relationships obtained from equation 14 are illustrated in Figure 2-2. In the first instance, we consider errors in δD when the δD values of the sample and standard are approximately matched. To a good approximation, values of ξ then depend only on the difference in peak height between sample and standard and on the magnitude of ε (Figure 2-2a). If sample and standard peaks are perfectly matched in height but not δD value, ξ varies approximately with the difference in δD and with the product of h and ε (Figure 2-2b). In this case, errors increase with peak height (as opposed to the *difference* in peak heights) and with increasing mismatch in δD values. In the third instance, errors in δD increase as the magnitude of K increases (Figure 2-2c) regardless of mismatch in peak height between sample and standard. Given the relationships in Figure 2-2, steps to minimize H_3-related errors in hydrogen irmMS analyses should be, in order of importance, 1) match sample and standard peak heights, 2) reduce the magnitude of K, 3) match sample and standard δD values, and 4) with due attention to limitations imposed by shot noise (Merritt and Hayes, 1994), minimize peak heights. This final step is counterintuitive, but is a result of the fact that H_3^+ increases disproportionately with increasing H_2.

Detector Frequency Response

Equations 2 through 4 assume that the mass-2 signal recorded by the data system accurately reflects the partial pressure of H_2 in the ion source. In fact, the relationship is only approximate. The mass-2 ion current follows P_{H_2} but the signal voltage is affected by time constants associated with the signal-processing pathway. Although the time constant of the mass-2 amplifier could easily be <1 ms, an important requirement is that the time constants of both mass-2 and -3 amplifiers be approximately equal for greatest measurement accuracy (Merritt and Hayes, 1994). Because of the large feedback resistance typical of the mass-3 amplifier ($\sim 10^{12}\Omega$), it is difficult to reduce time constants in that circuit below ~500 ms.

If the time constant associated with the mass-2 signal pathway is so large, or if the chromatographic peaks are so narrow that their shape is not accurately reproduced by the signal-processing system, large errors in the calculated H_3^+ peak area, and so also the D/H ratio, will result. The nature of this problem is illustrated in Figure 2-3. As the the time constant becomes larger, the signal peak
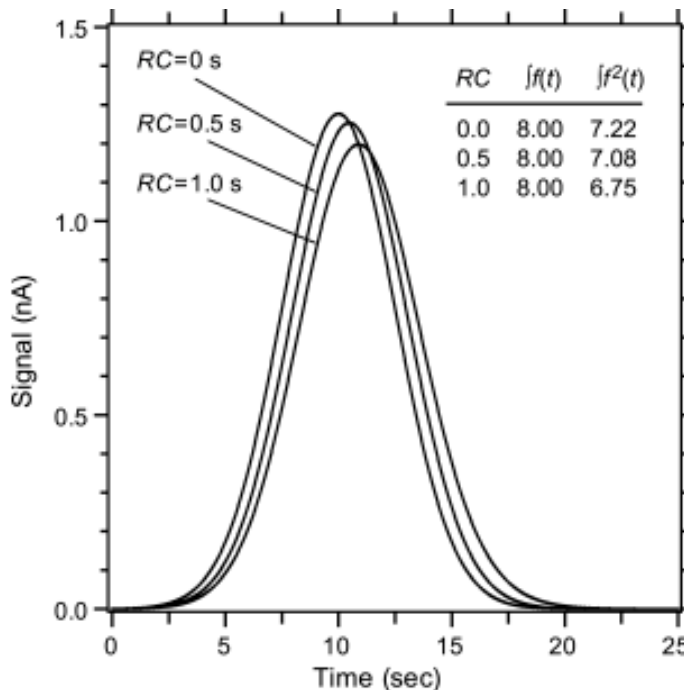
Figure 2-3. Decrease in the area under the square of signal intensity when peak shape is broadened by electronic time constants. All three curves represent the same 10-s-wide Gaussian curve filtered by three different time constants. This decrease in the ratio of integrated areas leads to an underestimate of H_3^+ contributions.

is progressively broadened. Although the integrated area under $f(t)$ remains constant despite this broadening, the area under $[f(t)]^2$ does not. Instead, the integral of $[f(t)]^2$ decreases as the signal is broadened, resulting in underestimation of the H$_3^+$ contribution to i_3.

To examine the importance of frequency response quantitatively, we have calculated values of ε as a function of the time constant of the mass-2 signal pathway. Results are shown in Figure 2-4 for both Gaussian and rectangular peaks. The plotted results reflect calculations that consider only the effects of frequency response. As shown in Figure 2-4, errors related to the analog time constants increase sharply with decreasing peak width and increasing time constant, and can be quite large. For Gaussian peaks with $\sigma = 3$ s, an amplifier time constant of 1 s results in a value for ε of approximately -5%, and a time constant of 500 ms results in a value for ε of about -1%. These values of ε can be used directly in Figure 2-2 to estimate the magnitude of errors in δD. Note that in all cases the contribution of H$_3^+$ is underestimated. There are thus very clear benefits to maximizing
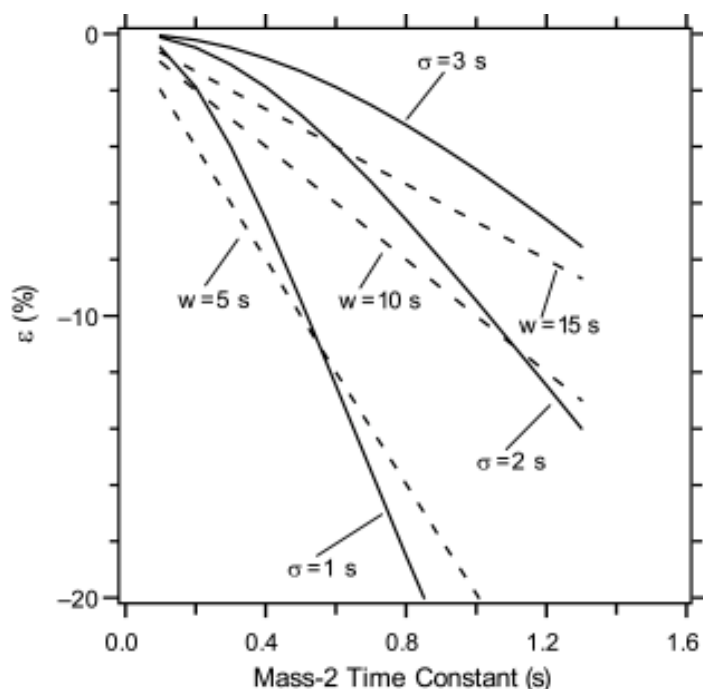
Figure 2-4. Estimated values of ε as a function of peak width and mass-2 time constant. Data are for Gaussian (solid lines; σ = standard deviation) and rectangular (dashed lines; w = width) peaks with no background H$_2$ signals.

the frequency response of both mass-2 and -3 detectors for hydrogen irmMS. Time constants of 500 ms or less should probably be considered a minimum requirement for chromatographic peaks with width $(4\sigma) \approx 10$ s.

Analog-to-Digital Conversion Rate

Errors will be introduced by the pointwise H_3^+ correction when signals change significantly across individual integration intervals. The magnitude of the errors will depend on how fast signals are changing relative to the sampling rate. Numerical simulations confirm that ε decreases with sampling rate, and increases as peaks get taller and narrower (Figure 2-5). For peaks having a width (4σ) of >4 s, an integration interval of 250 ms results in $0.0 \geq \varepsilon \geq -0.3\%$. Again, the contribution of H_3^+ to i_3 is underestimated. For square peaks, errors are negligible because ion currents are approximately constant over most of the peak.
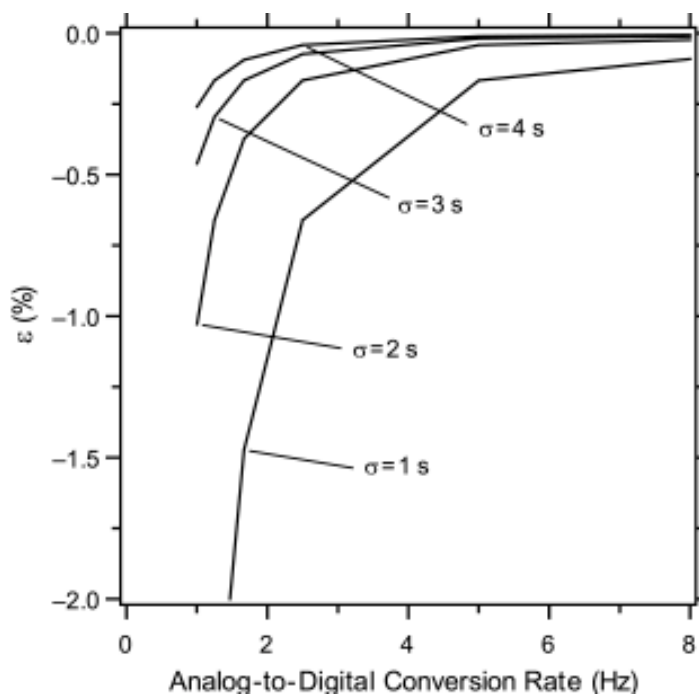
Figure 2-5. Estimated values of ε as a function of peak width and analog-to-digital conversion frequency. All data are for Gaussian-shaped peaks (σ = standard deviation) with no background H_2 signals.

Table 2-3. Peak characteristics and δD values of *n*-alkane standard

C no.	H_2 (nM)[a]	H (V)[b]	*FWHM* (s)[c]	δD (‰)[d]	σ_{di} (‰)[e]	Δ (‰)[f]	σ_p (‰)[e]	σ_m (‰)[e]	σ_Δ (‰)[e]
17	20.7	1.6	3.4	−144.3	0.40	0.3	5.2	0.74	0.8
18	31.4	2.5	3.8	−55.2	0.69	≡ 0[g]			
19	41.9	3.6	4.0	−119.4	0.92	−2.6	3.2	0.47	1.0
20	52.2	5.1	4.5	−48.7	0.40	1.8	2.7	0.39	0.6
21	10.2	1.2	4.1	−215.0	1.21	2.3	3.8	0.56	1.3
22	20.9	2.2	4.0	−62.2	0.75	3.0	2.3	0.33	0.8
23	31.3	3.4	4.0	−46.5	1.21	1.1	2.1	0.31	1.3
24	42.0	4.7	4.3	−55.4	1.10	3.8	2.7	0.40	1.2
25	52.1	5.8	5.0	−256.5	1.39	−1.4	2.2	0.32	1.4
26	10.4	1.4	4.5	−57.7	0.64	−4.5	4.1	0.59	0.9
27	20.7	2.6	4.5	−226.5	0.98	−0.6	3.6	0.52	1.1
28	31.2	3.8	5.1	−52.3	0.92	≡ 0[g]			
29	41.6	4.3	6.3	−182.1	0.06	1.1	2.6	0.37	0.4
30	51.7	4.6	7.9	−42.7	0.58	−3.1	3.0	0.44	0.7
					mean:	0.0	2.3		1.0

[a] Injected on-column for typical analysis.
[b] Peak height for typical analysis.
[c] Full width at half maximum for typical analysis.
[d] Mean δD value from offline dual-inlet measurements ($n = 3$).
[e] Standard deviations of the mean dual-inlet δD value (σ_{di}), the population of IRMS δD measurements (σ_p), the mean IRMS δD measurements (σ_m), and Δ (σ_Δ).
[f] $\Delta \equiv \delta D_{IRMS} - \delta D_{di}$.
[g] *n*-C_{20} and *n*-C_{28} were the isotopic reference peaks.

Sample Analyses

As a test of the overall analytical system, including data-processing algorithms, the *n*-alkane test solution was analyzed 48 times over a period of 30 days. For these analyses, time constants of 0.2 s (mass 2) and 1.3 s (mass 3) were used. Problems with mismatched time constants are minimized in these samples because peaks are widely separated. As a result, overall integration intervals can be significantly wider than the actual peaks. Data were collected in 250-ms integration intervals and corrected with the pointwise algorithm using values of *K* determined from the *n*-alkane standards via the peak-RMS method described in Chapter 3. The C_{18} and C_{28} *n*-alkanes were chosen as isotopic reference peaks for each analysis because they are at approximately the same concentration in our standard mixture and have approximately the same δD values.

Results obtained via isotope-ratio-monitoring are compared to those obtained from conventional analyses in Table 2-3. The relationship between δD values obtained by the two methods is shown for a typical analysis in Figure 2-6. For all such analyses, a linear relationship was obtained
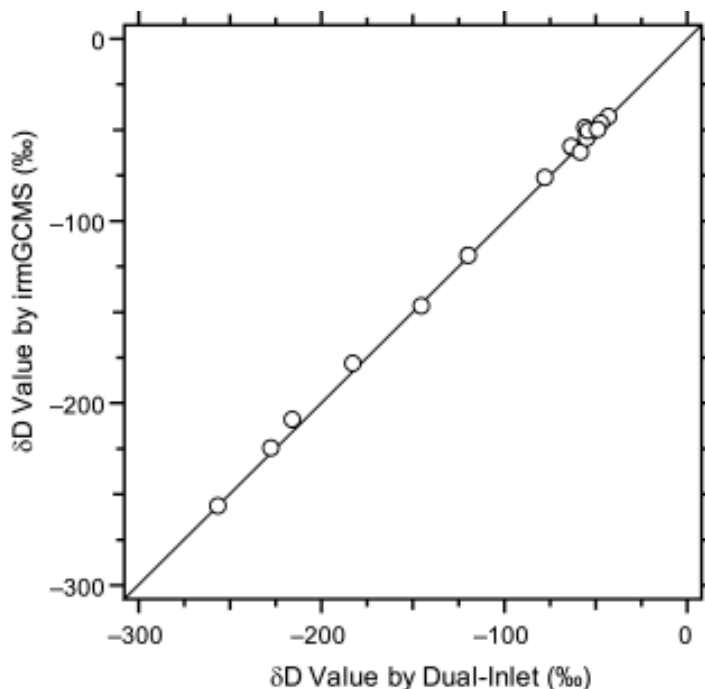
Figure 2-6. Typical relationship between δD values measured by conventional dual-inlet versus isotope-ratio-monitoring techniques. Least-squares regression of these data gives $y = 0.987x - 0.6$, with $r^2 = 0.9988$. The solid line is $y = x$, and is indistinguishable from the regression line at this scale.

with $r^2 > 0.99$. and with a slope ranging from 0.95 to 1.02. The slope of this regression was typically reproducible to within ~0.01 when multiple samples were analyzed over the course of a day. Differences in δD values are designated by the symbol Δ in Table 2-3. Accuracy, expressed in terms of the RMS value of Δ, is 2.5‰. Precision, expressed as the standard deviation of the population of results for each alkane (σ_p), ranges between 2.1 and 5.2‰. Systematic errors are minimized by the normalization procedure. In this case, the average value of Δ is exactly zero because the normalization is based on the alkane δD values themselves (in practical analyses, *e.g.,* Sessions *et al.*, 1999, normalizations developed from alkane test runs are applied to diverse analytes in separate chromatographic runs). In contrast, precision is unaffected by normalization which serves only to increase or decrease the average value (*i.e.,* Δ).

Errors in δD are uncorrelated with peak height ($r^2 = 0.002$; Figure 2-7). The normalization applied to these data is based only on δD value, not peak height. δD and concentration do not covary in our *n*-alkane sample mixture ($r^2 < 0.001$), so any correlation between Δ and peak height
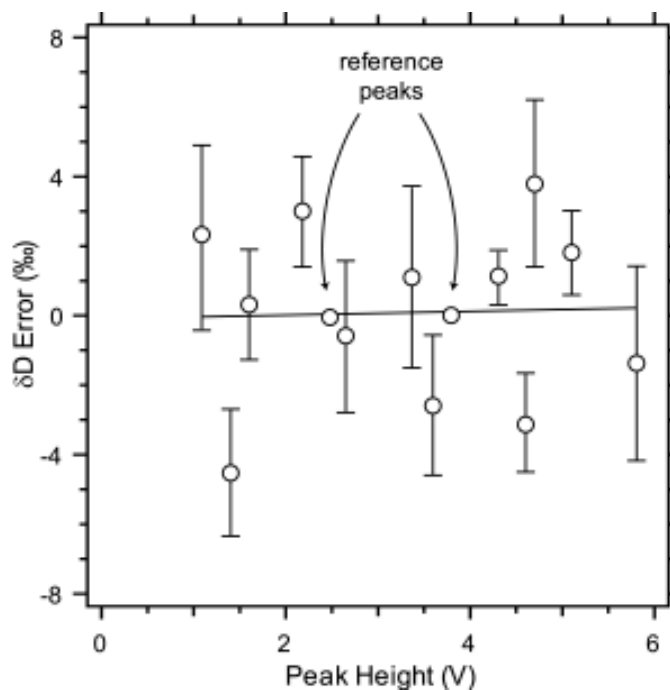
Figure 2-7. Measured errors in δD as a function of peak height for C_{17} to C_{30} *n*-alkanes. Error bars are $\pm 2\sigma_\Delta$ from 48 replicate analyses.

should be unaffected by normalization. To test this assertion, we calculated the correlation coefficient between peak height and errors in the δD values obtained prior to normalization ($r^2 = 0.004$). The lack of correlation indicates no significant systematic errors are introduced by the pointwise correction of H_3^+. Because we have determined the value of K from the chromatograms themselves, this level of accuracy and precision is probably better than can be achieved for real samples where a larger uncertainty in the value of K exists. This analysis does demonstrate, however, that the pointwise algorithm can accurately accommodate GC peaks with a wide range in peak height and width, and which appear on a substantially changing H_2 background.

As shown in Figure 2-7, the scatter of the results around $\Delta = 0$ is larger than expected on the basis of the reproducibility of the δD values. The error bars are $\pm 2\sigma_\Delta$, where $\sigma_\Delta = \sqrt{\sigma_m^2 + \sigma_{di}^2}$ (see notes to Table 2-3). This range takes into account the expected random variations in the mean values of both the irmGCMS results and the dual-inlet results. Approximately 95% of the error bars would be expected to include $\Delta = 0$, but only six of the twelve samples do so. There is no

apparent correlation between values of Δ and σ_p for a given alkane ($r^2 = 0.08$), between Δ and carbon number ($r^2 = 0.10$), or between Δ and δD of the alkane ($r^2 = 0.001$) or δD of the previous alkane ($r^2 = 0.03$) as might be expected in the case of memory effects. However, the alkanes for which Δ is significantly different from zero all have δD in the range –50 to –125‰, and are therefore likely derived from petroleum sources (Schoell, 1984). With one exception, the alkanes for which Δ is not signficantly different from zero all have δD in the range –150 to –275‰, and are probably derived from biological sources (Sessions *et al.*, 1999). We suggest that the systematic errors apparent in the former group may therefore be related to the origin of these materials. For example, minor impurities in petroleum-derived alkanes could lead to systematic differences between the compound-specific irmGCMS analyses and the bulk-property conventional analyses.

As shown by Figure 2-2, a correlation between peak height and Δ would be expected if errors in K were responsible for the scatter in the results. In more general terms, uncertainties in K must propagate and lead to uncertainties in δD. The results of the sensitivity tests summarized in Figure 2-2 indicate that, if uncertainties in K are on the order of 2% (as in this case), related errors in δD will be on the order of a few permil for typical sample-to-standard mismatches of peak height and δD value. From this perspective, the RMS error of 2.5‰ is not surprising. Until further experience yields a more complete understanding of factors controlling K, the results of the sensitivity tests reported here should — when questions of accuracy are preeminent — be given precedence over more impressive measurements of internal precision.

CONCLUSIONS

We have shown on theoretical grounds that a correction based only on peak height can be very accurate, but only to the extent that peak shapes and background currents are constant. In typical irmMS conditions, where neither is constant, peakwise corrections can introduce large errors. The more general, pointwise algorithm avoids these problems. This method is independent of peak shape and background signals, and is applicable to a wide range of hydrogen irmMS applications (including gas chromatography and elemental analysis). The accuracy of pointwise H$_3^+$ correction

is limited by 1) the frequency response of the mass-2 signal-processing pathway, 2) the analog-to-digital sampling rate of the data system, and 3) the highest frequency at which H_2 signals change. Analog-to-digital conversion rates of at least 4 Hz and electronic time constants < 500 ms should be used to minimize H_3^+-related errors under typical GC conditions.

To test the proposed pointwise correction algorithm, a suite of 14 homologous *n*-alkanes for which concentrations vary over a five-fold range was analyzed using our irmGCMS system. The analyses produced an RMS error of 2.5‰ for means of 48 analyses. The average precision of a single measurement was 2.3‰. There is no correlation between error and peak height in these analyses, indicating that pointwise correction of H_3^+ does not introduce systematic errors. Assuming the "correct" value for *K* can be determined, the correction of irmMS data for H_3^+ by the pointwise correction algorithm should not limit the precision of the measurements.

REFERENCES

Coplen, T. B. (1988) Normalization of oxygen and hydrogen isotope data. *Chemical Geology* **72**, 293–297.

Friedman, I. (1953) Deuterium content of natural water and other substances. *Geochimica et Cosmochimica Acta* **4**, 89–103.

Hilkert, A. W., Douthitt, C. B., Schlüter, H. J., and Brand, W. A. (1999) Isotope ratio monitoring GCMS of D/H by high temperature conversion isotope ratio mass spectrometry. *Rapid Communications in Mass Spectrometry* **13**, 1226–1230.

Kelly, S. D., Parker, I. G., Sharman, M., and Dennis, M. J. (1998) On-line quantitative determination of $^2H/^1H$ isotope ratios in organic and water samples using an elemental analyser coupled to an isotope ratio mass spectrometer. *Journal of Mass Spectrometry* **33**, 735–738.

Merritt, D. A. and Hayes, J. M. (1994) Factors controlling precision and accuracy in isotope-ratio-monitoring mass spectrometry. *Analytical Chemistry* **66**, 2336–2347.

Ricci, M. P., Merritt, D. A., Freeman, K. H., and Hayes, J. M. (1994) Acquisition and processing of data for isotope-ratio-monitoring mass spectrometry. *Organic Geochemistry* **21**, 561–571.

Schimmelmann, A., Lewan, M. D., and Wintsch, R. P. (1999) D/H ratios of kerogen, bitumen, oil, and water in hydrous pyrolysis of source rocks containing kerogen types I, II, IIS, and III. *Geochimica et Cosmochimica Acta* **63**, 3751–3766.

Schoell, M. (1984) Recent advances in petroleum isotope geochemistry. *Organic Geochemistry* **6**, 645–663.

Schoeller, D. A., Peterson, D. W., and Hayes, J. M. (1983) Double-comparison method for mass spectrometric determination of hydrogen isotopic abundances. *Analytical Chemistry* **55**, 827–832.

Scrimgeour, C. M., Begley, I. S., and Thomason, M. L. (1999) Measurement of deuterium incorporation into fatty acids by gas chromatography/isotope ratio mass spectrometry. *Rapid Communications in Mass Spectrometry* **13**, 271–274.

Sessions, A. L., Burgoyne, T. W., Schimmelmann, A., and Hayes, J. M. (1999) Fractionation of hydrogen isotopes in lipid biosynthesis. *Organic Geochemistry* **30**, 1193–1200.

Sternberg, J. C. (1966) Extracolumn contributions to chromatographic band broadening. In Giddings, J.C. and Keller, R.A. (Eds.), *Advances in Chromatography*, Vol. 2. Marcell Dekker, New York, pp. 205–270.

Tobias, H. J. and Brenna, J. T. (1997) On-line pyrolysis as a limitless reduction source for high-precision isotopic analysis of organic-derived hydrogen. *Analytical Chemistry* **69**, 3148–3152.

Tobias, H. J. and Brenna, J. T. (1996a) Correction of ion source nonlinearities over a wide signal range in continuous-flow isotope ratio mass spectrometry of water-derived hydrogen. *Analytical Chemistry* **68**, 2281–2286.

Tobias, H.J. and Brenna, J.T. (1996b) High-precision D/H measurement from organic mixtures by gas chromatography continuous-flow isotope ratio mass spectrometry using a Palladium filter. *Analytical Chemistry* **68**, 3002–3007.

Tobias, H. J., Goodman, K. J., Blacken, C. E., and Brenna, J. T. (1995) High-precision D/H measurement from hydrogen gas and water by continuous-flow isotope ratio mass spectrometry. *Analytical Chemistry* **67**, 2486–2492.

Chapter 3 — Determination of the H$_3$ factor in hydrogen isotope-ratio-monitoring mass spectrometry*

ABSTRACT

The H$_3$ factor, K, is a parameter required in high-precision, mass spectrometric analyses of hydrogen-isotopic abundances. When H$_2$ is used as the sample gas, $R^* = R - Ki_2$, where R^* is the true HD/H$_2$ ratio, R is the observed (mass 3)/(mass 2) ion-current ratio, and i_2 is the ion current at mass 2. Four different methods for the determination of K were defined and tested under conditions characteristic of isotope-ratio-monitoring systems. Three of these were peak-based. The fourth employed steady flows of H$_2$ from a conventional inlet system. Results obtained using the latter method were more precise (standard deviation of $K = 0.1$ versus ~0.6 ppm mV^{-1} for the peak-based methods). However, use of the resulting values of K for correction of isotope-ratio-monitoring GCMS results led to systematic errors as large as 9‰, whereas use of the peak-based values led to no systematic errors. Values of K were only weakly dependent on the pressure of He, declining approximately 5% for each 10-fold increase in P_{He}. Small variations in partial pressures of H$_2$O and CH$_4$, potential contaminants under isotope-ratio-monitoring conditions, had no significant effect on values of K.

INTRODUCTION

The abundance of ^{2}H (D) is low relative to that of ^{1}H (H): at natural abundance, most organic materials contain less than 100 ppm D. To avoid confounding contributions from other, more abundant heavy isotopes (*e.g.*, ^{13}C in CH$_4$), highly precise measurements of hydrogen isotopic ratios typically employ molecular H$_2$ as the sample gas for mass spectrometric determination of H$_2$ and HD abundances. An unfortunate consequence of the use of H$_2$ for these measurements is that the reaction

$$H_2^+ + H_2 \rightarrow H_3^+ + H \cdot \tag{1}$$

occurs readily in the ion source of the mass spectrometer (Friedman, 1953). Since H$_3^+$ is not resolved from HD$^+$ by typical isotope-ratio mass spectrometers, a correction is required. In materials containing a natural abundance of D, H$_3^+$ can account for as much as 5 to 30% of the *m/z*-3 signal, so the correction for H$_3^+$ is significant.

In "conventional" isotope-ratio measurements, both sample and standard gases enter the ion source as pure H$_2$ via dual, viscous-leak capillaries. Ion-source pressures are typically 10^{-7} mbar or lower during these measurements, and H$_2$ is the only neutral species present in significant quantities. Under these conditions, reaction 1 is the only important source for H$_3^+$ (Friedman, 1953), so that the production of H$_3^+$ is given by

$$[H_3^+] \propto [H_2^+][H_2] = K[H_2]^2 \tag{2}$$

The proportionality constant in this equation (K) is commonly known as the "H$_3$ factor" and, for dual-inlet measurements, it is both readily measured and reliably stable. In practice, the value of K is usually determined by measuring the (mass-3)/(mass-2) ion-current ratio of a sample over a range of pressures and using least-squares regression to find the value of K (*i.e.*, the slope) in the expression

$$R = \frac{i_3}{i_2} = \frac{(i_{HD} + i_{H_3})}{i_{H_2}} = \frac{i_{HD}}{i_{H_2}} + Ki_{H_2} = R^* + Ki_{H_2} \tag{3}$$

where R is the measured ion-current ratio, R^* is the corrected HD/H$_2$ ratio, i_2 and i_3 are the ion

currents measured at mass-2 and -3, and i_{H_2}, i_{HD}, and i_{H_3} are the ion currents due solely to H_2^+, HD^+, and H_3^+ ions, respectively. Once the value of K is known, equation 3 serves as the basis for correction of subsequent dual-inlet analyses (Friedman, 1953). In modern isotope-ratio mass spectrometers, K typically has a value of 5 to 30 ppm mV^{-1} (equivalent to 5 to 30‰ nA^{-1}), and is stable to within ~1% relative over a period of many hours. D/H ratios can accordingly be determined with a precision of 1‰ or better.

In contrast, recently developed methods utilize isotope-ratio-monitoring mass spectrometry (irmMS) for the measurement of D/H ratios (Sessions *et al.*, 1999; Scrimgeour *et al.*, 1999; Hilkert *et al.*, 1999; Kelly *et al.*, 1998; Tobias and Brenna, 1997). In these analyses, H$_2$ is carried to the ion source in a stream of carrier gas (typically He), and D/H ratios are obtained by the integration of mass-2 and -3 ion currents across sample peaks. The fundamental differences between isotope-ratio-monitoring and conventional, dual-inlet analyses are *i*) the dynamic conversion of samples into H$_2$, *ii*) the presence of He carrier gas, and *iii*) measurement across large variations in the partial pressure of H$_2$. All of these factors potentially lead to changes in both the mechanism and magnitude of H$_3^+$ formation.

In a companion paper (Chapter 2), we discuss the steps necessary to correct isotope-ratio-monitoring data for H$_3^+$, and show that a form of the pointwise correction first described by Tobias *et al.* (1995) is the most broadly applicable. Conceptually, the pointwise correction is very similar to the approach used for dual-inlet analyses, and it depends critically on two of the same requirements: that K can be easily measured, and that it is reliably stable. In this report, we examine those requirements under typical isotope-ratio-monitoring conditions, show that the value of K is remarkably stable under widely varying ion source conditions, and evaluate several alternative methods that can be used to determine the value of K.

EXPERIMENTAL SECTION

Mass Spectrometry

Hydrogen isotope-ratio-monitoring measurements were made using a Finnigan MAT 252 isotope ratio mass spectrometer (IRMS) which was modified in our laboratory. The system consists of a Varian 3400 gas chromatograph (GC) equipped with a cool on-column injector, coupled to the IRMS via a pyrolysis reactor and conventional open split. Operation of the pyrolysis reactor, which quantitatively converts organic H to H$_2$, was described by Burgoyne and Hayes (1998). Currently, we use a 3.18-mm O.D. by 0.50-mm I.D. alumina tube (99.8% purity, Vesuvius-McDanel, Beaver Falls, PA) to conduct the gas through a ~15-cm zone heated to 1400ºC. No water-removal system is employed in our system. Pyrolysis over graphite reduces background water signals to < 2 pA, better than can be achieved with drying systems based on Nafion membranes (Leckrone and Hayes, 1997).

Approximately 0.2 mL/min of the analyte gas stream is introduced to the IRMS via an open split. Gas flowing to the open split is controlled in conjunction with a vent installed upstream from the pyrolysis reactor so that the solvent peak from GC injections can be diverted from the reactor in a manner analogous to that used for carbon irmGCMS (Merritt *et al.*, 1995). While the pyrolysis reactor is not damaged by introduction of the solvent peak, the resulting accumulation of tar-like pyrolysis products downstream from the reactor adversely affects peak shape in subsequent samples.

The MAT 252 was modified to prevent scattered or low-energy ^{4}He$^+$ ions from reaching the mass-3 collector by placing an electrostatic lens after the mass-3 slit, just before the mass-3 Faraday detector. The lens consists of two plates, 8.00 mm long (along the beam path) and 4.34 mm apart. When the IRMS is operating at 6.6 kV accelerating potential, the lens is held at ~5.3 kV, thus providing a potential energy barrier which repels ions with less than 80% of nominal energy. The voltage on each plate is controlled independently to facilitate steering of the ion beam after the slit, which is necessary to accommodate the limited space available for the detector. Two shields are placed between the lens and the Faraday cup and are held at ground potential and –95 V, respectively. These shields help prevent leakage of secondary electrons from the Faraday cup, a process

that would otherwise be stimulated by the strong electric field of the energy-filtering system. The system described here reduces the ion current reaching the mass-3 detector to < 60 fA with 200 µL/min He flowing into the IRMS (the maximum flow rate the MAT 252 can accept). In the absence of the energy filter, the scattered ion current reaching the mass-3 collector is > 10 pA. This system is similar in its operation and performance to that described by Hilkert *et al.*(1999) for the Finnigan Delta$^+$XL mass spectrometer.

Isotope-ratio-monitoring data were processed using Visual Basic codes which we have developed for use in Excel (Microsoft, Redmond, WA). These use the pointwise correction algorithm described in Chapter 2. Data were collected using digitization intervals of 250 (for *n*-alkane analyses) or 125 ms (for all other experiments). Except where noted, the time constant of the mass-2 amplifier was 200 ms.

Determination of *K*

We evaluated four separate methods for determining the value of *K* for use in isotope-ratio-monitoring systems. These were as follows:

1)   "*Bellows method*." This is the method commonly used with dual-inlet analyses, in which pressure of an H$_2$ test gas in the sample reservoir is adjusted sequentially to yield different signal levels. In the present work, helium was supplied via the GC interface to maintain the ion source pressure at levels typical of isotope-ratio monitoring (~10^{-5} mbar indicated pressure). Ion currents were integrated for five seconds at each signal level, and linear regression of the measured ion current ratio on the mass-2 ion current yielded the value of *K* via equation 3. This method was used both under computer control (using the Isodat software) and manually. In the latter case, data were collected in isotope-ratio-monitoring mode and signals were integrated using Excel. The only significant difference between computer- and manually-controlled measurements was that the version of Isodat software employed here (v7.2-00) does not correct data for background signals prior to calculating the regression, whereas background signals *were* removed during integration in Excel.

2) "*Peak-RMS method.*" The *n*-alkane standard described by Sessions *et al.* (Chapter 2), in which concentrations of the 15 *n*-alkanes vary by five-fold, was first analyzed using the irmGCMS system. Then multiple sets of δD values were calculated using a range of values of *K*, keeping all other parameters constant. The best value of *K* was taken as that which produced the smallest root-mean-square (RMS) error.

3) "*Peak-slope method.*" Using the same data collected for method 2, the value of *K* was chosen as that which produced no correlation between peak height and the error in δD. That is, *K* was varied until a linear regression of δD error on peak height produced a slope of zero. Methods 2 and 3 are effective in determining *K* only because of the very large concentration differences in the sample and because the mixture of standard alkanes was designed with no correlation between δD and the concentrations of the analytes, thus allowing separation of mass-dependent (*i.e.*, ion-current-ratio) effects from peak-height-dependent H_3^+ effects.

4) "*Instantaneous method.*" The electronic time constant of the mass-2 amplifier was adjusted to carefully match that of the mass-3 amplifier at 1.30 s. Broad peaks of varying size were produced by slowly injecting a mixture of CH_4 and He into the GC using a syringe. The resulting hydrogen peaks were integrated at 62 ms intervals, and *K* was calculated by regression of *R* versus i_2 for the individual data points comprising the peak. This method was tested in part to examine whether *K* is truly constant during rapid changes in P_{H_2}. For example, rapid changes in space-charge distribution within the ion source of the IRMS during the introduction of an H_2 peak could lead to varying rates of H_3^+ formation that do not follow equation 2.

Variable Ion Source Conditions

To investigate the magnitude of changes in *K* that typical isotope-ratio-monitoring conditions might produce, we systematically measured *K* with changing ion-source pressure ($\approx P_{He}$), under changing partial pressures of H_2O and CH_4 , and with changing background concentrations of GC column bleed. These conditions were chosen for investigation because *i*) He is abundant during

isotope-ratio-monitoring analyses, *ii*) H$_2$O and CH$_4$ are likely to participate in proton-exchange reactions (Leckrone and Hayes, 1998; McLafferty, 1980), and *iii*) varying column bleed contributions represent the largest change which occurs over the course of a typical GC analysis. Although the partial pressure of He is generally constant throughout isotope-ratio-monitoring experiments, small fluctuations may arise when, for example, solvent peaks are backflushed, external standards are injected, etc. In all examinations of such ion-source effects, values for *K* were calculated using the bellows method (see above).

Partial pressures of He and CH$_4$ were varied by means of pressure regulators and capillary leaks. For the He experiments, relatively high flow rates were controlled by the addition of a needle valve after the capillary leak. The H$_2$ was introduced using a separate leak and did not flow through the needle valve. Pressures of He in the ion source were calculated from gauge readouts using an estimated ion-source conductance of 18 L/s (for ^{4}He), a pumping speed of 50 L/s at the Penning gauge, and a 6.8-fold decrease in sensitivity to He (relative to N$_2$, the calibration gas) by the Penning gauge. On this basis, pressures of He in the ion source are typically 10^{-4} mbar (gauge readings of ~10^{-5} mbar) during isotope-ratio-monitoring analyses. In this experiment, they were varied from 10^{-7} to 10^{-4} mbar. The partial pressure of CH$_4$ was measured in terms of the *m/z*-16 ion-beam current, and varied from 0.1 to 11 nA. For comparison, the background CH$_4$ ion current during actual irm-GCMS analyses is not detectable above the ~0.3 pA background current at *m/z* 16, which is presumably due to ^{16}O$^+$. GC column bleed was varied by changing the temperature of the GC and allowing ~5 minutes for the column bleed to stabilize at each temperature. The amount of column bleed at each temperature was quantified using the *m/z*-2 ion-beam current, which varied from ~0 at a column temperature of 40ºC to 0.6 nA at 325ºC.

Changes in *K* with the partial pressure of H$_2$O in the ion source were studied by addition of a Nafion-membrane humidistat to the system (Leckrone and Hayes, 1997). The arrangement is shown in Figure 3-1. Helium carrier gas, which had been dried by passing through the pyrolysis reactor and which had a partial pressure of water corresponding to an *m/z*-18 ion current of ~1 pA, flowed through a Nafion tube immersed in a variable-temperature cold bath. The outside of the Nafion membrane was purged with He directly from a gas cylinder. The concentration of H$_2$O in this gas
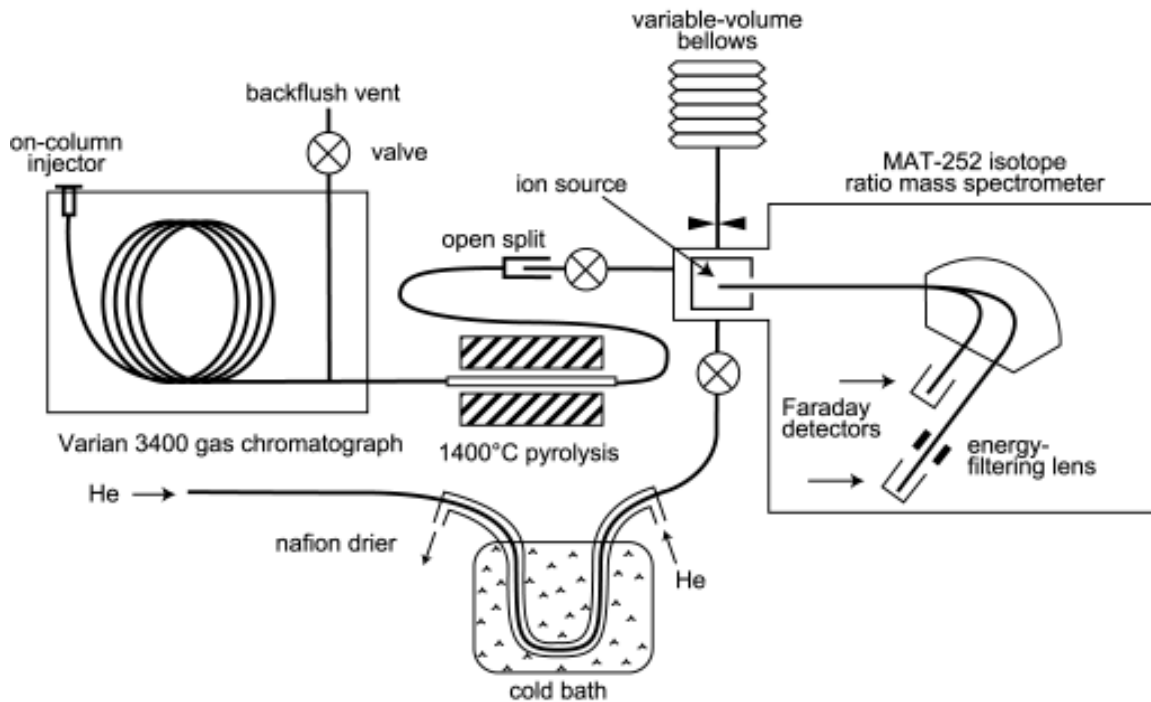
Figure 3-1. Diagram of the hydrogen isotope-ratio-monitoring analytical system. Operation of the various components is described in the text.

was higher than that in the pyrolyzed carrier gas, so the Nafion membrane served to add H_2O to the carrier gas stream. Changing the temperature of the cold bath over the range $-40°$ to $+30°C$ resulted in H_2O ion currents ranging from 10 to 600 pA (Leckrone and Hayes, 1997).

RESULTS AND DISCUSSION

The methods used for measuring the magnitude of K embody three general approaches. The bellows method employs measurements of constant H_2 signals. The peak-RMS and peak-slope methods compare multiple peaks of different sizes, and the instantaneous method uses dynamic measurements of a rapidly changing H_2 signal. Each approach has strengths and weaknesses, and no single approach appears to be the best for all situations.

Static Measurements of K

Two problems affect methods based on measurements of constant H_2 signals. First, substantial mass-2 and -3 background currents are present under isotope-ratio-monitoring conditions. These potentially result both from He (as $^4He^{2+}$ and $^3He^+$ ions, or from $^4He^+$ scattered into the mass-2 collector, which is not protected by an energy-filtering lens) and from hydrogen in the carrier gas. Significant background H_2 signals can be generated, for example, by the pyrolysis of H_2O in the carrier gas. With background currents present, the relationship between R and i_2 will be nonlinear (Figure 3-2) if an appreciable portion of the background is due to He and/or if the isotopic composition of the hydrogenic background differs significantly from that of the sample. For these reasons, measurements using the bellows method under the control of Isodat (which did not correct for background signals) produced values of K that varied systematically with the range of H_2 signals employed, and that were up to 10% smaller than those determined with background correction.
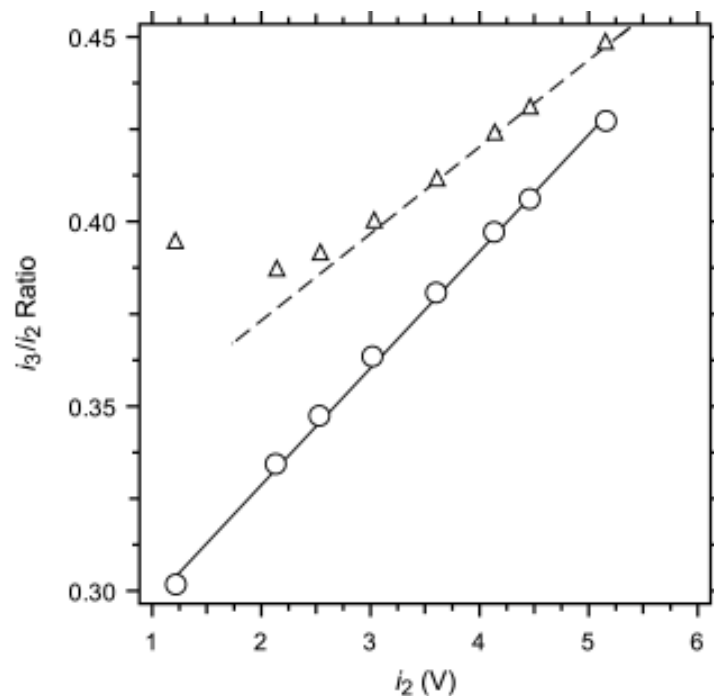
Figure 3-2. Typical "H₃ plot" used to calculate the value of K. Uncorrected data (triangles) are nonlinear because of mixing between the sample gas and background signals. After correcting for background ion currents a linear relationship is obtained (circles). Note that the use of uncorrected data to determine the value of K will result in erroneously low values (dashed line with lower slope).

In our system, background currents due to H are small enough that they can be neglected, and the entire background (due therefore to He) can simply be subtracted to give a linear relationship (Figure 3-2). Note that if the H background were significant, this analysis would become considerably more difficult because the H background — which would contribute to formation of H$_3^+$ — cannot simply be subtracted along with the He background (see Chapter 2). Some value of K would have to be assumed to correct for the H$_2$ background, with the true value of K then being found through successive approximations.

In principle, these difficulties can be overcome by subtracting the portion of the background signal due to He and by minimizing the H portion of the background. In practice, however, distinguishing the contributions of He and H to the background can be challenging. By examining the background signals in a He carrier gas that was passed sequentially through CuO at 800°C (to combust H$_2$ to H$_2$O) and then through liquid nitrogen (to trap H$_2$O), we were able to estimate the relative contribution of H to the background signals in our instrument. This process is tedious, however, and would not be suitable for use on a frequent basis. An alternate possibility, if background signals are not too large, is to measure the value of K at very large values of i_2 where the effects of background signals are minimized.

The second problem facing measurements based on constant ion currents is that these measurements do not fully duplicate the conditions encountered during isotope-ratio-monitoring experiments. Specifically, the rapid changes in P_{H_2} that occur as sample peaks pass through the ion source are not reproduced. Also, trace levels of gases such as H$_2$O, CH$_4$, CO, and N$_2$ may increase throughout the course of an analysis as column bleed and atmospheric leaks increase in the GC. The accuracy and applicability of a static measurement of K to isotope-ratio-monitoring conditions are therefore uncertain.

Peak-Based Measurements of K

The peak-based measurements provide an ideal basis for comparison with the static measurements because they are derived by completely independent means. The large variations in peak height in our alkane test mixture allow use of both the peak-RMS and peak-slope methods to deter-
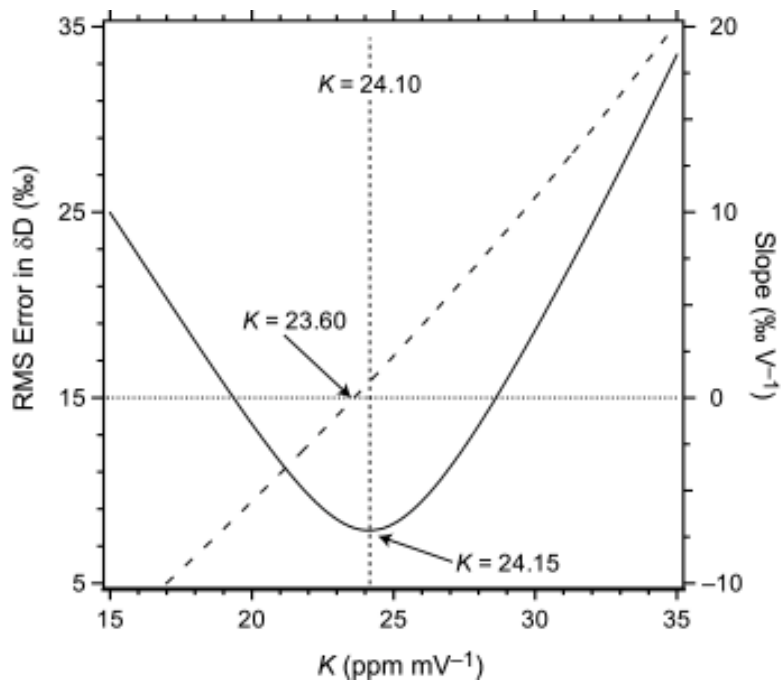
Figure 3-3. Comparison of H₃ factors determined by three methods for a typical *n*-alkane analysis. Vertical dotted line gives the value of *K* obtained by the bellows method. *K* is determined by the peak-RMS method as the minimum in the δD error vs *K* curve (solid line). *K* is determined by the peak-slope method where the slope of the regression of δD error on peak height is zero (dashed line).

mine values of *K*. In the peak-RMS method, the relationship between the RMS error of the *n*-alkane standard and the value of *K* was always a smooth, parabolic curve (Figure 3-3). The peak-slope method produced a nearly linear relationship when the slope of the regression was plotted as a function of *K*.

To determine whether these different methods produce equivalent results, we measured *K* using the bellows, peak-RMS, and peak-slope methods over two periods of time, as follows. Typically, each morning before any samples were run, one or two aliquots of the *n*-alkane standard were analyzed, followed by measurement of *K* using the bellows method, followed by one or two additional injections of the *n*-alkane standard. Observations were made over two separate time periods: ~65 days during January–March, 1999, and ~30 days during January, 2000. In all, values of *K* were accumulated from 27 bellows measurements and 105 alkane measurements.
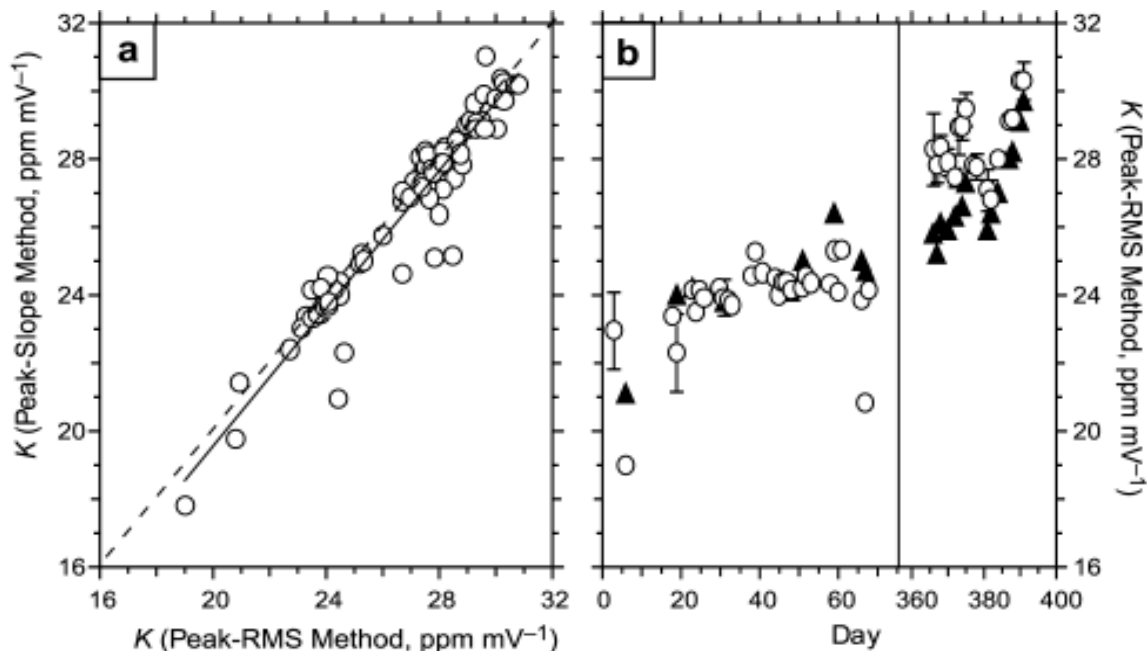
Figure 3-4. (a) Comparison of values of K determined for 105 n-alkane analyses using the peak-RMS and peak-slope methods. Solid line is the least-squares regression which has a slope of 1.01. The light, broken line is $y = x$. (b) Comparison of values of K determined using the peak-RMS (open circles) and bellows (triangles) methods over two separate periods of time. Error bars for the peak-RMS method represent 1σ for days on which three or more measurements were made. Error bars for the bellows method are the size of the symbols. Note the break in scale at 75 days.

Values of K determined by the peak-RMS and peak-slope methods are compared in Figure 3-4a. The two methods give essentially identical results. Regression of the values of K determined by the peak-slope method against those determined by the peak-RMS method (for the same samples) yields $y = 1.01x - 0.7$, with $r^2 = 0.92$. The pooled standard deviation for replicate measurements of K on a single day was 0.64 ppm mV^{-1} for the peak-RMS method and 0.77 ppm mV^{-1} for the peak-slope method (53 degrees of freedom). These standard deviations do not differ significantly. Furthermore, both methods of calculating K can be used on the same data with little extra effort, and comparison of the results can provide insight into the performance of the analytical system.

Values of K determined by the peak-RMS method are compared to those determined by the bellows method in Figure 3-4b. The standard deviation of replicate measurements of K using the bellows method was, in general, better than 0.1 ppm mV^{-1}. During the period January – March, 1999, the two methods gave values for K that were usually indistinguishable. However, during January, 2000, the bellows method produced values that were consistently 1 to 2 ppm lower than

those obtained using the peak-RMS method. In this case, systematic errors of up to 9‰ in the δD values of the *n*-alkanes were observed when the bellows method was used to determine the value of *K*. As expected, systematic errors were dependent on peak-height mismatch between sample and standard peaks (Chapter 2), and were largest in pairs with the greatest mismatch. These systematic errors were absent when the peak-RMS method was used to determine *K*. The peak-RMS method, or other similar approaches, therefore appear to be the more appropriate way to measure the value of *K* for isotope-ratio-monitoring measurements.

A more difficult question is *why* do the two methods produce different values? The only significant change in the analytical system between the two time periods over which we compared the two methods is that the pyrolysis furnace was rebuilt using a longer heated zone, slightly different geometry (during the former period the alumina tube rested beside the heating element, and during the latter it was inside and concentric with the cylindrical heating element), and the addition of a small amount (~5 mg) of Pt wire catalyst. Because the positioning of the thermocouple relative to the reactor tube changed slightly, it is possible that the temperature of the hot zone also changed slightly in the rebuilt furnace. Separate experiments with much larger amounts of Pt (up to 500 mg) in the reactor have demonstrated a memory effect due to dissolution of H$_2$ in the Pt metal, but the magnitudes of those effects were dependent on the D/H ratio of peaks, rather than on peak size. A few measurements during the period January–March, 1999 (when there was no Pt catalyst present) also produced significantly different values of *K* using the bellows and peak-RMS methods (Figure 3-4b).

One possible explanation for the discrepancy between peak- and bellows-based values of *K* is that subtle changes in the pyrolysis reactor resulted in different levels of trace gases reaching the mass spectrometer, which in turn altered the magnitude of *K* during chromatographic runs. However, we have not been able to observe any measurable changes in the value of *K* over the course of a chromatographic run, or over very large fluctuations in the partial pressures of CH$_4$ and H$_2$O (see below). A second possible explanation is that some isotope-exchange process (or perhaps merely contamination) existed in the pyrolysis reactor, on metal fittings, in the GC, etc. If such an effect were dependent on peak size, it could account for the observed results. This potential explanation

highlights the subtle question of what the "correct" value for K means. Any process that alters the D/H ratio of the n-alkane standard would likely also alter samples to a similar extent, so that even though the peak-RMS method produced an incorrect value for K, its use would lead to correct δD values. Conversely, the bellows method might produce "correct" values for K but erroneous δD values.

Dynamic Measurement of K

The instantaneous method of measuring K is an attempt to combine the realistic conditions of the peak-based measurements with decreased time requirements. In theory, the use of changes in P_{H_2} across a single peak to measure the value of K is very attractive. The value of K could be determined separately for each peak in a chromatogram simply through appropriate data processing, without requiring any additional standards, chromatograms, or instrument time.

In practice, however, there are several difficulties with this approach. First, the time constants of the two signal pathways must be very closely matched for the instantaneous ion current ratio to reflect the D/H ratio of gas in the ion source. Even in the absence of H_3^+, mismatched time constants would result in large changes in the measured ion current ratios across a peak. The time constants can be closely matched by varying the feedback capacitance of the electrometers, but the time constants of both signal pathways are then determined by the slower mass-3 electrometer. When the time constants of the signal pathways are slower than the highest frequency contained in the peak being examined, the interaction between the nonlinearly-changing ratio and the nonlinear damping of the time constants produces a pattern like that shown in Figure 3-5.

Computer-numerical simulations of this phenomenon (using the approach described in Chapter 2) produce similar patterns, and suggest that at smaller amplifier time constants (RC < 0.3 s for a Gaussian peak with $\sigma = 2$ s) this effect is minimized, with all the data falling on a straight line with slope = K. We were unable to obtain time constants faster than 1.3 s for our mass-3 electrometer due to its large feedback resistance ($\sim 10^{12} \, \Omega$) in combination with unavoidable capacitance in the collector system, so this prediction remains untested. A possible alternative is to produce peaks which rise and fall very slowly, but the technical difficulty of producing those peaks negates the primary motivation for the instantaneous method, *i.e.,* analytical convenience.
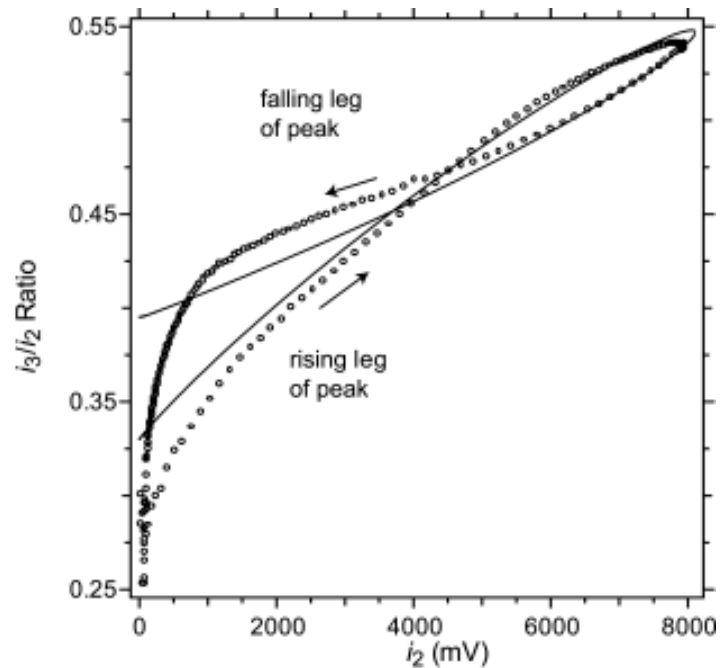
Figure 3-5. Instantaneous i_3/i_2 ratios collected across a single peak. Each point represents an individual pair of background-corrected i_2 and i_3 measurements. Solid line is the calculated ratio for a Gaussian peak with width (4σ) of 10 s, amplifier time constant of 1.3 s, $K = 24$ ppm mV^{-1}, and true i_3/i_2 ratio of 0.33.

The second significant problem facing the instantaneous method is that the peak being examined must be isotopically homogeneous. Sample peaks from a GC will clearly be affected by isotope chromatography, with partial separation of the H$_2$ and HD peaks. Even if deactivated capillaries are used to deliver reference peaks from an external peak generator, differences in the diffusivities of H$_2$ and HD could lead to greater broadening of the H$_2$ peak. Furthermore, differences in the pumping speeds of H$_2$ and HD in the ion source ($^2S/^3S \approx \sqrt{3/2}$) will tend to broaden the HD peak. If the latter two problems prove to be insignificant, the offset caused by isotope chromatography might be corrected by data processing, as is done prior to peak integration for irmGCMS data (Ricci *et al.*, 1994). Further examination of this approach seems well-justified, as the potential benefits in speed and accuracy are compelling.

Uncertainties in the Measurement of K

As described in Chapter 2, relatively small errors in the value of K can result in significant errors in δD if the sample and standard peaks are not closely matched in both size and δD value. For example, a 1% error in the value of K would result in a δD error of >1‰ if the sample and standard are mismatched in height by only 2 V (see Figure 2-2). It is extremely important, therefore, to accurately assess uncertainties associated with measurements of the value of K and to propogate those uncertainties to resulting δD values.

Repeated measurements of K using the bellows method consistently give standard deviations which are <0.1 ppm mV^{-1} but, as described above, the use of this method can lead to significant errors in measured δD values. On the other hand, if the source of the systematic errors can be identified and eliminated, it is likely to remain the most precise method of measuring K.

For the 21 days on which K was measured via the peak-RMS method using at least three injections of the n-alkane standard, the daily standard deviation of those measurements ranged from 0.1 to 1.2 ppm and averaged 0.5 ppm mV^{-1}. Given the typical magnitude for K of ~25 ppm mV^{-1} during this period, 0.5 ppm mV^{-1} amounts to a 2% uncertainty in the value of K. Measuring the value of K with an uncertainty of <1% would therefore require four or more measurements of the n-alkane standard (*i.e,.* standard error of the mean $= \sigma / \sqrt{n} = 0.25$). This is a very time-consuming requirement, and provides great motivation for 1) determining the cause of systematic errors in the bellows method, or 2) improving electrometer time constants so that the instantaneous method might be used.

Factors Controlling K

We considered it possible that the systematic differences between values of K determined by the bellows versus peak-RMS methods were due to subtle changes in the chemical composition of gases entering the IRMS ion source. To investigate this possibility, we examined changes in K with varying ion source pressure and varying partial pressures of CH_4 and H_2O. Large increases in P_{He} result in small decreases in the value of K, ~5% for each 10-fold increase in P_{He} (Figure 3-6a). These changes are small enough that normal fluctuations in He flow rate, if buffered by an open
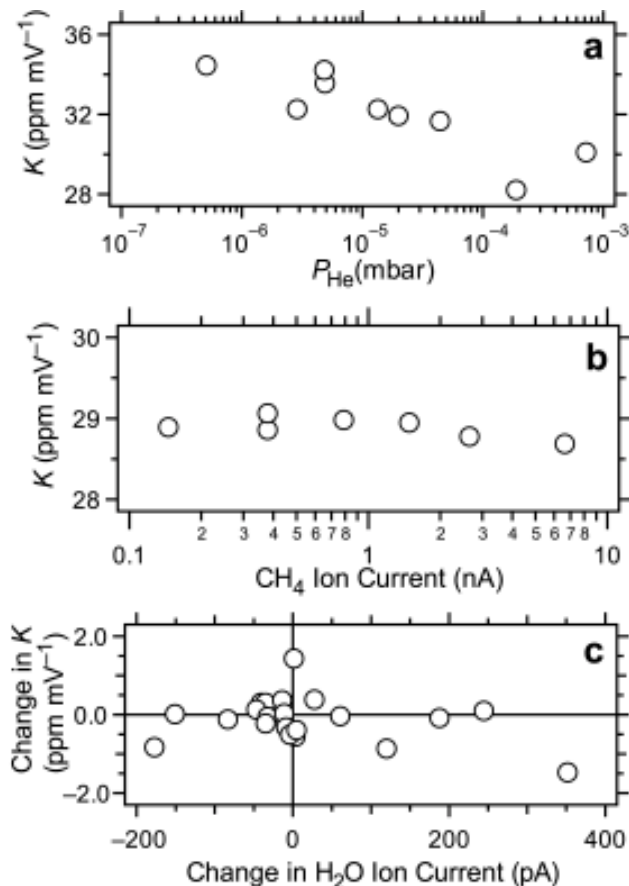
Figure 3-6. Changes in the value of K associated with He (panel a), CH$_4$ (panel b), and H$_2$O (panel c) background signals. In panel c, relative changes in the value of K are plotted against changes in H$_2$O$^+$ ion current over the same interval in order to remove the effects of instrumental drift.

split, should have virtually no influence on the value of K. The observed reduction in the rate at which H$_3^+$ is formed may be due to a decrease in the number of H$_2^+$/H$_2$ collisions due to dilution of the H$_2$ by He.

No significant change in K was observed with changing pressures of CH$_4$ (Figure 3-6b). This was unexpected, since CH$_4$ can mediate proton transfer and is widely used as a reagent gas for chemical-ionization mass spectrometry (McLafferty, 1980). On the other hand, the presence of CH$_4$ produces a substantial increase in mass-2 and mass-3 background signals. For example, a 0.25 nA CH$_4^+$ ion beam is accompanied by 10 pA and 9 fA mass-2 and mass-3 ion beams, respectively. This "background" mass 3/2 ratio is approximately 30-fold higher than the D/H ratio of samples

with a natural abundance of D. Thus, while the value of K might not change, the presence of large amounts of CH$_4$ during an analysis (*i.e.*, due to incomplete pyrolysis of sample components) could lead to substantial measurement errors (innacurately high values of δD).

Analysis of results obtained at varying partial pressures of H$_2$O is somewhat more complex, because up to twelve hours were required for the H$_2$O pressure in the ion source to equilibrate with the carrier gas stream after the Nafion humidistat was adjusted. Changes in K due to H$_2$O partial pressure are therefore superimposed on changes due to instrument drift. To compensate for this, we compared relative changes in the value of K between consecutive measurements (generally 1 to 2 hours apart) to changes in H$_2$O ion currents over the same period (Figure 3-6c). There is no correlation between changes in K and P_{H_2O}, indicating that water does not significantly affect the value of K at concentrations typical of isotope-ratio-monitoring analyses.

When background column bleed contributions cycled between 0 and 600 fA (*m/z*-2 ion current) as column temperature varied between 40 and 325ºC, there were no measurable changes in the value of K (mean value, 20.0 ± 0.1 ppm mV^{-1}, $n = 7$). Background mass spectra contain no ion currents that are clearly attributable to Si-containing compounds produced by the pyrolysis of GC column bleed.

In summary, the presence of CH$_4$, H$_2$O, and GC column bleed in the analyte stream does not appear to enhance (or retard) the formation of H$_3^+$. Such effects could presumably occur through the transfer of protons to H$_2$, but this process is apparently insignificant at the partial pressures of CH$_4$ and H$_2$O we examined. Other species such as CO and N$_2$ may also be present in the ion source, but are even less likely to participate in proton-transfer reactions. It appears unlikely, therefore, that differences in the chemical composition of the analyte stream could account for the differences observed between the bellows and peak-RMS methods of measuring K. On the other hand, these results offer some assurance that the value of K remains stable throughout GC analyses, despite small changes in carrier gas composition. This supports our observation (Chapter 2) that a single value of K can be used to accurately correct a wide range of peak sizes across a chromatogram even when large temperature programs are employed.

CONCLUSIONS

Approaches to accurate correction of H_3^+ contributions during hydrogen-isotope-ratio-monitoring mass spectrometry have been outlined (Chapter 2), but these calculations depend crucially on the accuracy and stability of the H_3 factor (K). A critical evaluation of several methods for determining the value of K indicates that static measurements of a range of H_2 signals (the approach conventionally used in dual-inlet analyses) is highly precise ($\sigma < 0.1$ ppm mV^{-1}) but can lead to systematic errors in δD when applied to isotope-ratio-monitoring data. The source of these systematic errors is presently unknown. Peak-based measurements, on the other hand, produce values for K that are significantly less precise ($\sigma \approx 0.6$ ppm mV^{-1}) but that consistently produce more accurate δD values. Accordingly, the peak-based determinations of K are the most appropriate for use in isotope-ratio monitoring. Determination of K from instantaneous D/H ratios measured across a single peak is theoretically possible and highly appealing, but would require that amplifier time constants be faster than can currently be achieved and that peaks be isotopically homogeneous. The uncertainty associated with measuring the value of K can limit the precision of the analytical method unless sample and standard peaks are carefully matched in both size and δD value.

The rate of H_3^+ production (*i.e.,* the magnitude of K) in our MAT-252 IRMS decreases by ~5 % for each order-of-magnitude increase in the partial pressure of He in the ion source. Given the very small variations in P_{He} typically encountered in systems in which the flow of He is regulated by an open split, the resultant changes in K would be undetectable. The presence of CH_4 and H_2O, possible contaminants of the gas stream during non-ideal operation of the pyrolysis reactor, has no significant effect on K. Likewise, the introduction of GC column bleed has no measurable effect on K. We conclude that isotope-ratio-monitoring analyses do not require additional measures beyond those used in conventional dual-inlet analyses to stabilize the H_3 factor.

REFERENCES

Burgoyne, T.W. and Hayes, J.M. (1998) Quantitative production of H_2 by pyrolysis of gas chromatographic effluents. *Analytical Chemistry* **70**, 5136–5141.

Friedman, I. (1953) Deuterium content of natural water and other substances. *Geochimica et Cosmochimica Acta* **4**, 89–103.

Hilkert, A.W., Douthitt, C.B., Schluter, H.J. and Brand, W.A. (1999) Isotope ratio monitoring GCMS of D/H by high temperature conversion isotope ratio mass spectrometry. *Rapid Communications in Mass Spectrometry* **13**, 1226–1230.

Kelly, S.D., Parker, I.G., Sharman, M. and Dennis, M.J. (1998) On-line quantitative determination of $^2H/^1H$ isotope ratios in organic and water samples using an elemental analyser coupled to an isotope ratio mass spectrometer. *Journal of Mass Spectrometry* **33**, 735–738.

Leckrone, K.J. and Hayes, J.M. (1998) Water-induced errors in continuous-flow carbon isotope ratio mass spectrometry. *Analytical Chemistry* **70**, 2737–2744.

Leckrone, K.J. and Hayes, J.M. (1997) Efficiency and temperature dependance of water removal by membrane dryers. *Analytical Chemistry* **69**, 911–918.

McLafferty, F.W. (1980) *Interpretation of Mass Spectra*. University Science Books, Mill Valley, CA.

Merritt, D.A., Freeman, K.H., Ricci, M.P., Studley, S.A. and Hayes, J.M. (1995) Performance and optimization of a combustion interface for isotope ratio monitoring gas chromatography/mass spectrometry. *Analytical Chemistry* **67**, 2461–2473.

Ricci, M.P., Merritt, D.A., Freeman, K.H. and Hayes, J.M. (1994) Acquisition and processing of data for isotope-ratio-monitoring mass spectrometry. *Organic Geochemistry* **21**, 561–571.

Scrimgeour, C.M., Begley, I.S. and Thomason, M.L. (1999) Measurement of deuterium incorporation into fatty acids by gas chromatography/isotope ratio mass spectrometry. *Rapid Communications in Mass Spectrometry* **13**, 271–274.

Sessions, A.L., Burgoyne, T.W., Schimmelmann, A. and Hayes, J.M. (1999) Fractionation of hydrogen isotopes in lipid biosynthesis. *Organic Geochemistry* **30**, 1193–1200.

Tobias, H.J., Goodman, K.J., Blacken, C.E. and Brenna, J.T. (1995) High-precision D/H measurement from hydrogen gas and water by continuous-flow isotope ratio mass spectrometry. *Analytical Chemistry* **67**, 2486–2492.

Tobias, H.J. and Brenna, J.T. (1997) On-line pyrolysis as a limitless reduction source for high-precision isotopic analysis of organic-derived hydrogen. *Analytical Chemistry* **69**, 3148–3152.

Chapter 4 — Hydrogen Isotope Exchange in Organic Molecules

ABSTRACT

To quantify rates of hydrogen isotopic exchange in organic molecules under typical sedimentary conditions, we incubated icosane, pristane, and cholestene with D_2O on a variety of sedimentary substrates over the temperature range $7° – 111°C$ for up to four months. Significant amounts of D were incorporated by all analytes in most of the experiments. A range of processes are responsible for this incorporation, including exchange, structural rearrangements, and hydrogen addition. The δD value of icosane incubated on organic-free montmorillonite increased by up to 87‰ over ~3 months. The changes represent the effects of exchange processes only, and correspond to exchange half-times of 10 ka at $60°C$ and 100 ka at $7°C$. These half-times are much faster than is predicted by extrapolation of literature data for other compounds at higher temperatures.

Icosane incubated on lacustrine sediment with 20% TOC yielded exchange half-times identical to those in organic-free silica, whereas icosane incubated on a marine clay with 1.5% TOC yielded half-times about one order of magnitude slower than those in montmorillonite. These results are inconclusive regarding the effects of complex, natural organic matter on hydrogen exchange, but do suggest that acidic, organic-rich environments are less favorable than marine ones for preserving organic D/H ratios. Cholest-5-ene was reactive on all substrates, producing cholest-4-ene and 20R- and 20S-diacholestene as major products. D incorporation in these products was extensive, but <50% of hydrogen atoms mobilized by each rearrangement were replaced by D. When 10% XAD resin was added to sediments, both the extent of rearrangement and the incorporation of D decreased dramatically.

57

INTRODUCTION

Hydrogen isotope ratios (^{2}H/^{1}H, or D/H) of individual organic compounds offer great potential for the reconstruction of D/H ratios of paleoenvironmental water, and hence climatic variables (Sauer *et al*., 2001; Xie *et al*., 2000). Whereas similar attempts using bulk isotopic analyses have had to contend both with complex mixtures of organic material and with the rapid exchange of O- and N-bound hydrogen (*e.g.,* Krishnamurthy *et al*., 1995), the analysis of individual compounds like *n*-alkanes and sterols potentially avoids both problems. With this opportunity comes new questions about the isotopic fidelity of C-bound hydrogen over geologic timescales. Current evidence suggests that even hydrogen in alkanes might exchange on timescales less than the age of the Earth at temperatures as low as 4ºC (Alexander *et al.*, 1982), but uncertainty about rates still encompasses many orders of magnitude. The interpretation of hydrogen isotopic records obtained from geologic materials must be based in part on quantitative information about rates of isotopic exchange, but that information is nearly nonexistent. The goal of this chapter is therefore to provide such quantitative data through experimental measurements and compilation of literature data.

Several factors complicate the issue of hydrogen exchange. Uncatalyzed exchange between alkyl H and H_2O proceeds with a reaction half-time $>10^9$ years at temperatures below 100ºC (Koepp, 1978). On the other hand, mineral surfaces are frequently potent catalysts (Huizinga *et al*., 1987) and vary widely in their form, surface area, and activity. The catalytic properties of sedimentary minerals are further modified by the abundance of water, cation chemistry, pH, and interactions with organic matter (Alexander *et al*., 1982; Larcher *et al*., 1986). The significance of hydrogen exchange for any particular component of sedimentary organic matter therefore depends not only on the molecular structure, but also on the geochemical setting in which it exists.

The multiplicity of relevant processes presents an experimental dilemma. Exchange experiments using pure compounds on organic-free sediments will not accurately reproduce the catalytic effects of natural sediments. On the other hand, if natural sediments are used for exchange experiments then the compounds of interest can react with, or be released from the complex organic matter present. Effects of exchange, isomerization, fractionation, and isotopic mixing can be mutu-

ally confounding. Yet isotopic changes through time can be understood and predicted only by separating these effects.

The experimental approach adopted here is a compromise. It represents an attempt to bracket natural rates of hydrogen exchange through the use of both organic-free and natural sediments as experimental substrates. Compound-specific hydrogen isotopic analyses were used to measure the abundance of D in compounds incubated with D_2O. The low natural abundance of D (~0.015%) and high precision of isotope-ratio analyses make this an exquisitely sensitive measurement of D incorporation, with the potential to measure reaction half-times approaching 10^5 years over a period of just months. Processes occurring over geologic timescales are therefore experimentally accessible with no extrapolation from higher temperatures or more active catalysts.

We examined hydrogen exchange in four different types of compounds: *n*-alkanes, pristane, cholestene, and androstanol. The first two were chosen as unreactive analytes to examine exchange with a minimum of interfering processes. Androstanol and cholestene were chosen as representative of the steroid class of compounds, which are likely targets for paleoclimate studies because of their potential source-specificity (Sauer *et al.*, 2001). Because these molecules are more reactive, however, the number of processes leading to hydrogen isotopic variations is greater.

To examine the role of sediment chemistry in exchange processes, hydrogen exchange was measured for five different substrates. Substrates were chosen to bracket the range of sediment mineralogy and organic content which might be encountered in a typical geologic sequence. Based on previous reports, montmorillonite was expected to catalyze rapid hydrogen exchange, while silica was expected to provide no catalysis and to serve as a control. On one hand, increasing contents of organic matter were expected to impede access to catalytic sites and thus decrease rates of exchange. On the other hand, the organic matter could also break down to yield compounds that incorporated D as a result of cleavage reactions. The following substrates were tested: *i*) organic-free montmorillonite; *ii*) organic-free microcrystalline silica; *iii*) a marine clay with low organic content; and *iv*) a silica-rich lacustrine sediment with very high organic content. A fifth substrate consisted of organic-free montmorillonite mixed with 10% XAD resin, to test whether the hydro-

gen-exchange characteristics of complex, organic-rich sediments can be duplicated using a mixture of well-defined components.

EXPERIMENTAL

Analytes

Test compounds were obtained from Sigma Chemicals (St. Louis, MO) and were tested for purity by GCMS prior to use. The test compounds were: *n*-icosane, pristane, 5α-androst-3β-ol, and cholest-5-ene. Standard solutions containing 2.5 mg/mL of each analyte were prepared in dichloromethane (DCM) and analytes were added to each sample in this form.

Substrates

Montmorillonite. The reference material SAz-1, also known as "Cheto" montmorillonite, was obtained from the Clay Minerals Society (University of Missouri). SAz-1 is a homogenized Ca-montmorillonite from the Bidahochi Formation, Apache County, AZ. It has a specific surface area of 97 m^2/g and a cation exchange capacity of 1.2 meq/g (Olphena and Fripiat, 1979). Montmorillonite was cleaned prior to use by three-fold ultrasonication in 9:1 DCM/methanol (MeOH) with centrifugation between extractions, followed by air-drying at 120ºC for >2 days. This temperature was chosen to reduce adsorbed moisture and to sterilize the substrate. The total carbon content of the cleaned montmorillonite, measured by elemental analyzer (EA) with quantification by IR absorption, was $0.011 \pm 0.004\%$ on a dry-weight basis. The aqueous pH of this substrate, measured by adding 20 mL of distilled H$_2$O to 10 g of dry SAz-1, was 8.20.

A portion of cleaned SAz-1 was blended with XAD-2 resin (10% XAD by weight) to make the "clay + XAD" substrate. XAD-2 resin, a 2% cross-linked styrene-divinylbenzene copolymer, was obtained from Aldrich (Milwaukee, WI) as 200-400 mesh beads. The XAD resin was cleaned by repeated ultrasonication in MeOH, methyl *tert*-butyl ether (MTBE), and hexane prior to mixing with SAz-1. Blank extractions and GCMS analyses for both SAz-1 and clay + XAD substrates produced no detectable organic compounds.

Silica. Powdered silica, obtained from Sigma Chemicals, is described by the supplier as "A naturally occurring microcrystalline silica which has been finely ground." The reported grain size is $0.5 - 10$ µm, with 80% between $1 - 5$ µm. The silica was cleaned and dried as for montmorillonite. The total carbon content of cleaned silica was $< 0.004\%$ on a dry-weight basis. Because the silica was found to catalyze substantial hydrogen exchange (see below), trace and major element chemistry of the silica was analyzed at the Notre Dame ICP-MS Research Facility. Results of those analyses are attached as Appendix A, and show that transition metals are present in the range 0.1 to 10 µg/g, and platinum-group elements are present at 0.2 to 4 ng/g. Aqueous pH of cleaned silica was 5.73.

Marine Clay. Sediment from the Gulf of Mexico (831 m depth, 27.740°N, 90.771°W) was collected by Chris Reddy and Miguel Goñi in April, 1998 (box coring, *R.V. Pelican)* and subsequently stored at –40ºC at WHOI. Approximately 1 kg of sediment, representing the top 5 cm of a box core, was used for these experiments. The sediment was air-dried at 40ºC over a period of weeks, then crushed to a fine powder in an agate mortar. The sediment was air-dried at 120ºC for two days immediately prior to use. The sample is tan and odorless, and contains a large proportion of clay based on its settling time in water. The organic carbon content is $1.6 \pm 0.7\%$, with a $\delta^{13}C$ value of –10.4‰ measured by elemental-analyzer IRMS. Although the marine clay was treated with HCl to remove carbonate prior to analysis of organic carbon, this $\delta^{13}C$ value indicates a significant amount of inorganic carbon remained. Carbonate content, determined by weight-loss after acidification to pH 1 with HCl, was 2%. Aqueous pH of the marine clay, measured after drying then rehydrating with distilled H_2O, was 7.57.

Lacustrine Sediment. Sediment was collected from the middle of Great Pond, a small, freshwater lake in Truro, Massachusetts (see details in Sauer *et al.*, 2001), in October 1998 using a stainless steel Ekman dredge in ~9 m water depth. About 5 kg of wet sediment was collected from the top 10 cm, and was frozen at –40ºC within five hours of collection. The collected sediment was 92.6% water by weight, and was air-dried then crushed as for Gulf of Mexico sediment. Because of the nature and abundance of organic matter in this sediment, it was not heated above 40ºC at any time prior to incubation. Organic matter comprises $19.8 \pm 1.9\%$ of sediments (dry weight) and has

a $\delta^{13}C$ value of –28.8‰. It is derived primarily from phytoplankton in the lake, although some higher-plant components are also present (Sauer *et al.*, 2001). The inorganic fraction of Great Pond sediment is primarily diatom frustules. No carbonate was detectable in the sediment by addition of HCl, although 4.4% weight loss was measured after acidification. The difference probably represents organic matter lost during the 110ºC drying used to drive off HCl. Aqueous pH of dried then rehydrated sediment was 4.45.

Sample Preparation and Measurement

Experiments were conducted in two rounds. The first, begun in February, 1999, used only marine clay and lacustrine sediment substrates, and only organic compounds naturally occurring in the substrates were examined. The second was undertaken in July, 2000, to address several shortcomings of the earlier experiments, in particular the possibility that the generation of hydrocarbons from natural organic matter was responsible for the changes observed in δD values. In these later experiments, selected test compounds were added to the precleaned silica, montmorillonite, and clay + XAD substrates, and to the marine clay. Procedures used to prepare and extract samples were also modified during this second round. The two rounds of experiments are described separately below, although they are similar in their general approach.

Round 1 experiments. Aliquots of dry substrate plus 99.5% D_2O (Cambridge Isotope Labs, Andover, MA) were loaded into precombusted, 16-mm ID, medium-wall Pyrex tubes, each ~10 cm long and sealed at one end. Lacustrine sediment samples contained 3 g sediment plus 3 mL D_2O. Marine clay samples contained 6 g sediment plus 7 mL D_2O, due to the lower organic content of that sediment. Sample tubes were covered with Parafilm to prevent exchange with water vapor, frozen in liquid N_2, evacuated to 50 mTorr, and flame-sealed.

Sealed tubes were placed into homemade incubation chambers consisting of 2-L Pyrex beakers surrounded by insulation and filled with SiC powder as a heat-exchange medium. A constant temperature (± 2ºC) was maintained in the chamber via a resistance-heating cartridge, K-type thermocouple, and electronic temperature controller (all from Omega Engineering, Stamford, CT). Three parallel experiments at 29º, 60º, and 111ºC were conducted. Three thermocouples arranged radially

in each incubation chamber were used to monitor temperature gradients. Measured horizontal gradients were ≤ 5ºC in all experiments, and vertical gradients were ≤ 2ºC.

Selected tubes were removed from incubation after 60 and 120 days. Tubes were cracked open and wet sediment was washed into 60-mL centrifuge tubes with organic-free H_2O. Samples were washed three times to remove D_2O prior to drying. Specifically, sediment was stirred into H_2O containing 0.1 M sodium pyrophosphate (an antiflocculant) for 10 minutes, then centrifuged at 2500 rpm ($1050 \times g$) for 10 minutes. Samples were then washed onto precombusted GF/F glass fiber filters and air-dried at 40ºC for several days. Dry samples were crushed lightly with mortar and pestle, then extracted in an Accelerated Solvent Extractor (ASE). Extraction conditions were: 9:1 DCM/MeOH, 1 soak for 10 minutes at 40ºC, 3 soaks for 5 minutes each at 100ºC, with a total of 20 mL solvent collected per sample.

Extracts were dried under N_2 at 40ºC, then redissolved in 2 mL hexane to remove moderately polar compounds from the extract. Extracts were fractionated using solid-phase extraction with aminopropyl stationary phase as described by Sessions *et al*. (1999). The four fractions (F1: hydrocarbons; F2: ketones and esters; F3: alcohols; F4: fatty acids) were analyzed by capillary GC with a HP 5973 mass-selective detector (MSD). *n*-Alkanes were further purified by urea adduction using isooctane as the solvent. δD values of selected *n*-alkanes were measured on the irmGCMS system described in Sessions *et al*. (2001a) with H_2 gas pulses as the isotopic reference peaks.

Round 2 experiments. Samples were prepared in precombusted, 12-mm OD, thin-wall Pyrex tubes. Until ~1 hour before loading, all substrates, D_2O, empty tubes, pipettes and spatulas were stored at 120ºC to maintain sterility. D_2O was contained in a screw-cap Teflon pressure vessel. Each sample contained 1 g dry substrate, 80 mL of spike solution (200 mg each of icosane, pristane, androstanol, and cholest-5-ene), and 2 mL of D_2O. To reduce plugging by clay-rich substrates, alternating portions of clay and D_2O were added, with spike compounds at the end. Concentrations of spike compounds added to the marine clay samples were ~1000-fold higher than analogous compounds (*n*-C_{29}, cholesterol) indigenous to the sediment. Tubes were evacuated and sealed as before. Samples were incubated at 30º and 60ºC in heated chambers, and at 7ºC in a laboratory refrigerator.

Sample tubes were removed from incubation after 35 and 88 days and immediately frozen. Each tube was cracked open and the sample was freeze-dried for approximately 20 hours in its tube. Blanks for the freeze drier using precleaned montmorillonite showed no evidence of pump oil contamination. Dried samples were transferred to Pyrex centrifuge tubes, then extracted by 3-fold ultrasonication in 9:1 MTBE/MeOH at room temperature. This procedure was designed specifically to minimize exposure to metal surfaces and high temperatures, which might induce hydrogen exchange. Extracts were treated with acetic anhydride/pyridine at 65ºC to make the acetate derivative of androstanol, then analyzed by GC (DB-5ms analytical column, 60m × 0.32mm ID × 0.25µm stationary-phase thickness) with the column effluent split between FID and MSD. Icosane was further purified by two-fold, and in some cases three-fold, urea adduction followed by silica-gel column chromatography.

D/H ratios were measured on a Finnigan-MAT Delta+XL isotope-ratio mass spectrometer coupled to an Agilent Technologies GC (HP-Ultra1 analytical column, 25m × 0.32mm ID × 0.56µm stationary phase thickness) via the Finnigan thermal conversion interface. Coinjected compounds served as isotopic-reference peaks. Due to problems with incorporation of D by minor sample components (see discussion), androstanol and cholestene were not analyzed for δD. The C_{16}–C_{30} *n*-alkane standard described by Sessions *et al.* (2001a) was analyzed several times every day as an external standard. To reduce H_3^+-related errors, peak heights for analytes and coinjected standards were matched to within ~30%. The value of the H_3-factor used to correct data was determined by measuring a series of *n*-alkanes of varying peak height (Sessions *et al*., 2001b).

Calculations

The isotope exchange reaction $R^1H + D_2O \rightarrow RD + {}^1HDO$ follows pseudo-first-order reaction kinetics and has a rate constant described by

$$kt = \ln(F_i - F_e)/(F_t - F_e) \tag{1}$$

where *k* is the rate constant, *F* is the fractional abundance of D [$\equiv D/(D + {}^1H)$] in a compound, and subscripts designate fractional abundances *i*nitially, at *e*quilibrium, and at time *t* (Wedeking and

Hayes, 1983). For the purpose of comparing exchange rates to geologic timescales, it is more convenient to discuss the exchange half-time, where $t_{1/2} = \ln(2)/k$.

In practice, values of F_i, F_t, and F_e were used in equation 1 to calculate $t_{1/2}$ for each experiment. F_i and F_t were calculated from measured δD values. Water added to these experiments was 99.5% D_2O, but the D content of water following exchange could not be easily measured. A value of 0.995 was therefore assumed for F_e. It is likely that the actual D abundance was lower due to exchange with mineral surfaces, but a 10% error in F_e (a very large error) produces an error in $t_{1/2}$ of 10%, much smaller than analytical uncertainties. Overestimation of F_e leads to an underestimation of exchange rate, and hence overestimation of $t_{1/2}$.

RESULTS AND DISCUSSION

Several unexpected results were observed. First and foremost, significant increases in the D content of all analytes were observed in most of the experiments. These increases ranged from a few parts per million in icosane and pristane up to a few atom% in cholestene. Second, cholestene proved to be reactive on all of the substrates tested, producing a variety of sterene and diasterene products that incorporated significant amounts of D. The experiments were designed to study hydrogen exchange, but these observations show that a variety of processes can influence the D/H ratio of organic compounds. We therefore begin our discussion with a description and summary of relevant processes, with the goal of defining specific terminology to support a more precise discussion of the experimental results.

Data from exchange experiments are then discussed in three sections, grouped according to the processes observed. In the first section, exchange of alkyl hydrogen is described for incubations of icosane and pristane on organic-free silica and montmorillonite substrates. These experiments provide the least ambiguous view of exchange processes. Next, evidence for the inhibition of exchange by organic matter is discussed from the incubations of icosane and pristane on the marine clay and lacustrine sediment substrates. Finally, reactions of cholestene on all substrates are used

to examine the range of processes which affect D/H ratios in steroid compounds. For reasons described below, no D/H analyses were obtained for androstanol.

Taxonomy of Exchange Processes

Diverse processes can lead to changes in the hydrogen-isotopic compositions of organic compounds. Here, to facilitate discussion of our observations, we establish formal definitions for processes relevant to the current experiments. The examples provided illustrate individual processes, though two or more processes are often combined in complex reactions.

Processes that change the D/H ratio of an organic compound include: hydrogen exchange, structural rearrangement, hydrogen addition or loss, fractionation, and isotopic mixing. The term *exchange* is used here to encompass all chemical reactions in which the structure of the molecule (*i.e.*, the pattern of bonding, including the number and position of double bonds and hetero atoms) does not change, but which provide the opportunity for hydrogen in the reactant to be replaced. Conceptually, pure exchange involves the abstraction and replacement of a single hydrogen with no effect on the rest of the molecule (Figure 4-1). When exchange occurs at a chiral carbon atom, such as C-3 in cholesterol, stereochemical inversion of the chiral center may result. Although the two stereoisomers can then be distinguished by certain analytical techniques, the process is otherwise identical to the inversion of an achiral, tetrahedral center. Exchange accompanying stereochemical inversion is therefore included in our use of the term *exchange*. The less-specific term *incorporation* is reserved for situations in which the D content of a molecule increased following incubation in D_2O, but the process responsible for that increase is unspecified or unknown.

Reactions in which the structure of a molecule changes but the net inventory of hydrogen in the molecule remains constant (constitutional isomerization) also provide the opportunity for replacement of hydrogen in the product. Examples of such *rearrangment* include double-bond isomerizations, methyl shifts, and rearrangements of sterene backbones to form diasterenes. Reactions which increase the net inventory of hydrogen in the molecule are termed *addition*. Addition processes include the hydrogenation of double bonds (Figure 4-1), as well as cleavage reactions such as decarboxylation of organic acids. A reaction in which hydrogen is lost, such as the dehydration of
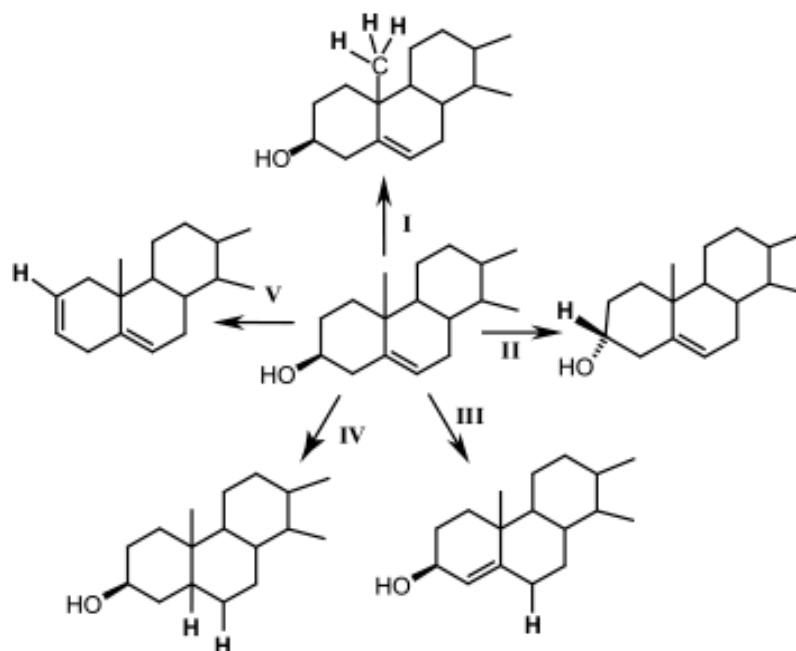
Figure 4-1. Examples of processes that can change the δD value of a sterol molecule. (I) exchange, (II) exchange accompanying stereochemical inversion, (III) rearrangment, (IV) hydrogen addition, (V) fractionation during hydrogen loss. Hydrogen atoms affected by each reaction are shown in bold.

alcohols, is frequently accompanied by a kinetic isotope effect which fractionates hydrogen isotopes in the product. *Fractionation* can also occur during physical processes such as adsorption, dissolution, and evaporation, and can produce very large shifts in δD.

Isotopic mixing is the final process to be considered. For example, *n*-alkanes released from kerogen can have a hydrogen isotopic composition differing from free *n*-alkanes in a sediment, and the D/H ratio of the pooled alkanes will change through time as a result of mixing between these two sources. Isotopic mixing has been discussed extensively with regard to carbon isotopes (*e.g.*, Pearson and Eglinton, 2000), and the principles involved are directly relevant to hydrogen isotopes.

Hydrogen Exchange in Pristane and Icosane

Analyte recovery. The recovery of pristane and icosane from each sample is listed in Table 4-1. Analyte recovery data for experiments using clay + XAD and marine clay substrates are included

Table 4-1. Recovery of pristane and icosane from incubation experiments

Sample[a]	Substrate	Temp. (°C)	Time (d)	Pristane	*n*-Icosane
M7-35		7	35	44%	60%
M7-88		7	88	65	81
M30-35	montmorillonite	30	35	53	65
M30-88		30	88	40	57
M60-35		60	35	74	78
M60-88		60	88	77	100
X7-35		7	35	69	84
X7-88[b]		7	88	<1	17
X30-35	montmorillonite +	30	35	59	63
X30-88	10% XAD resin	30	88	68	85
X60-35		60	35	66	75
X60-88[b]		60	88	<1	58
S7-35		7	35	13	47
S7-88		7	88	29	81
S30-35[b]	silica	30	35	<1	17
S30-88		30	88	23	68
S60-35		60	35	23	75
S60-88		60	88	24	97
MC7-35		7	35	82	50
MC7-88		7	88	27	64
MC30-35	marine clay	30	35	73	52
MC30-88[b]	(Gulf of Mexico)	30	88	<1	135
MC60-35		60	35	71	52
MC60-88		60	88	30	88

[a] Sample numbers follow the code Stt-dd: S = substrate type, tt = incubation temperature (°C), dd = incubation time (days).
[b] Sample was accidentally dried at 45°C.

for comparison. Recovery of pristane and icosane was frequently between 60 and 80%, with the deficiency attributed to extraction and handling losses. In several experiments (X7-88, X60-88, S30-35, and MC30-88; sample ID's appear in Table 4-1) up to 83% of icosane and >99% of pristane was lost. Extracts from these samples were mistakenly blown to dryness under N_2 at 45°C, and the losses are attributed to evaporation. Partial evaporation of nonpolar hydrocarbons should result in depletion of D in the residual analyte (Hopfner, 1969). Any enrichment of D measured in the incubated samples must then represent a minimum value due to exchange processes, and such values are reported below with due notation. Anomalously high recovery of icosane in MC30-88 appears to be the result of some systematic error in quantitation, since androstanol and cholestene were also recovered from that sample at high levels (145% and 72%, respectively). Pristane was recovered from montmorillonite in much higher proportions than from silica, and with great vari-

ability from marine clay samples. These differences in pristane recovery are not due to evaporative losses and remain unexplained.

Hydrogen isotopic analyses. Significant problems arose during irmGCMS analyses. Many products, present at low abundance but containing large amounts of D, appeared in the mass-3 ion-current. Isotope-ratio chromatograms for the non-incubated test compounds and for the products of experiment MC60-35 are compared in Figures 4-2 and 4-3. MC60-35 is a representative sample with D enrichment near the middle of the range observed for all experiments. The number and abundance of D-enriched peaks generally increased in hotter, longer experiments, and increased with substrate in the order $MC < S < M < X$. The typical range of integrated mass-3/mass-2 signal ratios for analytes containing D at natural abundance is $0.30 - 0.45$, whereas, in the incubated samples, this ratio frequently reached 10 or higher, equivalent to a δD value of ~30,000‰. D-enriched analytes in clay + XAD experiments appeared as an unresolved hump, and are attributed to breakdown of the XAD copolymer.

Memory effects caused further problems. In addition to D-enriched trace components, rearrangement of cholest-5-ene produced significant amounts of diasterenes (discussed below) containing up to 25 mole% D. To prevent contamination of the pyrolysis reactor and mass spectrometer, these products were backflushed (Figure 4-3). While no memory effects have been observed during analysis of samples with natural abundances of D (Sessions *et al.*, 2001a), this was not true for these samples. After 10 to 15 injections of sample extracts, the mass-3/mass-2 ion-current ratio of GC-column bleed increased from ~0.2 to over 7.2. At the same time, mass-3/mass-2 ratios observed for standard *n*-alkanes (*i.e.,* in a mixture of external standards *not* coinjected with incubated samples) shifted upward by ~150‰. Removing a 2-m section from the head of the analytical column and replacing all septa, fittings, and transfer capillaries did not substantially reduce the D/H ratio of column bleed. These dramatic changes appear to represent exchange of hydrogen between injected analytes and the column stationary phase (5%-phenyl-methylpolysiloxane). Since the amount of D injected was too small to homogeneously label the stationary phase to the level observed in column bleed, exchange must occur preferentially in limited portions of the stationary phase that are both more reactive and thermally labile.
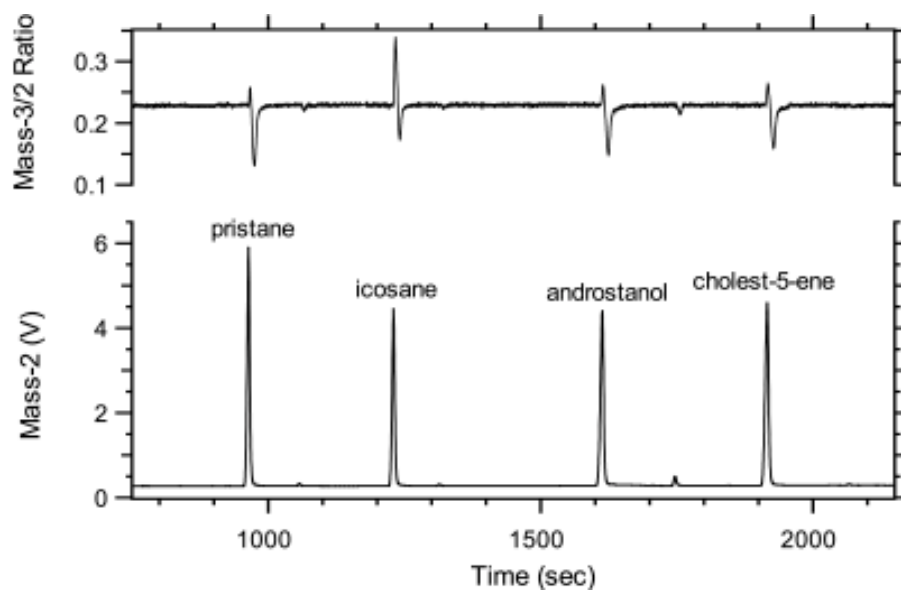
Figure 4-2. Isotope-ratio chromatogram of the initial solution of test compounds added to each incubation experiment. The δD values of these analytes range from −55 to −360‰.
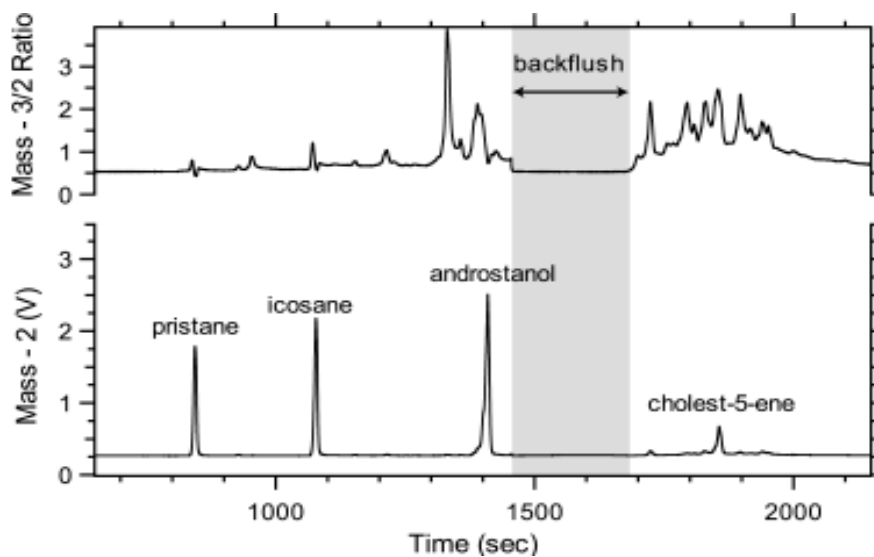
Figure 4-3. Isotope-ratio chromatogram of the total extract from exchange experiment MC60-35. Backflush prevented D-enriched diasterenes from reaching the mass spectrometer. Note scale change of the mass-3/2 ratio from Figure 4-2.

The problems described above prevented accurate hydrogen-isotopic analysis of all analytes in clay + XAD samples, and of androstanol and cholestene in all samples. Isotopic measurements of pristane were possible in some samples, but with greatly reduced precision and accuracy. Problems were largely avoided for icosane through purification by urea adduction, with precision and accuracy for icosane δD values nearly as good as for non-incubated compounds. The following discussion therefore focuses primarily on icosane results.

Hydrogen exchange in icosane. Measured changes in the δD value of icosane are reported in Table 4-2. The precision and accuracy of these measurements depended strongly on the presence of D-enriched components in each sample. The following approach was used to estimate uncertainty due to random error. Icosane in the initial spike mixture was analyzed a total of 13 times over the 3-month period in which D/H data was collected, more than any other analyte. The δD value of icosane was –54.6‰ and the observed standard deviation of the population of results was 5.6‰. While precision from replicate analyses on a given day was typically much better, we take this long-term value to represent the minimum attainable accuracy for icosane. For each measurement of δD, the uncertainty (σ) was then assigned as the *largest* of *i)* 5.6‰ (*i.e.*, the standard deviation

Table 4-2. Measured δD values and changes in δD for icosane and coinjected standards[a]

Sample	Icosane δD	Icosane σ_p[b]	Icosane n	n-C$_{16}$ ΔD[c]	n-C$_{19}$ ΔD[c]	n-C$_{23}$ ΔD[c]	σ_{ext}[d]	ΔD[c] icosane	$2\sigma_\Delta$[e]
initial[f]	−54.6	5.6	13	−81.0[f]	−128.3[f]	−48.6[f]	5.8		
M7-35	−49.3	2.9	4	0.8	0.9	−1.3	5.8	5.3	6.4
M7-88	−42.8	0.6	3	−13.3	−10.4	−3.7	5.1	11.8	7.2
M30-35	−8.6	5.7	6	1.0	3.3	15.6	6.0	46.0	NA[g]
M30-88	−31.8	3.9	3	−4.9	−4.4	2.7	6.0	22.8	7.2
M60-35	−34.2	12.5	4	−12.6	−4.7	−2.2	6.8	20.4	12.9
M60-88	−0.9	22.7	4	−42.3	−14.4	6.6	6.8	53.7	23.0
S7-35	−52.7	4.3	3	−6.8	4.2	4.2	5.2	1.9	7.2
S7-88	−51.5	0.7	4	4.0	6.8	−0.7	4.8	3.1	6.4
S30-35[h]	−42.8	2.5	3	6.0	3.9	1.2	5.1	11.8	7.2
S30-88	−58.5	6.1	4	−7.9	−5.2	2.3	6.1	−3.9	6.8
S60-35	−2.5	2.6	4	2.6	4.2	−1.8	6.5	52.1	6.4
S60-88	+33.4	9.0	4	−8.7	−4.7	−4.6	6.5	88.0	9.5

[a] C$_{16}$, C$_{19}$, C$_{22}$, and C$_{23}$ n-alkanes were coinjected with each sample. n-C$_{22}$ (δD = −62‰) was used as the isotopic reference peak.
[b] Standard deviation of population of replicate measurements.
[c] $\Delta D = \delta D$ (sample) − δD (initial), (‰).
[d] RMS accuracy of external standards analyzed on the same days as sample (‰).
[e] Estimated uncertainty for change in δD calculated as described in text (‰).
[f] δD values for icosane and coinjected n-alkanes prior to incubation (‰).
[g] Not available; see explanation in text.
[h] Sample was accidentally dried at 45°C.

obtained for icosane in the spike solution), *ii)* the standard deviation of replicate measurements of the analyte (σ_p in Table 4-2), or *iii)* the RMS accuracy of *n*-alkane external standards analyzed on the same day (σ_{ext} in Table 4-2). In practice, values for *ii* and *iii* were usually similar and were greater than 5.6‰ in only one-quarter of the icosane analyses. The variance of a mean δD value was calculated as σ^2/n, where *n* was typically 3 or 4 replicate analyses, and the variance of the change in δD (σ_Δ^2) was then the sum of the variances of the two δD measurements.

The possibility of systematic errors was examined for each sample by measuring coinjected C_{16}, C_{19}, and C_{23} *n*-alkanes. These compounds were never in contact with D_2O, and only briefly in contact with each sample, so any changes in their δD values must represent systematic analytical errors. The changes in δD of these coinjected compounds were typically smaller than $2\sigma_\Delta$ (Table 4-2). Exceptions include samples S30-88, S60-88, M7-88, M60-35, and M60-88 in which some coinjected alkanes show negative changes (*i.e.,* δD was more negative when coinjected with the sample than when analyzed alone) slightly greater than the stated uncertainty. Depletion of D due to evaporation or handling of the coinjected *n*-alkanes cannot be the cause of these changes since similar shifts do not appear in subsequent analyses utilizing the same standard solution. More likely, the changes are due to interference from D-enriched background components. In these samples the change in δD (and calculated H-exchange rate) of icosane may therefore be slightly underestimated. Sample M30-35 appears unusual, in that either C_{22} and C_{23} are too enriched in D by 15‰ or more, or C_{16} and C_{19} are too depleted in D by 15‰ or more, depending on which compound is chosen as the isotopic reference peak. Because of the uncertainty associated with this sample, data from M30-35 are not considered in subsequent calculations.

Several processes could produce the observed increases in δD of icosane. The coelution of more D-enriched compounds with icosane is possible but unlikely, because only linear hydrocarbons would survive both solid-phase extraction and urea adduction. We know of no other linear hydrocarbons that are both plausible products of icosane degradation and which coelute with icosane, including icosene and methyl-nonadecane. Fractionation of hydrogen isotopes in icosane could be caused by incomplete recovery from the samples, but should lead to changes in δD that are correlated with analyte recovery, a situation which is not observed. Production of new icosane mol-

ecules — with concomittant incorporation of D — is unlikely for two reasons. First, there is no probable source for the generation of new icosane in these samples. Second, any mechanism for the production of icosane would probably also create other homologous *n*-alkanes, which are not observed. In the absence of evidence for other processes affecting icosane, we interpret the measured changes in δD of icosane as representing hydrogen exchange.

Calculated exchange half-times for icosane are summarized in Table 4-3. In several samples, no significant change in δD was measured. The detection limits for these samples (minimum $t_{1/2}$ values) were calculated from $2\sigma_\Delta$ values reported in Table 4-2. The reaction rate for a first-order kinetic reaction is described by the Arrhenius relationship

$$\ln k = \ln A - \left(\frac{E_a}{RT}\right)$$

(2)

where k is the rate constant, A is the pre-exponential factor or frequency factor, E_a is the activation energy, R is the gas constant, and T is the absolute temperature. For a first-order reaction, plots of $\ln k$ versus inverse temperature should be linear, with a slope equal to $-E_a/R$ and an intercept equal to $\ln A$. Values of $\ln k$ are plotted in Figure 4-4. Samples for which no change in δD was detected, as well as sample M30-35, are plotted in gray in Figure 4-4.

The data in Figure 4-4 give the following Arrhenius parameters for exchange on silica: $E_a = 41 \pm 4$ kJ mol^{-1}, $A = 164 \pm 5$ yr^{-1}. These values are calculated by treating the maximal value for k obtained in experiment S7-88 as the actual exchange rate. For exchange on montmorillonite, these

Table 4-3. Calculated hydrogen exchange half-lives for icosane.

Sample	$t_{1/2}$ (ka)	2σ range (ka)
M7-35	> 66.6	
M7-88	90.9	56.4 – 233
M30-35	9.27	8.26 – 10.6
M30-88	47.0	35.7 – 68.7
M60-35	20.9	12.8 – 56.9
M60-88	20.0	14.0 – 34.9
S7-35	> 59.2	
S7-88	> 168	
S30-35[a]	36.1	22.4 – 92.7
S30-88	> 158	
S60-35	8.19	7.29 – 9.33
S60-88	12.2	11.0 – 13.7

[a] Sample was accidentally dried at 45°C.
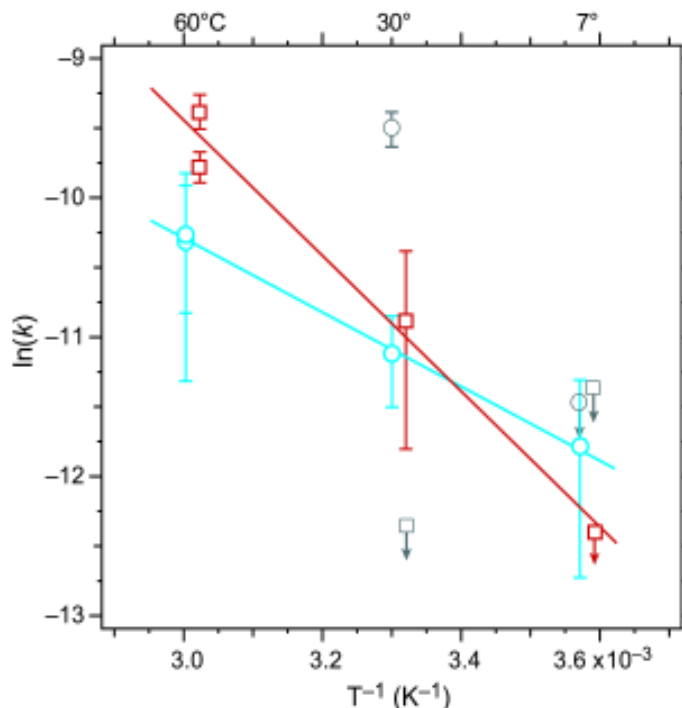
Figure 4-4. Arrhenius plot of exchange rates for icosane on silica (red squares) and montmorillonite (blue circles). Error bars are ±2σ range. Data points with arrows represent maximum values of *k* based on no measured change in δD. Gray data points were not used to calculate regression lines. Data for silica are offset slightly to the right for clarity.

parameters are: $E_a = 22 \pm 0.7$ kJ mol^{-1}, and $A = 0.1 \pm 1.3$ yr^{-1}. The stated uncertainties are the 95% confidence limits derived from the scatter of data points.

Several conclusions can be drawn. The slope of each relationship is significantly different from zero, indicating that the measured changes in δD are kinetically controlled. The values of *A*, the frequency factor, are quite small and are consistent with the reaction involving a molecule adsorbed to a catalytic surface (Larcher, 1985). The Arrhenius parameters are also different for each substrate, though it is not clear that this difference is significant.

Hydrogen exchange in pristane. The precision and accuracy of δD analyses of pristane were significantly poorer than those for icosane (Table 4-4). Although large changes in δD were measured for many experiments, large systematic errors were also observed in the coinjected standards, particularly phytane. In many cases these errors were larger than the changes measured for pristane. As shown in Figure 4-5, much of this reduction in accuracy is probably due to coelution of

D-enriched background components. However, the reduced accuracy of analyses of the external *n*-alkane standard (σ_{ext} in Table 4-4) also attests to the occurrence of isotopic memory effects in the irmGCMS system. The results in Table 4-4 do suggest that hydrogen exchange in pristane is faster than in icosane (compare values of ΔD for icosane and pristane in Tables 4-2 and 4-4). Values of $t_{1/2}$ calculated from changes in δD are roughly one order of magnitude faster for pristane than are corresponding values for icosane. However, the problems created by D-enriched background components in these experiments (for which adduction techniques are not applicable) are such that the results of pristane analyses are not interpreted further.

Comparison with previous studies. The experiments described here are capable of detecting exchange processes with half times as long as 168 ka over experiments lasting 3 months. This is a significant improvement over previous methods used to study hydrogen exchange, which measured the loss of tritium by scintillation counting and for which detection limits are on the order of a few years (Alexander *et al*., 1982; Alexander *et al*., 1981). On the other hand, extrapolation of exchange rates measured for different molecules and at higher temperatures (below) suggests that values of $t_{1/2}$ calculated from the present results are anomalously fast.

Several types of data are available for comparison with the icosane exchange rates. Mackenzie and McKenzie (1983) have compiled rate constants for stereochemical inversion at C-20 in C_{29}

Table 4-4. Measured δD values and changes in δD for pristane and coinjected standards[a]

| | pristane | | | C_{10} FAME | phytane | | ΔD[c] | |
Sample	δD	σ_p[b]	*n*	ΔD[c]	ΔD[c]	σ_{ext}[d]	pristane	$2\sigma_\Delta$[e]
raw[f]	−360.4	1.2	4	−218.7[f]	−317.5[f]	3.2		
M7-35	−233	30	5	25	158	20.2	127	27
M7-88	−10	55	4	NA	242	14.3	351	55
M30-35	−250	33	4	−24	87	20.6	111	33
M30-88	+624	326	3	NA	472	20.6	984	376
S7-35	−285	13	4	5.3	96	6.9	75	13
S7-88	−294	10	3	−13	17	5.3	66	12
S30-88	−242	26	3	25	129	5.3	118	31
S60-35	+132	15	3	−37	116	10.6	492	18

[a] C_{10} and C_{12} fatty acid methyl esters and phytane were coinjected with each sample. C_{12} FAME ($\delta D = -250$‰) was used as the isotopic reference peak.
[b] Standard deviation of population of replicate measurements.
[c] $\Delta D = \delta D$ (sample) − δD (initial), (‰).
[d] RMS accuracy of external standards analyzed on the same days as sample (‰).
[e] Estimated uncertainty for change in δD calculated as described in text (‰).
[f] δD values for pristane and coinjected compounds prior to incubation (‰).
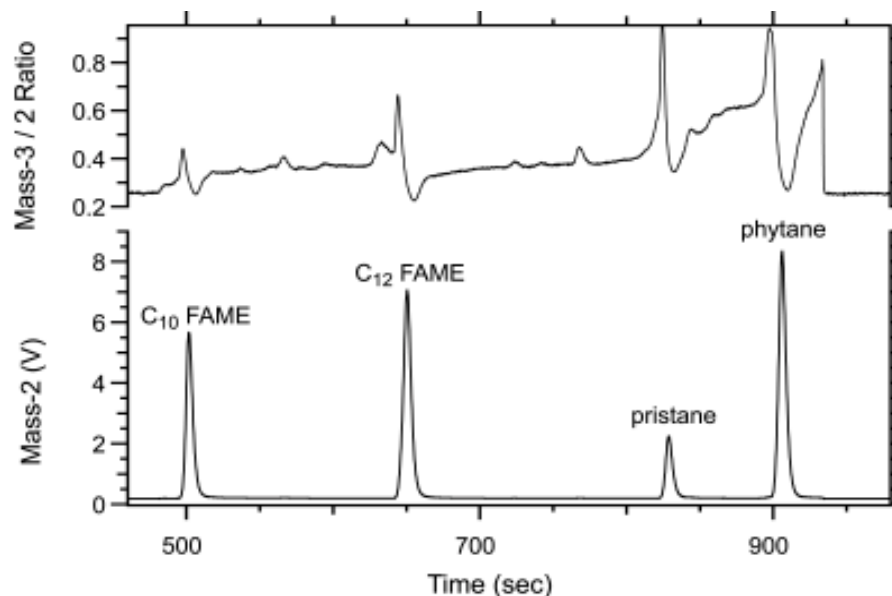
Figure 4-5. Isotope-ratio chromatogram for a typical analysis of pristane. C_{10} and C_{12} FAME and phytane are coinjected standards. Note that the peaks are represented by minima in the ratio trace. The rising baseline in the ratio trace is due to elution of components that are heavily labeled with D.

steranes and at C-22 in C_{31} hopanes from sediments in the North Sea Basin (Figure 4-6; six representative points are shown from the > 40 reported for North Sea samples). Mackenzie and McKenzie (1983) also calculated rates of stereochemical inversion for hopanes produced during laboratory maturation of shale at 203 and 253ºC. Abbott *et al*. (1985) studied the stereochemical inversion of chiral centers in pristane on clay over the temperature range 224–261ºC, with sulfur added as an initiator of free-radical reactions. Inversion in pristane was ~2 orders of magnitude faster than in hopanes incubated under similar conditions (Mackenzie and McKenzie, 1983), perhaps due to catalysis by elemental sulfur.

Assuming that hydrogen exchange always accompanies stereochemical inversion (Larcher, 1985), and then only at the chiral center, the inversion rates plotted in Figure 4-6 correspond to the stereochemical exchange of a single tertiary hydrogen. Alexander *et al*. (1984) showed that exchange at tertiary centers in pristane was roughly four-fold slower than for the rest of the molecule. In their proposed mechanism, the relative acidity of the tertiary hydrogen promotes exchange by stabilizing the formation of a carbocation intermediate. But while the tertiary hydrogen is readily abstracted by a clay surface, it is also returned intact, allowing exchange at adjacent carbon atoms
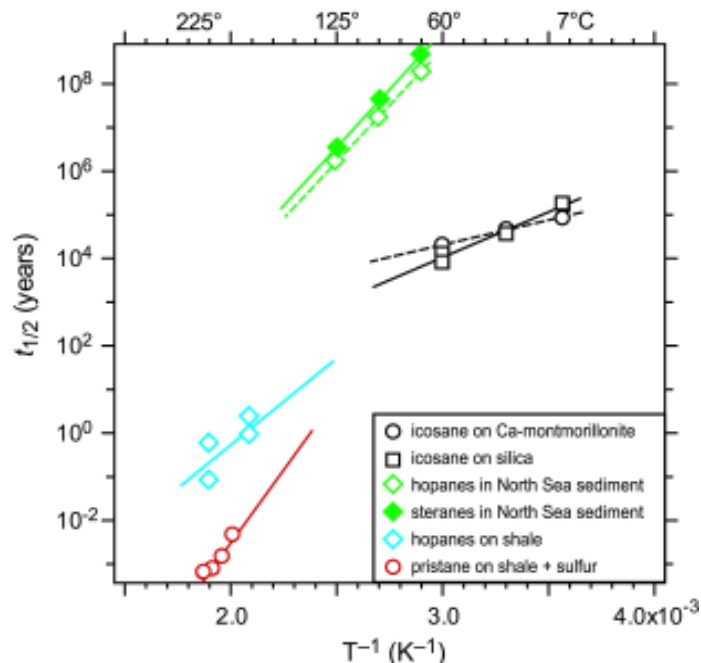
Figure 4-6. Comparison of exchange rates for icosane (this study) with stereochemical inversion rates for polyisoprenoids. Green diamonds: inversion of hopanes (open symbols) and steranes (filled symbols) in North Sea sediments (Mackenzie and McKenzie, 1983). Blue diamonds: inversion of hopanes during laboratory maturation of shale (Mackenzie and McKenzie, 1983). Red circles: inversion of pristane incubated on shale + elemental sulfur (Abbott *et al.*, 1985).
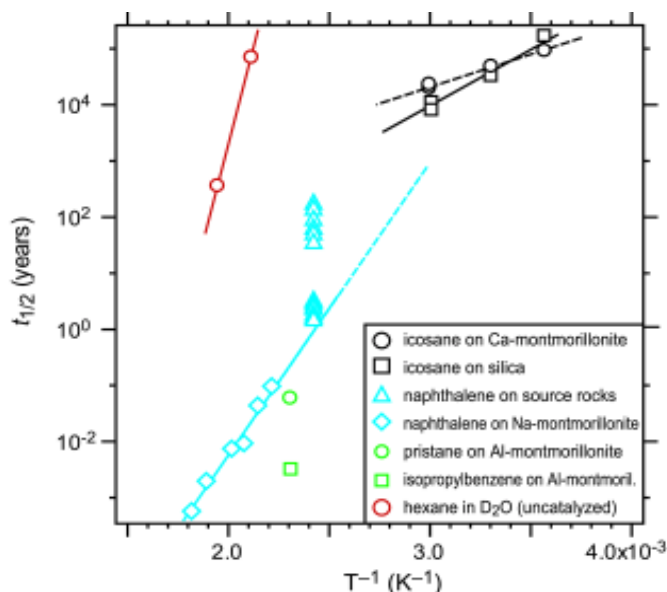
Figure 4-7. Comparison of exchange rates for icosane (this study) with other laboratory exchange experiments. Red circles: hexane in D_2O (Koepp, 1978). Blue triangles: naphthalene incubated on crushed, dry source rocks (Alexander *et al.*, 1981). Blue diamonds: naphthalene on dry Na-montmorillonite (Alexander *et al.*, 1982). Green circle: pristane on dry Al-montmorillonite (Alexander *et al.*, 1984). Green square: alkyl H in isopropylbenzene on dry Al-montmorillonite (Alexander *et al.*, 1984).

(methyl as well as methylene) but not at the tertiary center. Larcher (1985) documents experiments in which no detectable exchange or inversion occurred in steranes under conditions identical to those leading to significant exchange in pristane. This difference was interpreted as due to steric hindrance of the sterane chiral centers interacting with the clay surface. Given this limited information, it is impossible to quantitatively relate rates of stereochemical inversion in triterpenoids to rates of pure exchange in icosane. Although the stereochemical inversion of steranes at C-20 may be slower than hydrogen exchange in icosane, the two processes are mechanistically similar. The ~5 orders of magnitude that separate values of $t_{1/2}$ for these two processes in Figure 4-6 then seem improbably large.

Koepp (1978) equilibrated *n*-hexane and cyclohexane with D_2O at 200º and 240ºC in glass vessels with no catalyst, measuring exchange by bulk hydrogen-isotope-ratio techniques. The calculated exchange rates (Figure 4-7) were at least three orders of magnitude slower than rates of hopane stereochemical inversion on shale (Mackenzie and McKenzie, 1983; compare Figures 4-6 and 4-7), perhaps in part because of the lack of catalytic mineral surfaces in Koepp's experiments.

Alexander and coworkers (Alexander *et al*., 1981, 1982, 1984; Larcher, 1985) obtained hydrogen exchange rates from a series of laboratory incubations by measuring the loss of tritium from analytes. Alexander *et al*. (1981) measured exchange rates in 2-methoxynaphthalene incubated at 138°C on dry, crushed petroleum source rocks containing between 1% and 20% extractable organic matter. In Figure 4-7, exchange rates in 2-methoxynaphthalene have been converted to equivalent rates in naphthalene using the ratio of exchange rates of 4.8×10^3 (2-methoxynaphthalene/naphthalene) measured by Alexander *et al*. (1981) at 100ºC. Alexander *et al*. (1982) measured exchange rates for napththalene incubated on clean, dry Na-montmorillonite over the temperature range 177–275ºC. Exchange on montmorillonite was several orders of magnitude faster than on source rocks, but there is no correlation between organic content and $t_{1/2}$ for the source-rock experiments. The implication is that mineralogy, but not organic content, affects the rate of exchange. The activation energy for exchange of naphthalene H on Na-montmorillonite was 103 ± 5 kJ/mol, roughly two-fold higher than that measured for icosane.

Further experiments by Alexander *et al.* (1982, 1984) and Larcher (1985) have elucidated several factors which affect the rate of hydrogen exchange. First, there is a strong correlation between exchange rate and mineral surface acidity. Surface acidity in montmorillonite increases with the identity of interlayer cations in the order $Na < Ca < Al < H$, and increases in the absence of water. Second, the presence of an adjacent tertiary center greatly increases the rate of exchange at primary or secondary hydrogen positions, although, for reasons described above, exchange of the 3° hydrogen is slower than that of the 1° or 2°. Third, exchange of methyl hydrogen in isopropylbenzene at 160ºC ($t_{1/2}$ = 1.15 days) is slower than that of aromatic hydrogen in naphthalene at 120ºC ($t_{1/2}$ = 0.2 days). This strongly supports the expectation that exchange in aromatic compounds proceeds much more rapidly than in alkyl compounds.

The experiments of Alexander *et al.* are difficult to compare with ours because the tritium-loss method necessitates the use of high temperatures and activated substrates and analytes. Nevertheless, an attempt is made by comparison to naphthalene on dry Na-montmorillonite as follows. The use of water-saturated substrates in our experiments should slow rates by ~100-fold compared to dry substrates, while Ca interlayer cations in SAz-1 montmorillonite should speed rates by 10-fold relative to Na (Alexander *et al.*, 1982). Exchange in pristane is at least 100-fold slower than naphthalene (Alexander *et al.*, 1984). Based on a comparison of exchange in the alkyl tails of ethylbenzene and isopropylbenzene (Larcher, 1985), exchange in *n*-alkanes is at least another 10-fold slower than in pristane. Thus, rates of exchange in naphthalene, if extrapolated to 60ºC (Figure 4-7), are estimated to be four orders of magnitude faster than in icosane. Because they are in fact similar to the rates observed here, a major discrepancy is apparent.

Mechanisms for rapid exchange. Several other lines of evidence also suggest that the rates of hydrogen exchange measured here for icosane are anomalously fast. Specifically, the observed rates are similar on different substrates. Surface hydroxyl groups in hydrated silica have $pK_a = 6.5 - 6.8$ (Schindler and Stumm, 1987), whereas hydrated kaolinite (a 1:1 layer clay with no permanent charge, and hence much-reduced acidity compared to montmorillonite) has surface pKa values of $3.0 - 4.0$ (Larcher, 1995). Alexander *et al*. (1982) have shown that catalysis of hydrogen exchange varies strongly with the surface pH of clay minerals, so a large difference in activity is expected.

Also, E_a for hydrogen exchange in icosane is much lower than that reported for naphthalene, whereas it is expected to be higher based on the stability of reaction intermediates.

Several potential explanations for accelerated exchange in icosane can be immediately dismissed. Sample preparation or workup procedures could alter D/H ratios through exchange or fractionation, but the magnitude of these changes should be independent of incubation temperature. For both silica and montmorillonite substrates, ΔD varies significantly with incubation time and temperature. Microbial activity might plausibly produce hydrogen exchange with some temperature dependence. All materials were heat-sterilized to reduce this possibility, though the samples were not prepared under strictly sterile conditions. Some bacteria have been adapted to live in 100% D_2O over time (Kushner *et al.*, 1999), but rapid transfer of organisms from H_2O to D_2O should severely inhibit their growth, if not kill them outright. In short, microbial activity cannot be excluded but is unlikely.

A more plausible cause for the observed rapid exchange can be suggested. Consider a compound with two groups of exchangeable H atoms. Group X includes ¼ of the molecule's hydrogen and exchanges with a half-time of 10^3 years. Group Y, the remainder, has an exchange half-time of 10^5 years. Groups X and Y could represent, for example, hydrogen at different carbon positions in the same molecule, or hydrogen in molecules adsorbed to different surfaces. The overall progress of hydrogen exchange is shown in Figure 4-8. In an exchange experiment lasting much less than one half-time, nearly all exchange would be due to group-X hydrogen. The change in δD for the compound would be exactly one-quarter that of the X hydrogen because of dilution by unexchanged Y hydrogen. The calculated $t_{1/2}$ would be 4000 years, four times that of group X but only 4% that of group Y. Extrapolating the 4000-year half-time to longer periods of time, Figure 4-8 shows that initial exchange would be reproduced well, but that the time needed to reach 50% exchange ($= t_{1/2}$) is underestimated by more than an order of magnitude.

Our experiments monitored exchange over $\sim 10^{-5}$ half-times, whereas previous, high-temperature experiments reported in Figures 4-6 and 4-7 typically monitored reaction progress over several half-times. Any mechanism that produced rapid exchange for a short period of time, or at a few positions or in a few molecules, would lead to overestimation of long-term rates by our approach.
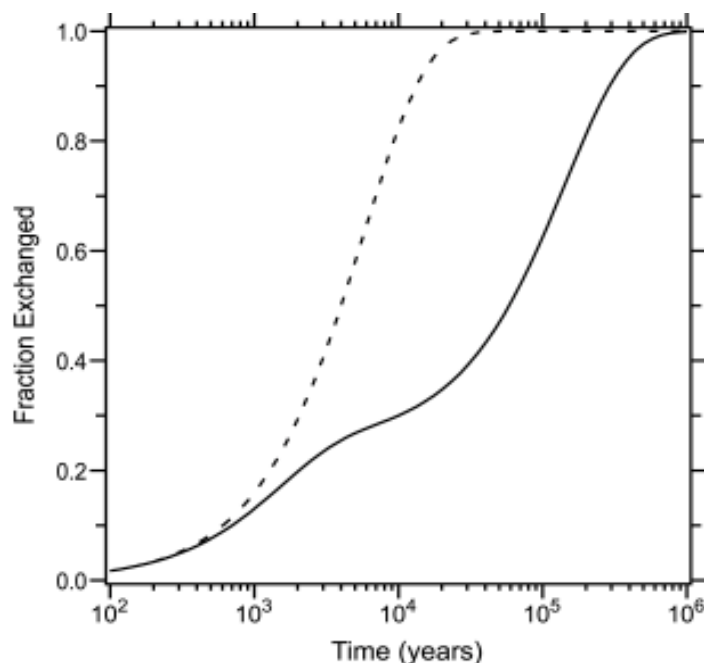
Figure 4-8. Hydrogen exchange over time (solid line) in a system with two populations of exchanging H. One population, comprising 25% of the H, has $t_{1/2} = 1,000$ yrs. The other, comprising 75% of the H, has $t_{1/2} = 100,000$ yrs. The dashed line reflects the exchange predicted from a short exchange experiment.

Such mechanisms might include temporary activation of substrates by drying or grinding; adsorption geometry that promotes exchange at a particular position; or rapid exchange in a few molecules due to trace contamination of the substrates by a potent catalyst. A simple calculation illustrates the point. Only 570 ppm of icosane containing just one atom of D per molecule would produce an increase in δD of 87‰, the largest change measured for icosane.

If this explanation for rapid exchange in icosane is correct, there are two important conclusions. The first is that rates of hydrogen exchange can be extremely variable, even for a simple molecule such as icosane. Whether such variability exists in natural sediments, or is an artifact of our experiments, is unknown. The second is that, for any experiment that measures a small increment of exchange, extrapolation of the results to longer timescales must rely heavily on the assumption of homogeneous exchange rates. If this assumption is not valid, the experimental approach described here may be limited in its applicability.

Effects of Organic Matter on Hydrogen Exchange

Interpreting the incorporation of D by alkanes is substantially more complicated when sample substrates contain complex organic matter. In addition to the possibility that interactions between that organic matter and catalytic surfaces alter exchange rates, other processes leading to incorporation of D must be considered, such as the synthesis of new analyte molecules. These effects cannot be separated in the experiments described here. Our approach, therefore, is to calculate *apparent* exchange rates for marine clay and lacustrine sediment samples, and to compare them to rates determined for organic-free substrates in order to describe the net effect of organic matter on D/H ratios.

Hydrogen exchange in organic-lean marine clay. Measured changes in δD for icosane and pristane incubated on the marine clay are given in Table 4-5. Reaction half-times are not calculated for pristane because of large systematic errors in isotopic analyses of the coinjected phytane standard. Icosane was added to this sediment at a concentration at least 1000 times higher than indigenous n-C_{20}. Indigenous alkanes were not present in sufficient concentration to allow D/H measurements after urea adduction, so only icosane was analyzed. Errors for coinjected standards are not shown in Table 4-5, but are similar in magnitude and direction to those reported in Tables 4-2 and 4-3. In general, analytical precision (*i.e.,* uncertainty in measured ΔD values) was better for marine clay experiments than for silica or montmorillonite, but changes in δD were correspondingly smaller, resulting in larger relative errors in $t_{1/2}$.

Table 4-5. Changes in δD and exchange half-times for icosane and pristane incubated on marine clay

Sample	Icosane				Pristane	
	ΔD[a]	$2\sigma_\Lambda$[b]	$t_{1/2}$ (ka)	2σ range	ΔD[a]	$2\sigma_\Lambda$[b]
MC7-35	0.3	6.9	>61.8	51.4 - ∞	13.4	6.6
MC7-88	3.0	6.4	>168	102 - ∞	41.4	6.6
MC30-35					18.7	6.6
MC30-88[c]	−0.1	7.2	>139	123 - ∞		
MC60-35	0.8	7.2	>59.2	46.9 - ∞	15.7	23
MC60-88	9.7	7.2	99.3	59.6 - 298	123	31

[a] ΔD = δD (sample) − δD (initial), (‰).
[b] Estimated uncertainty for ΔD calculated as described in text (‰).
[c] Sample was accidentally dried at 45°C.

Hydrogen exchange in organic-rich lacustrine sediment. In samples using the lacustrine sediment substrate, indigeneous *n*-alkanes from C_{21} to C_{31} were sufficiently abundant after urea adduction for δD analysis. There is a strong odd-over-even predominance in these *n*-alkanes, suggesting that they are derived from higher plant waxes. No spike compounds were added to these samples. δD values are given in Table 4-6. Incubation temperatures and times were slightly different for these samples, including a hotter 111ºC experiment. Because of the complexity of the chromatograms for lacustrine sediment samples, no standards were coinjected with the samples and accuracy is correspondingly more difficult to assess. Two observations support the accuracy of the measured δD values for the *n*-alkanes. First, changes in δD are remarkably consistent across the suite of *n*-alkanes. Second, there are no systematic differences between large (odd carbon number) and small (even carbon number) peaks.

On the other hand, *n*-alkanes from 60- and 120-day experiments produced indistinguishable δD values, rather than the expected two-fold difference. This type of result is not unprecedented (*e.g.*, pristane in samples S7-35 and S7-88, icosane in samples M30-35 and M30-88) but the consistency across five related compounds suggests that the discrepancy is due to experimental rather than analytical factors. Possible explanations are discussed below.

Values of $t_{1/2}$ for two representative *n*-alkanes, C_{25} and C_{26}, are given in Table 4-7. Exchange half-times for the other *n*-alkanes are similar. Uncertainties in $t_{1/2}$ were calculated by assuming an uncertainty (σ) in each δD measurement which is the larger of *i)* 9.5‰ (the RMS accuracy of *n*-alkane external standards associated with these analyses), or *ii)* σ_p in Table 4-6. Sample LS111-60

Table 4-6. Measured δD values for *n*-alkanes extracted from lacustrine sediment samples

n-alkane	initial		LS29-60		LS29-120		LS60-60		LS111-60[c]
	δD (‰)	σ_p[a]	ΔD[b] (‰)	σ_p	ΔD (‰)	σ_p	ΔD (‰)	σ_p	ΔD (‰)
C_{23}	−159	2.1	47	5.7	48	9.2	96	2	692
C_{25}	−162	6.4	41	5.7	40	0.7	86	4	611
C_{26}	−151	16	45	4.9	59	13	76	5	496
C_{27}	−168	9.2	35	1.4	24	0.7	81	15	595
C_{29}	−165	11	33	13	32	4.2	80	25	517
C_{31}	−160	8.5	37	2.1	94	7.8	79	35	686

[a] Standard deviation of population of δD measurements.
[b] ΔD = δD(sample) − δD(initial)
[c] Only one analysis performed for this sample.

was analyzed only once, so for that sample the standard deviation of ΔD for the six different *n*-alkanes in the sample (82‰) was used as the uncertainty. This large uncertainty reflects the high level of D enrichment in these samples.

Effects of organic matter. Hydrogen exchange rates for the organic-lean marine clay and organic-rich lacustrine sediment samples are compared to those for montmorillonite and silica in Figure 4-9. Exchange rates for alkanes in lacustrine sediment samples are indistinguishable from those for icosane on clean silica, and are similar to those for icosane on clean montmorillonite. The activation energy for exchange in lacustrine sediment samples is 36 ± 6 kJ/mol, is indistinguishable from that for silica (41 ± 4 kJ/mol), and is similar to that for montmorillonite (22 ± 0.7 kJ/mol). In contrast, the single marine clay experiment which produced a measurable shift in δD of icosane yielded a value for $t_{1/2}$ of ~100 ka, approximately an order of magnitude slower than for the other three substrates.

Larcher *et al*. (1986) have shown that, in carboxylic acids, the alkyl tail of the molecule is deactivated towards hydrogen exchange when the carboxyl head of the molecule is adsorbed on clay surfaces. The strong ion-dipole interaction between the carboxyl group and clay surface apparently inhibits the catalytic interaction between the alkyl tail and clay surface, where relatively weak van der Waals interactions dominate. By inference, a large amount of polar organic matter — sufficient to cover mineral surfaces — might inhibit hydrogen exchange in other nonpolar molecules.

The present results are ambiguous in this regard. If the similarities in exchange rate and Arrhenius parameters between the lacustrine sediment and silica incubations are taken to indicate that organic

Table 4-7. Apparent hydrogen exchange half-times for *n*-alkanes from lacustrine sediment samples

Sample	*n*-C$_{25}$		*n*-C$_{26}$	
	$t_{1/2}$ (ka)	2σ range (ka)	$t_{1/2}$ (ka)	2σ range (ka)
LS29-60	17.8	12.2 – 33.2	16.2	10.3 – 38.9
LS29-120	36.6	24.8 – 69.6	24.8	16.6 – 49.1
LS60-60	8.5	7.1 – 10.6	9.6	7.2 – 14.4
LS111-60	1.2	0.94 – 1.6	1.5	1.1 – 2.2
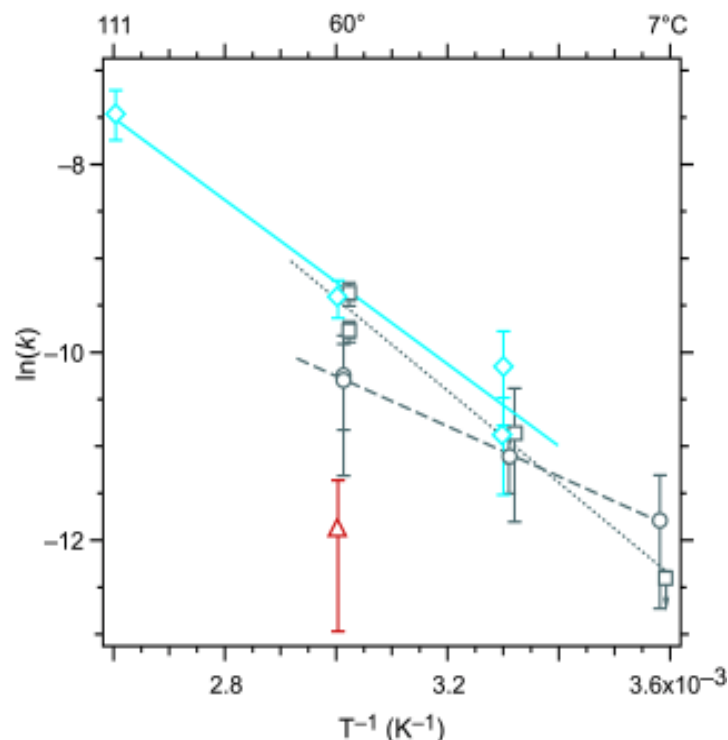
Figure 4-9. Arrhenius plot of exchange rates for icosane on marine clay (red triangle) and pentacosane in lacustrine sediments (blue diamonds). Data for icosane on montmorillonite (circles) and on silica (squares) from Figure 4-4 are shown in gray. Error bars are ±2σ. Data for silica and montmorillonite substrates are offset slightly to the right for clarity.

matter does not affect exchange, then the slower exchange on the marine clay relative to montmorillonite must be attributed to some other factor. Clay and silt-sized silicate minerals comprise >90% of the marine clay substrate, so differences in mineralogy are not a likely explanation.

Conversely, if the slower exchange in marine clay samples is attributed to inhibition by organic matter, then exchange in lacustrine sediments, with its 10-fold higher organic content, must be enhanced by some other mechanism. One possibility is the incorporation of D into new icosane molecules. Results from samples LS29-60 and LS29-120 indicate that δD values of lacustrine sediment alkanes are not changing with time, but the strong temperature dependence suggests that the changes in δD are kinetically controlled (Figure 4-9). The observed changes in δD are consistent with the production of trace amounts of *n*-alkanes from lacustrine sediment organic matter during a brief period at the beginning of each experiment. Possible causes include exposure to oxidizing conditions at the start of each experiment, or thermolysis of highly labile components.

Another potential mechanism is that organic acids are catalyzing exchange in lacustrine sediment samples. Larcher *et al.* (1986) found that hydrogen exchange of isoprenoid acids in pure D_2O was 2–5 times faster than when incubated on dry, deuterated Al-montmorillonite, opposite the pattern observed in experiments with hydrocarbons (*e.g.*, Larcher, 1985). They concluded that the organic acids were themselves acting as catalysts for hydrogen exchange. Given the high concentrations of organic acids in the lacustrine sediment substrate (data not shown), similar mechanisms are plausible here.

In summary, we see no conclusive evidence that organic matter slows hydrogen exchange. In fact, incorporation of D was much more rapid in the organic-rich lacustrine sediments than in the organic-poor marine clay. Until the mechanisms underlying these differences are understood, it is difficult to predict which sedimentary environments are best suited for preservation of organic D/H ratios.

Comparison with previous work. Useful comparisons for the lacustrine sediment results are the experiments of Hoering (1984) and Leif and Simoneit (2000), who used hydrous pyrolysis of Messel Shale with D_2O to study the release of *n*-alkanes from kerogen. After three days at 330ºC, *n*-alkanes were produced that contained between 0 and 14 D atoms/molecule, with most containing 4–6 D atoms (Hoering, 1984). In separate experiments using identical conditions, heptadecane added to the shale contained only 0–2 D atoms per molecule after pyrolysis, thus eliminating pure exchange as an explanation. Examination of pristane mass-spectral fragments revealed a bimodal distribution of D labeling: fragments corresponding to $C_{13}(H,D)_{27}{}^{+}$ generally contained 0-2 D atoms or 5-8 D atoms. This was interpreted as evidence that deuteration of pristane, and probably of *n*-alkanes as well, occurred preferentially at one end of the molecule. The observed patterns of D labeling were rationalized in terms of free-radical chain reactions occurring when alkanes formed by cleavage of bonds to kerogen.

Leif and Simoneit (2000) later reproduced Hoering's results but proposed a different mechanism for incorporation of D. The pattern of D labeling in *n*-alkanes released by hydrous pyrolysis was closest to that of alkadienes added as "molecular probes," rather than to that in alkene or alkane probes. Pyrolysis of C_{32} *n*-alkane in pH 11 D_2O produced the typical cracking products of

shorter-chain alkanes and terminal alkenes, but with no D incorporation detectable — at least by conventional GCMS — in either product. Similar experiments at pH 7 resulted in D incorporation by both alkene and alkane fractions. Since basic conditions should inhibit acid-catalyzed ionic mechanisms but have no effect on free radical reactions, they concluded that D incorporation by alkanes released during pyrolysis was due to acid-catalyzed double-bond isomerization of transient alkene species. Leif and Simoneit (2000) also showed that pyrolysis of icosane on Messel Shale resulted in incorporation of an average of 0.14 D/molecule, while pyrolysis on elemental sulfur under otherwise identical conditions resulted in incorporation of 3.9 D/molecule. These data support the role of reduced sulfur species, including H_2S, in promoting free-radical reactions of organic compounds.

Such extensive incorporation of D by newly-formed alkanes should be detectable at extremely low concentrations in our experiments. For example, if new *n*-alkane molecules contained 5 D atoms (*i.e.*, the average determined by Hoering), the measured changes in δD for lacustrine sediment samples could represent the production of 66–990 ppm of new alkanes, although this interpretation is complicated by the possibility of exchange. Assuming an analytical accuracy of 10‰ in ΔD values, and incorporation of 5 D atoms/molecule, the detection limit (95% confidence intervals not overlapping) for new alkanes in this experiment would be ~50 ppm. *n*-Alkanes are present in the lacustrine sediment substrate at about 10 $\mu g/g$ dry weight per compound (P. Sauer, unpublished data), so that detection limit corresponds to the production of ~1.5 ng of each *n*-alkane per gram of dry sediment per year. Similar approaches (essentially isotope dilution measurements) might be useful for measuring oil generation rates at relatively low temperatures.

Deuterium Incorporation in Cholestene

Cholestene added to our experiments proved to be quite reactive, undergoing both double-bond isomerization and backbone rearrangements. The incorporation of D by products of these reactions was extensive, and readily observed by conventional GCMS. Here we focus on the rearrangment reactions of cholestene, changes in D content accompanying those rearrangements, and the implications of the observed processes for the preservation of hydrogen isotopic ratios in steroids.

Reactions of cholestene. Three major reaction products of cholest-5-ene are shown in Figure 4-10: cholest-4-ene (II), and 20R- and 20S-diacholestene (III). The position of the double bond in diasterenes was not established here, but is assumed to be $\Delta^{13(17)}$ based on the findings of Kirk and Shaw (1975). Other minor products appear in chromatograms, but are difficult to identify by comparison to published mass spectra because of peak shifts associated with the incorporation of D. Likely candidates for these minor components include diasterenes with differing configurations at C-10, partially rearranged sterenes (IV), and spirosterenes (V), all of which have been identified by Peakman *et al.* (1988) as rearrangement products of cholest-5-ene.

There are clear differences in the reactivity of cholestene on the four substrates tested (Table 4-8; Figure 4-11). With pure silica as the substrate, roughly half of Δ^5 cholestene was recovered intact, one-quarter was recovered as Δ^4, and one-quarter as the 20R-diasterene. The 20S-diasterene was formed in much lower quantities. Recovery was similar for marine clay samples, but with a slightly smaller relative amount of 20R-diasterene. In montmorillonite samples, diasterenes make
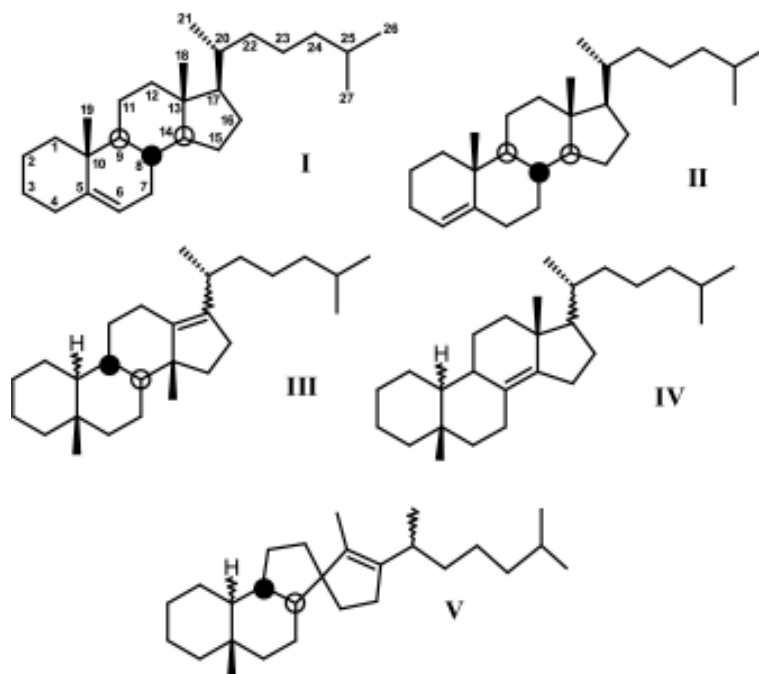
Figure 4-10. Structures of steroidal molecules discussed. (I) 20R-cholest-5-ene; (II) 20R-cholest-4-ene; (III) 20R- or 20S-diacholest-13(17)-ene; (IV) 5-methyl-18-nor-cholestene; (V) spirosterene.

Table 4-8. Recovery of steroid compounds from incubation experiments

Sample	Andro-stanol	Cholest-5-ene[a]	Cholest-4-ene[a]	20R-dia-cholestene[a]	20S-dia-cholestene[a]	total sterenes
M7-35	62%	4%	2%	48%	31%	85%
M7-88	64	13	5	59	35	112
M30-35	66	4	2	51	35	91
M30-88	53	30	6	37	18	92
M60-35	87	7	3	51	28	90
M60-88	73	9	4	43	20	76
X7-35	89	83	9	26	12	130
X7-88	34	29	0	8	0	36
X30-35	66	75	7	15	6	102
X30-88	77	85	10	19	6	121
X60-35	79	91	6	9	2	108
X60-88	76	61	6	6	0	74
S7-35	60	42	23	23	0	87
S7-88	81	68	22	43	5	138
S30-35	82	45	18	14	0	77
S30-88	66	48	17	29	0	94
S60-35	89	60	11	24	9	104
S60-88	89	52	8	19	7	87
MC7-35	81	55	15	12	2	85
MC7-88	68	55	13	12	2	83
MC30-35	74	89	21	10	1	121
MC30-88	145	72	24	10	0	105
MC60-35	76	60	25	27	4	115
MC60-88	67	38	15	16	3	73

[a] Recovery of each cholestene compound is expressed as a percentage of cholest-5-ene added initially.

up ~75% of the recovered products, with cholest-5-ene representing $< 30\%$. But with the addition of 10% XAD resin to the montmorillonite substrate the recovery of Δ^5 rose to $60-90\%$, with diasterenes accounting for $< 25\%$ of the recovered products. These results are consistent with the suggestion of van Kaam-Peters *et al*. (1998) that the diasterane/sterane ratio in sedimentary rocks is correlated with the ratio of clay to organic carbon, rather than the absolute clay content. The catalysis of these backbone rearrangement reactions at a significant rate by crystalline silica has not, to our knowledge, been previously reported.

The occurrence of these isomerization and backbone rearrangement reactions is well known, both in natural sediments (Brassell *et al*., 1984; Peakman and Maxwell, 1988; Rubinstein *et al*., 1975) and in the laboratory (Kirk & Shaw, 1975; Peakman *et al*., 1988), where they are catalyzed by liquid and solid acids. The progressive isomerization of cholestene, rearrangement to form
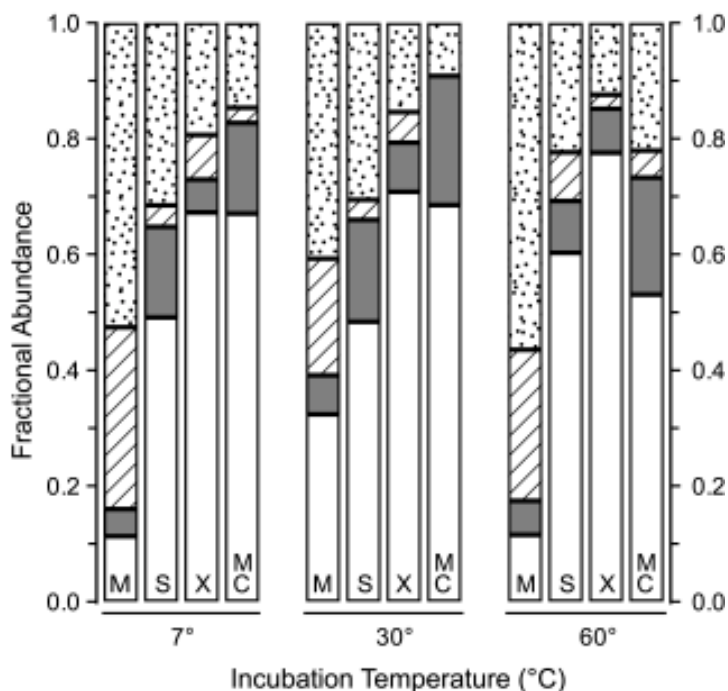
Figure 4-11. Relative abundance of cholest-5-ene (white), cholest-4-ene (gray), 20R-diacholestene (dots), and 20S-diacholestene (stripes) in the recovered products from incubation experiments. M is the montmorillonite substrate, S is silica, X is montmorillonite plus 10% XAD resin, and MC is marine clay. All data shown are for 88-day experiments.

diacholestene, and subsequent isomerization of the 20R- to 20S-diasterene can therefore be used to judge the relative reactivity of the substrates used in our experiments (Brassell *et al.*, 1984).

At equilibrium, the ratio of Δ^4/Δ^5 cholestene should approach a value of 1.5 on the basis of thermodynamic calculations (de Leeuw *et al.*, 1989). In toluenesulfonic acid/acetic acid/cyclohexane at 85ºC, the expected ratio was reached in a matter of hours (Kirk & Shaw, 1975). Many young sediments also contain Δ^4/Δ^5 ratios near the expected value (see references in de Leeuw *et al.*, 1989). In products of our experiments, this ratio ranged from $0.1-0.6$ and, with the possible exception of marine clay samples, shows no change with incubation temperature or time (Figure 4-12a)

The abundance of diasterenes, expressed as a fraction of total sterenes + diasterenes, varies from 0.9 in montmorillonite samples, to ~0.35 in silica samples, to $0.2-0.3$ in marine clay or clay + XAD samples (Figure 4-12b). The difference in reactivity on montmorillonite versus other substrates is particularly large for this reaction. For comparison, Cretaceous Falkland Plateau sedi-
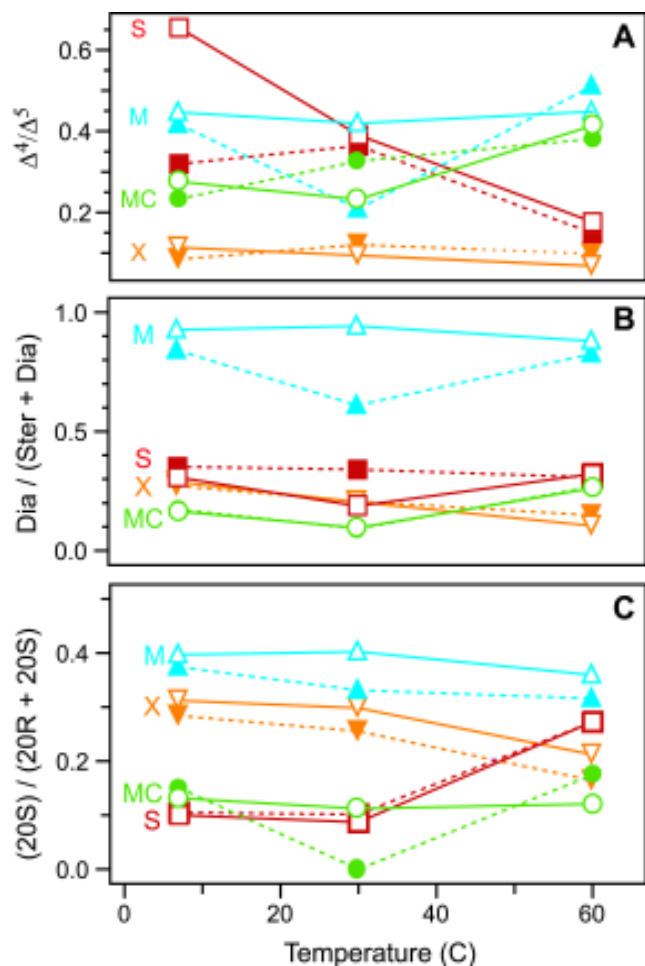
Figure 4-12. Changes in sterene abundance with substrate type, incubation time, and temperature. Open symbols are 35-day experiments, filled symbols are 88-day experiments. Substrates are labeled M, S, X, and MC as in Figure 4-11. (A) Relative abundance of Δ4 versus Δ5 cholestene. (B) Relative abundance of diasterenes versus sterenes. (C) Relative abundance of 20S- versus 20R-diasterenes.

ments at an *in-situ* temperature of over 40ºC show a fractional diasterene abundance of about 0.8 (Brassell *et al*., 1984), indicating that formation of diasterenes is rapid in our experiments.

When cholest-5-ene exists only as the 20R isomer, as it does here and in biosynthetic products, the first product of rearrangement is 20R-diacholest-13(17)-ene. This then progressively isomerizes to the 20S isomer, reaching a racemic (1:1) mixture at equilibrium (Brassell *et al.*, 1984). In our experiments, the fractional abundance of 20S-diasterene relative to (20S + 20R) ranges from ~0.4 in montmorillonite samples to ~0.1 in silica and marine clay samples (Figure 4-12c). Falkland

Plateau sediments exhibit fractional 20S abundances ranging from 0.08 to nearly 0.3 (Brassell *et al*., 1984), and Quaternary Guaymas Basin sediments at 49ºC have a fractional abundance of about 0.15, again suggesting that reaction rates in our experiments are particularly fast.

Extrapolation of reaction rates for cholestene measured in our experiments would imply complete rearrangement and isomerization within a few years. On the other hand, the yields do not increase systematically with increasing time or temperature on any of the substrates, suggesting that the reactions are not kinetically controlled in our experiments. Similar results were obtained by Mackenzie *et al*. (1981) for 20S/20R sterane isomerization in pyrolyzed shale, whereas 22S/22R hopane isomerization in the same experiments showed a modest increase in rate with temperature. They agree that such patterns of sterane isomerization are "difficult to explain."

Several conclusions can be drawn from the observed extents of rearrangment. First, both montmorillonite and crystalline silica can catalyze the reaction of cholestene, although montmorillonite is generally a better catalyst. Second, the addition of XAD resin substantially slows the rate of all three reactions. Third, the reactions proceeded quite rapidly in our experiments, but do not appear to be kinetically limited. All three conclusions are relevant to hydrogen isotopic exchange, both because of the D incorporation which accompanied these reactions, and because of the mechanistic similarity between acid-catalyzed isomerization and hydrogen exchange reactions.

Incorporation of D in rearranged sterenes. The extent of deuteration of Δ^4 and Δ^5 cholestene from representative samples was determined by comparison of their molecular mass spectra with those of the same (undeuterated) compounds in a standard solution (Table 4-9). Negative D enrichments are not possible, so negative numbers in Table 4-9 should be regarded as indistinguishable from zero. The enrichment patterns for *m/z* 257 and 355 (not shown) were identical to those of *m/z* 215 and 370, respectively, in both Δ^4 and Δ^5 compounds.

No significant differences in D labeling exist between the *m/z* 215 and 370 fragments, indicating that D was incorporated only on rings A – C. The Δ^4 compound was consistently more heavily deuterated than the Δ^5 (Figure 4-13). On average both sterenes contained ≤ 1 D atom per molecule, with a small proportion of molecules having up to three D atoms. This distribution cannot be

Table 4-9. Deuterium labeling patterns in cholestene from representative samples

Sample	cholest-4-ene								cholest-5-ene							
	m/z 215[a]				*m/z* 370[b]				*m/z* 215[a]				*m/z* 370[b]			
	D0[c]	D1	D2	D3	D0	D1	D2	D3	D0	D1	D2	D3	D0	D1	D2	D3
M7-88	45	54	2	−1	46	48	−1	7	78	19	2	1	81	17	3	−1
M30-88	75	28	-9	6	67	29	0	4	94	3	3	0	92	7	1	0
M60-35	40	55	4	0	35	56	4	5	80	15	4	1	85	10	4	1
X7-35	106	−10	3	1	99	−2	4	−1	98	1	1	0	100	0	0	0
X30-35	94	−3	5	5	92	3	6	−1	100	0	2	−2	101	−2	1	0
X60-35	87	9	2	2	92	5	3	0	101	−1	0	−1	87	9	2	2
S7-35	45	41	4	10	27	43	21	9	70	20	9	1	65	17	14	4
S30-35	46	39	4	11	36	46	16	2	87	8	3	2	87	9	2	2
S60-88	36	36	16	11	26	44	10	20	96	2	2	1	94	5	0	1
MC7-35	64	40	−6	3	54	41	6	−1	88	8	4	0	90	9	1	0
MC7-88	55	42	−4	8	50	51	−5	4	92	6	1	1	89	10	0	1
MC30-35	55	47	−6	4	43	54	4	0	97	4	−1	0	94	6	0	0
MC60-35	53	47	0	−1	46	51	0	3	85	14	1	1	86	11	2	0
MC60-88	29	70	−4	5	21	76	5	−2	71	14	12	3	69	33	−3	1

[a] Corresponds to A + B rings.
[b] Molecular ion.
[c] D1 indicates the proportion of molecules containing one deuterium atom, etc. Abundances are normalized to give 100% for the sum of all isotopomers, and have been corrected for the presence of carbon-isotopic peaks.
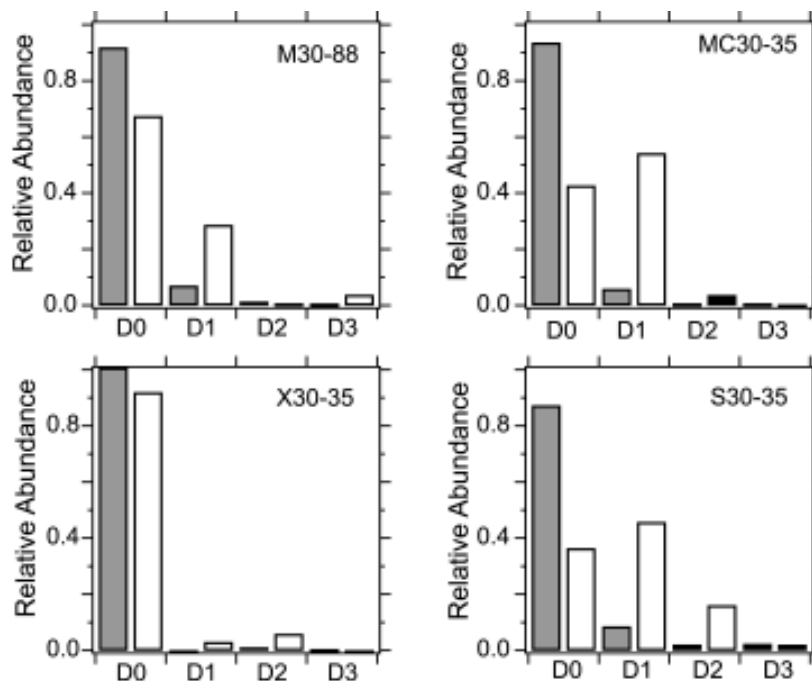
Figure 4-13. Relative distribution of deuterium in Δ^5 (solid) versus Δ^4 (white) cholestene in four representative samples. Abundances are normalized to give 100% for the sum of all isotopomers.

reconciled with a simple ionic mechanism for the isomerization of Δ^5 to Δ^4, which should result in exactly one D in every molecule of cholest-4-ene. In most samples, more than half of cholest-4-ene molecules contained no D. It is highly unlikely that hydrogen on or near mineral surfaces (including hydroxyl H, interlayer water, etc.) could fail to reach isotopic equilibrium with sample water after several days (Longstaffe, 1996). The absence of D in some cholest-4-ene molecules therefore seems to require that hydrogen from C-4 is, with high probability, transferred to C-6 during isomerization of Δ^5 to Δ^4. Observed differences in D incorporation during double-bond migration on various substrates could perhaps be rationalized as being due to differences in the efficiency of this transfer by different catalysts. For example, silica consistently produced a lower Δ^4/Δ^5 ratio than did montmorillonite, yet Δ^4 produced on silica contains more D.

Repeated isomerization between Δ^5 and Δ^4 cholestene can result in the replacement of up to three hydrogen atoms per molecule at C-4 and C-6, assuming that both axial and equatorial hydrogens can be abstracted during double-bond migration. The observed lack of enrichment beyond D_3 is consistent with the prediction by de Leeuw *et al*. (1989) that migration of the double bond to positions other than Δ^4 and Δ^5 is unlikely to occur under natural conditions.

The amount of D in Δ^5 cholestene in many samples is greater than expected based solely on double-bond isomerization. Using sample S7-35 as an example, approximately 25% of Δ^5 has converted to Δ^4 (Table 4-8). The ratio of rate constants of the forward and reverse reactions is 3/2 (de Leeuw *et al*., 1989), so the amount of Δ^5 resulting from backward reaction of Δ^4 should be <4% of the starting amount. Assuming a 50% probability of replacement with each shift of the double bond, the D distribution in Δ^5 should be 97:2:1:0 (D_0:D_1:D_2:D_3). In contrast, the measured distribution is 65:17:14:4 (Table 4-9). Isomerization of cholestene to the proposed first intermediate product in the formation of diasterene (5-methyl-10-norcholest-9-ene; Peakman and Maxwell, 1988) and back could result in replacement of one additional hydrogen at C-9. Inversion at C-20 in cholestene could result in exchange of one hydrogen, but comparison of D labeling in *m/z* 370 versus 215 (Table 4-9) fragments provides little evidence of this.

Diacholestenes contained between 0 and ~12 D atoms per molecule. With the exception of silica samples, D labeling in the 20R and 20S isomers is similar (Figure 4-14). In silica samples, the
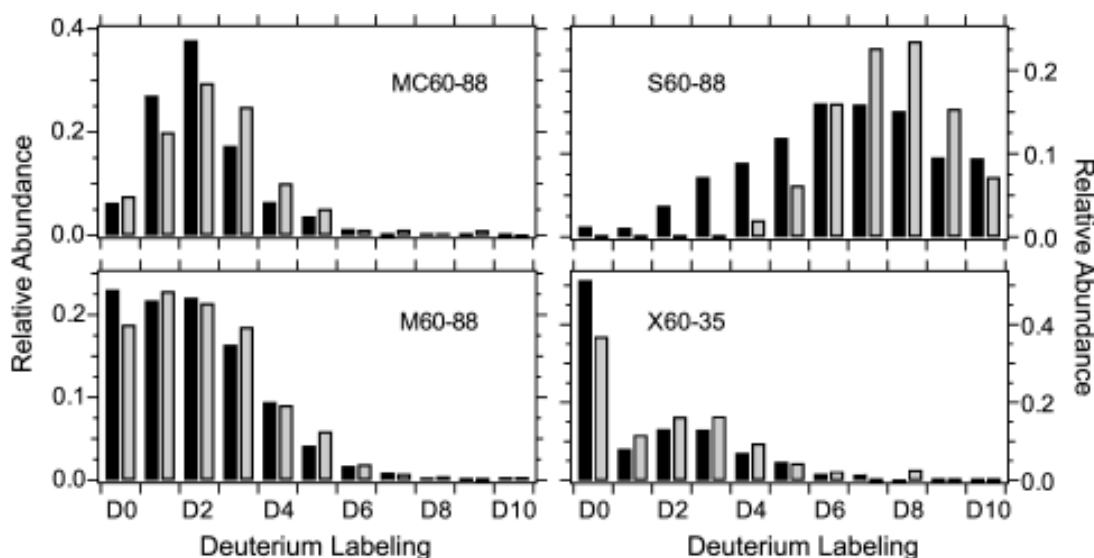
Figure 4-14. Distribution of deuterium in 20R- (black) versus 20S-diacholestene (gray) for four representative samples.

20R isomer appears to be enriched by ~1 D atom relative to the 20S isomer. The reasons for this difference are not known, but could be due to coelution of another compound with the 20R isomer. Since the first product of sterene rearrangement is the 20R diasterene (Kirk & Shaw, 1975; Peakman *et al.*, 1988), subsequent chiral inversion should lead to the 20S isomer with one additional D. The lack of enrichment in 20S diasterenes relative to 20R suggests that either *i*) exchange at C-20 might occur during backbone rearrangement to form the diasterene; *ii*) stereochemical inversion at C-20 might proceed without hydrogen exchange; or *iii*) hydrogen exchange at C-20 might proceed without chiral inversion. All of these possibilities are unexpected. Isomerization of the 20R and 20S isomers of cholestene *before* backbone rearrangment is possible, but no 20S-cholestene was observed in the reaction products.

Deuterium labeling of 20R-diacholestene is shown in Table 4-10 for representative samples of the four substrates. As with cholestene, there are differences in the extent of D incorporation on different substrates. Diacholestenes contained the largest abundance of D when they were incubated on silica, followed by montmorillonite, marine clay, then clay + XAD substrates. This pattern is distinct from that of diasterene abundance, which was greatest in montmorillonite samples, fol-

Table 4-10. Deuterium enrichment of 20R-diacholestene in representative samples

Sample	m/z	D0[a]	D1	D2	D3	D4	D5	D6	D7	D8	D9	D10
M7-88	257[b]	22	29	24	14	7	2	1	0	0	0	0
	355[c]	18	18	20	17	12	8	3	2	1	1	0
M30-88	257	31	26	21	13	6	2	1	0	0	0	0
	355	26	16	20	17	8	6	3	2	1	1	0
M60-88	257	23	22	22	16	9	4	2	1	0	0	0
	355	22	16	17	16	10	8	5	3	1	1	1
X7-35	257	64	13	11	7	2	1	0	0	0	0	0
	355	63	8	10	8	5	3	0	2	0	0	0
X30-35	257	46	11	15	12	8	4	2	0	1	0	1
	355	46	7	12	8	10	6	4	3	1	2	1
X60-35	257	51	8	13	13	7	5	2	1	0	0	0
	355	56	2	13	4	11	4	5	0	4	0	0
S7-88	257	1	3	9	18	24	21	14	7	3	1	1
	355	1	2	6	12	18	20	16	11	6	4	2
S30-88	257	0	1	6	13	21	21	18	10	5	3	2
	355	0	1	5	9	16	18	16	14	8	4	5
S60-88	257	1	1	4	7	9	12	16	16	15	10	9
	355	3	2	3	6	8	9	10	12	7	8	8
MC7-88	257	20	30	28	14	4	3	0	0	1	0	0
	355	24	24	27	11	9	3	0	2	0	0	0
MC60-88	257	6	27	38	17	6	4	1	0	0	0	0
	355	8	24	38	16	7	3	2	1	1	0	0

[a] D1 indicates the proportion of molecules containing one deuterium atom, etc. Abundances are normalized to give 100% for the sum of all isotopomers, and have been corrected for the presence of carbon-isotopic peaks.
[b] Corresponds to rings A–C.
[c] M–15 ion.

lowed by silica, then clay + XAD, then marine clay. Rearrangment and H exchange are not closely correlated, as for isomerization between Δ^4 and Δ^5 cholestene.

Akporiaye *et al*. (1981) catalyzed the rearrangement of cholest-5-ene to 20R- and 20S-diacholestene in deuterated acetic acid with toluene-*p*-sulfonic acid. Mass spectrometry indicated a D content of 16 atoms/molecule (range 13 – 20) in 20R-diacholestene, and 18 D atoms/molecule (range 13 – 25) in the 20S compound. Incorporation of D in our experiments was much lower than that described by Akporiaye *et al*. (1981). In particular, more than 50% of diasterenes formed in montmorillonite + XAD samples showed no measurable increase in D content, a stunning result considering the extent of rearrangement involved. Unless the presence of XAD alters the reaction mechanism in some way that effectively blocks exchange, it appears that organic hydrogen from the polymer replaces water as the source of hydrogen during exchange. Since δD values of organic

H differ significantly from those of water, this observation could bear strongly on the preservation of organic records of δD.

D/H records of steroids. Hydrogen-isotopic records based on steroid compounds are particularly interesting because of the source-specificity provided by many steroid molecules (Sauer *et al.*, 2001). To quantify the effects of hydrogen exchange and addition on isotopic records, three pieces of information are needed: *i)* the rates of exchange and incorporation, *ii)* the number of positions affected by these reactions, and *iii)* the isotopic composition of hydrogen that is added and/or removed. At present, rates of hydrogen exchange in isoprenoid skeletons can only be estimated to within a few orders of magnitude. As an alternative approach, the complexity of steroid molecules may offer opportunities to assess exchange rates via structural information. For example, we might find that the extent of double-bond isomerization or of stereochemical inversion in a steroidal biomarker, or the abundance of more significantly rearranged products, is correlated with the extent of hydrogen exchange in the parent steroid. The relative abundances of such products could then be used to predict the extent of exchange for molecules in that sediment.

Experiments in which cholestene is incubated with D_2O provide information about the number of hydrogen positions affected by typical sterene reactions (*i.e.*, the second requirement in the preceding list). An important result of our experiments is that, for all of the observed cholestene reactions, the number of hydrogens replaced by solvent hydrogen is considerably less than the number mobilized by rearrangment. Furthermore, the extent of exchange in a given reaction depended strongly on the mineral substrate. These results greatly complicate the prediction of hydrogen exchange in steroids from sedimentary records, but also indicate that structural changes in steroids do not necessarily obscure primary isotopic signals.

The third requirement, knowledge of the δD of added hydrogen, is presently the most difficult. Rearrangments involving ionic mechanisms, such as double-bond migration, offer the opportunity for direct incorporation of water hydrogen. Exchange with water is also possible. The δD value of H derived from H_2O will be offset from that of water by some fractionation factor. Yakir & DeNiro (1990) showed that during metabolism of carbohydrate compounds, exchange with water resulted in a value of $\varepsilon_{\text{org-water}}$ of +158‰, *i.e.,* the exchanged hydrogen was D-enriched relative to water. In

contrast, Luo *et al*. (1991) explained the strong depletion of D in NADPH as a result of the significantly higher equilibrium concentration of H^+ relative to D^+ in H_2O. Currently, not even the direction of this fractionation can be predicted with confidence. A second source of hydrogen is that added during hydrogenation of double bonds. In a preliminary report, Andersen *et al*. (2000) compared phytane with carotane (derived from β-carotene by the hydrogenation of 11 double bonds) in the Green River Shale and estimated that H added during hydrogenation has a δD value of –587‰.

Available data are thus not yet sufficient to provide a complete accounting of hydrogen isotopic changes during sterol diagenesis, but it is possible to make quantitative predictions. Using the information described in the preceding discussion, a hypothetical example tracing the δD value of cholesterol through diagenesis is given in Figure 4-15. There is not universal agreement that the reactions shown are representative of those occurring in sediments, nor are all of the known reactions included. The starting compound in Figure 4-15, 20R-cholest-5-ene-3β-ol, is assumed to have a δD value of –250‰, typical of sterol compounds measured by Sessions *et al*. (1999). Hydrogen resulting from replacement or exchange with water is assumed to have a δD value of 0‰, and
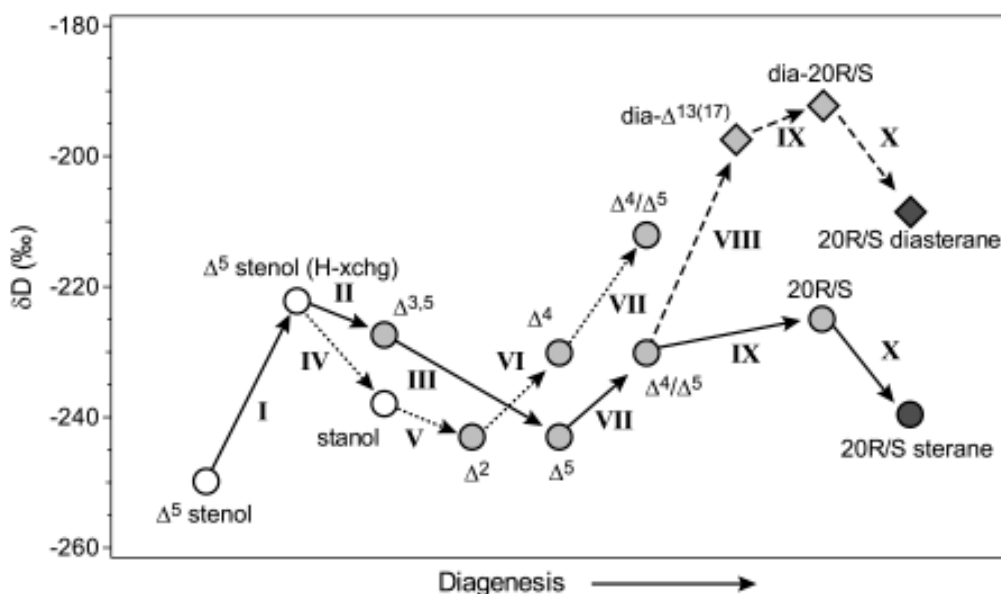
Figure 4-15. Hypothetical example of changes in δD of products derived from cholesterol through a sequence of typical diagenetic reactions. White symbols are alcohols, gray symbols are alkenes, black symbols are alkanes. Circles are molecules with the 10,13-dimethyl configuration of steroids, diamonds have the 5,14-dimethyl configuration of diasterenes. Assumptions used to calculate δD values are given in the text.

that resulting from hydrogenation a δD value of $-587‰$ (Andersen *et al.*, 2000). Where data regarding the number of exchanged hydrogen atoms are not available, complete replacement at every possible position is assumed to provide a worst-case estimate for the magnitude of changes in δD.

Prior to any molecular changes, exchange of hydrogen at C-2, C-3 and C-4 may be possible on short time-scales because the acidity of these positions is greatly increased by proximity to the electron-withdrawing hydroxyl group. For illustrative purposes, exchange is projected at all five hydrogen positions in Figure 4-15 (reaction I). One of the first diagenetic reactions affecting cholesterol will be dehydration to form the $\Delta^{3,5}$ diene, in which no hydrogen is gained but a previously-exchanged hydrogen at C-4 is lost (II; de Leeuw *et al.*, 1989). This loss may also be accompanied by a fractionation, which is not considered here. Selective hydrogenation of the Δ^3 position then produces the Δ^5-sterene (III) with the addition of two strongly-depleted hydrogens. An alternative pathway to Δ^5 cholestene, proposed by Peakman and Maxwell (1988) and others, is hydrogenation of cholesterol to cholestanol, dehydration to Δ^2 cholestene, then isomerization via Δ^3 to Δ^4 cholestene (IV – VI). These reactions result in the potential replacement of all four hydrogens at C-2 and C-3.

Δ^5 and Δ^4 cholestene will slowly isomerize (reaction VII), potentially replacing one hydrogen with each flip of the double bond. If this process is repeated, all three hydrogens on C-4 and C-6 will eventually be derived from water. However, isomeric equilibrium between Δ^4 and Δ^5 cholestene does not imply isotopic equilibration, since after the first hydrogen is replaced, each subsequent isomerization has at least a 50% chance of replacing the same hydrogen again. In addition, our results indicate that replacement of hydrogen occurs only about 50% of the time during double-bond migration. To reflect both of these factors, the calculations in Figure 4-15 assume only one hydrogen is incorporated from the solvent during double-bond isomerization.

Rearrangement of a sterene to a diasterene (reaction VIII) results, on average, in the replacement of five hydrogens. The number of positions affected may vary substantially with the reaction conditions, but our data suggest that the number is relatively constant for a given substrate. Two more reactions can affect both the sterene and diasterene molecules equally. Inversion at C-20 (IX) results in exchange of one hydrogen. Hydrogenation of the double bond (X) will add two hydrogens strongly depleted in D.

Several conclusions can be drawn from Figure 4-15, with the caveat that they are dependent on the assumed δD values of added and exchanged hydrogen. First, the change in δD values across the entire sequence of diagenetic products is relatively small. Out of 48 hydrogen atoms in diacholestane, three were added by hydrogenation, approximately twelve either exchanged with water or were replaced during rearrangment, and 33 remain intact from the parent cholesterol. Thus any of the steroid products may serve as crude indicators of primary D/H ratios. When intact sterols (as opposed to sterenes) are found, the number of hydrogen atoms subject to exchange and rearrangment drops to less than eight, with none due to addition. Second, sterene molecules represent particularly problematic targets for developing paleoclimatic records. Isomerization of Δ^4 and Δ^5 sterenes is incomplete in many sediments, and the extent of hydrogen turnover during rearrangment cannot be determined from Δ^4/Δ^5 molecular ratios. Downcore changes in δD of cholest-5-ene could be due solely to continuing isomerization. Similar problems exist for isomerization of $\Delta^{8(14)}$ and Δ^{14} sterenes, and possibly for isomerization of Δ^7 and $\Delta^{8(14)}$ (deLeeuw *et al.*, 1989).

Third, differences in δD between steranes and diasteranes may provide information about rates of hydrogen exchange. Because the rearrangement to form diasterenes is irreversible, any change in δD from this reaction is "locked in" once the saturated diasterane is formed. If δD values of steranes and diasteranes converge over time, the change is likely due to continuing hydrogen exchange. When δD values do not change relative to each other, exchange may be excluded.

CONCLUSIONS

We conducted incubation experiments using selected organic compounds, D_2O, and five different sediments as substrates. The pattern and extent of D incorporation by the analytes was studied by GCMS and irmGCMS. The goals of these experiments were to 1) measure or estimate rates of exchange in natural sediments at low ($<50°$) temperatures; 2) study the effect of sedimentary organic matter on rates of hydrogen exchange; and 3) make predictions about the long-term preservation of D/H ratios in steroid compounds. The unifying purpose of these goals is to provide a quantitative underpinning for the use of organic D/H ratios in reconstructions of paleoenvironmental conditions.

Multiple processes can affect the hydrogen isotopic compositions of sedimentary organic compounds. On clean montmorillonite and silica, exchange produced increases in icosane δD values of up to 87‰ over 85 days. These shifts correspond to exchange half-times on the order of 10 ka at 60°C, and 100 ka at 7°C, at least several orders of magnitude faster than predicted by other experimental and geologic evidence. The similarity of exchange rates between different substrates, and very low activation energies for exchange, also suggest that exchange in our experiments was artificially rapid. A possible explanation for this discrepancy is that our measurements, which will detect the incorporation of a few ppm D, are biased by the rapid exchange of a small fraction of the hydrogen pool, leading to overestimation of long-term rates.

Incubations utilizing siliceous lacustrine sediments with ~20% TOC measured exchange half-times for *n*-alkanes that were indistinguishable from those on organic-free silica and montmorillonite. Experiments using a marine clay with ~1.5% TOC produced exchange half-times at least an order of magnitude longer. These results are inconclusive regarding the effects of organic matter on rates of hydrogen exchange. If the reduced exchange rates in marine clay samples are attributed to the presence of organic matter, some other process (such as catalysis by organic acids) must be enhancing exchange in the lacustrine sediment samples. Alternatively, organic matter may have no influence on hydrogen exchange rates, which requires that some other, unidentified factor is slowing exchange in the marine clay samples.

Analysis of D labeling patterns in products of cholest-5-ene reveals several surprises about the retention of hydrogen during rearrangments. Isomerization of Δ^5 to Δ^4 cholestene results in the incorporation of D only ~50% of the time. The addition of XAD resin reduces incorporation of water-derived H to $<10\%$ of potential exchange. Backbone rearrangement of cholestene to diacholestene results in the incorporation of $0-9$ D atoms, roughly half the number when the reaction occurs in acidic solution. Again, the addition of XAD substantially reduces incorporation of water-derived H to $0-4$ atoms.

Consideration of the processes observed in these experiments allows the prediction that while hydrogen is replaced during diagenesis of sterols, overall changes in δD will not be large. Less than one-third of hydrogen atoms may be replaced during transformation of cholesterol to diacholestane.

Furthermore, the typical isotopic composition of sterols lies between those of water and of hydrogen added during hydrogenation of double bonds. These two sources of hydrogen push the D/H ratio of a steroid in opposite directions, and partially offset each other. Downcore comparison of δD values for steranes and diasteranes may provide direct evidence of hydrogen exchange, since isotopic fractionation between these two molecules should remain constant in the absence of exchange.

A central question which remains unanswered in all of our experiments is the relationship between complex, sedimentary organic matter and changes in δD. It is currently impossible to accurately simulate natural conditions without organic matter, yet its presence makes separation of competing processes more difficult. There are apparently conflicting observations about the effects of organic matter on exchange rates. Incorporation of D by alkanes incubated on organic-rich lacustrine sediments was as rapid as for those incubated on organic-free silica, yet the addition of XAD resin to montmorillonite greatly retards incorporation of water H by cholestene. Organic acids may deactivate catalytic clay surfaces by strongly binding to them, but may themselves be effective catalysts for exchange. To confidently utilize hydrogen isotopic records for the interpretation of paleoenvironmental conditions, an essential step will be to understand the interaction between complex organic matter and the preservation of isotopic compositions.

REFERENCES CITED

Abbott, G.D., Lewis, C.A. and Mazwell, J.R. (1985) Laboratory models for aromatization and isomerization of hydrocarbons in sedimentary basins. *Nature* **318**, 651–653.

Akporiaye, D.E., Farrant, R.D. and Kirk, D.N. (1981) Deuterium incorporation in the backbone rearrangement of cholest-5-ene. *Journal of Chemical Research* **S**, 210–211.

Alexander, R., Kagi, R.I. and Larcher, A.V. (1982) Clay catalysis of aromatic hydrogen-exchange reactions. *Geochimica et Cosmochimica Acta* **46**, 219–222.

Alexander, R., Kagi, R.I. and Larcher, A.V. (1984) Clay catalysis of alkyl hydrogen exchange reactions — reaction mechanisms. *Organic Geochemistry* **6**, 755–760.

Alexander, R., Kagi, R.I., Larcher, A.V. and Woodhouse, G.W. (1981) Aromatic hydrogen exchange in petroleum source rocks. In: *Advances in organic geochemistry 1981*, pp. 69–71. John Wiley & Sons.

Andersen, N., Bernasconi, S.M., Carlson, R.M. and Schoell, M. (2000) Early diagenetic incorporation of strongly deuterium-depleted hydrogen in poly-unsaturated biomolecules. American Geophysical Union annual meeting, San Francisco, CA.

Brassell, S.C., McEvoy, J., Hoffmann, C.F., Lamb, N.A., Peakman, T.M. and Maxwell, J.R. (1984) Isomerisation, rearrangement and aromatisation of steroids in distinguishing early stages of diagenesis. *Organic Geochemistry* **6**, 11–23.

de Leeuw, J.W., Cox, H.C., van Graas, G., van der Meer, F.W., Peakman, T.M., Baas, J.M.A. and van de Graaf, B. (1989) Limited double bond isomerisation and selective hydrogenation of sterenes during early diagenesis. *Geochimica et Cosmochimica Acta* **53**, 903–909.

Griffin, J.J., Windom, H., and Goldberg, E.D. (1968) The distribution of clay minerals in the world ocean. *Deep-Sea Research* **45**, 433–459.

Hoering, T.C. (1984) Thermal reactions of kerogen with added water, heavy water and pure organic substances. *Organic Geochemistry* **5**(4), 267–278.

Hopfner, A. (1969) Vapor Pressure Isotope Effects. *Angewandte Chemie* **8**(10), 689-699.

Huizinga, B.J., Tannenbaum, E. and Kaplan, I.R. (1987) The role of minerals in the thermal alteration of organic matter — IV. Generation of *n*-alkanes, acyclic isoprenoids, and alkenes in laboratory experiments. *Geochimica et Cosmochimica Acta* **51**, 1083–1097.

Kirk, D.N. and Shaw, P.M. (1975) Backbone rearrangements of steroidal 5-enes. *Journal of the Chemical Society, Perkin transactions 1*, 2284–2294.

Koepp, M. (1978) D/H isotope exchange reaction between petroleum and water: A contributory determinant for D/H-isotope ratios in crude oils? In: *Short papers of the Fourth International Conference, Geochronology, Cosmochronology, Isotope Geology 1978*, *USGS Open-File Report 78-701* (Ed. by R. E. Zartman), pp. 221–222. US Geological Survey, Reston, VA.

Krishnamurthy, R.V., Syrup, K.A., Baskaran, M. and Long, A. (1995) Late glacial climate record of midwestern United States from the hydrogen isotope ratio of lake organic matter. *Science* **269**, 1565–1567.

Kushner, D.J., Baker, A. and Dunstall, T.G. (1999) Pharmacological uses and perspectives of heavy water and deuterated compounds. *Canadian Journal of Physiology and Pharmacology* **77**(2), 79–88.

Larcher, A.V., Alexander, R., Rowland, S.J. and Kagi, R.I. (1986) Acid catalysis of alkyl hydrogen exchange and configurational isomerisation reactions: acyclic isoprenoid acids. *Organic Geochemistry* **10**, 1015–1021.

Larcher, A.V. (1985) A study of some clay-catalysed organic hydrogen exchange reactions and their significance to the maturation of sedimentary organic matter. Ph.D. thesis, Murdoch University, 238 pp.

Leif, R.N. and Simoneit, B.R.T. (2000) The role of alkenes produced during hydrous pyrolysis of a shale. *Organic Geochemistry* **31**(11), 1189–1208.

Longstaffe, F. (1996) An introduction to oxygen and hydrogen isotope exchange in clay minerals. In: *The isotope geology of clay minerals: From isotope crystal chemistry to petrogenesis*, *33rd Annual Meeting* (Ed. by F. Longstaffe & K. Kyser), pp. 31–34. Clay Minerals Society, Gatlinburg, Tennessee.

Luo, Y.-H., Sternberg, L., Suda, S., Kumazawa, S. and Mitsui, A. (1991) Extremely low D/H ratios of photoproduced hydrogen by cyanobacteria. *Plant and Cell Physiology* **32**(6), 897–900.

Mackenzie, A.S., Lewis, C.A. and Maxwell, J.R. (1981) Molecular parameters of maturation in the Toarcian shales, Paris Basin, France. IV. Laboratory thermal alteration studies. *Geochimica et Cosmochimica Acta* **45**, 2369–2376.

Mackenzie, A.S. and McKenzie, D. (1983) Isomerization and aromatization of hydrocarbons in sedimentary basins formed by extension. *Geological Magazine* **120**(5), 417–470.

Olphena, H.V. and Fripiat, J.J. (1979) Data Handbook for Clay Minerals and Other Non-metallic Minerals, pp. 346. Pergamon Press.

Peakman, T. and Maxwell, J.R. (1988) Early diagenetic pathways of steroid alkenes. *Organic Geochemistry* **13**, 583–592.

Peakman, T.M., Ellis, K. and Maxwell, J.R. (1988) Acid-catalyzed rearrangements of steroid alkenes - Part 2. A re-investigation of the backbone rearrangement of cholest-5-ene. *Journal of the Chemical Society, Perkins Transactions 1*, 1071–1075.

Pearson, A. and Eglinton, T.I. (2000) The origin of n-alkanes in Santa Monica Basin surface sediment: a model based on compound-specific $\Delta^{14}C$ and $\delta^{13}C$ data. *Organic Geochemistry* **31**, 1103–1116.

Rubinstein, I., Sieskind, O. and Albrecht, P. (1975) Rearranged sterenes in a shale: occurrence and simulated formation. *Journal of the Chemical Society, Perkin transactions 1*, 1833–1836.

Sauer, P.E., Eglinton, T.I., Hayes, J.M., Schimmelmann, A. and Sessions, A.L. (2001) Compound-specific D/H ratios of lipid biomarkers from sediments as a proxy for environmental and climatic conditions. *Geochimica et Cosmochimica Acta* **65**(2), 213–222.

Schimmelmann, A. (1991) Determination of the concentration and stable isotopic composition of non-exchangeable hydrogen in organic matter. *Analytical Chemistry* **63**, 2456–2459.

Schindler, P.W. and Stumm, W. (1987) The surface chemistry of oxides, hydroxides, and oxide minerals. In: *Aquatic Surface Chemistry: Chemical Processes at the Particle-Water Interface* (Ed. by W. Stumm), pp. 83–110. John Wiley & Sons, New York.

Sessions, A.L., Burgoyne, T.W. and Hayes, J.M. (2001a) Correction of H_3^+ contributions in hydrogen isotope ratio monitoring mass spectrometry. *Analytical Chemistry* **73**(2), 192–199.

Sessions, A.L., Burgoyne, T.W. and Hayes, J.M. (2001b) Determination of the H_3 Factor in hydrogen isotope ratio monitoring mass spectrometry. *Analytical Chemistry* **73**(2), 200–207.

Sessions, A.L., Burgoyne, T.W., Schimmelmann, A. and Hayes, J.M. (1999) Fractionation of hydrogen isotopes in lipid biosynthesis. *Organic Geochemistry* **30**, 1193–1200.

van Kaam-Peters, H.M.E., Köster, J., van der Gaast, S.J., Dekker, M., deLeeuw, J.W. and Damste, J.S.S. (1998) The effect of clay minerals on diasterane/sterane ratios. *Geochimica et Cosmochimica Acta* **62**(17), 2923– 2929.

Wassenaar, L.I. and Hobson, K.A. (2000) Improved method for determining the stable-hydrogen isotopic composition (δD) of complex organic materials of environmental interest. *Environmental Science and Technology* **34**, 2354–2360.

Wedeking, K.W. and Hayes, J.M. (1983) Exchange of oxygen isotopes between water and organic material. *Isotope Geoscience* **1**, 357–370.

Xie, S., Nott, C.J., Avsejs, L.A., Volders, F., Maddy, D., Chambers, F.M., Gledhill, A., Carter, J.F. and Evershed, R.P. (2000) Palaeoclimate records in compound-specific δD values of a lipid biomarker in ombrotrophic peat. *Organic Geochemistry* **31**, 1053–1057.

Yakir, D. and DeNiro, M.J. (1990) Oxygen and hydrogen isotope fractionation during cellulose metabolism in *Lemna gibba* L. *Plant Physiology* **93**, 325-332.

APPENDIX A - ICPMS Results for Silica Substrate

Element	Concentration (ug/g)	Element	Concentration (ng/g)
Al	1900	Au	0.57
Ba	16	Ir	0.17
Be	0.13	Os	0.34
Bi	0.01	Pd	4.1
Ca	140	Pt	0.91
Cd	0.02	Re	0.48
Ce	7.6	Rh	0.18
Co	0.60	Ru	0.55
Cr	6.4		
Cs	0.09		
Cu	2.0		
Dy	1.4		
Er	0.62		
Eu	0.25		
Fe	380		
Ga	0.52		
Gd	1.7		
Hf	0.25		
Ho	0.26		
K	250		
La	7.1		
Li	1.7		
Lu	0.05		
Mo	0.17		
Na	46		
Nb	0.64		
Nd	6.8		
Ni	0.44		
Pb	2.0		
Pr	1.6		
Rb	1.8		
Sb	0.06		
Sc	1.3		
Sm	1.4		
Sn	0.17		
Sr	110		
Ta	0.05		
Tb	0.23		
Th	0.68		
Tm	0.07		
U	0.40		
V	3.7		
W	0.10		
Y	9.4		
Yb	0.47		
Zn	1.5		
Zr	9.5		

Chapter 5 — Hydrogen isotope fractionation in methane-oxidizing and sulfate-reducing bacteria

ABSTRACT

Hydrogen isotopic compositions of lipids from *Methylococcus capsulatus*, an aerobic, methane-oxidizing bacterium, and from four species of sulfate-reducing bacteria (SRB) were measured to provide a preliminary perspective on hydrogen isotope fractionations in bacterial metabolism. By systematically varying the D/H ratios of CH_4 and H_2O supplied to *M. capsulatus*, and by observing concomitant changes in δD of lipids, we determined that $31 \pm 2\%$ of hydrogen in all *M. capsulatus* lipids is derived from methane. Examination of the relevant biochemical pathways indicates that no hydrogen is transferred directly (with C-H bonds intact) from methane to lipids, so other indirect pathways must exist. Possibilities include NADPH, and H_2O resulting from the oxidation of CH_4. There appears to be a positive isotopic fractionation between methane and lipids, so that methanotroph lipids are generally D-enriched relative to the methane they consume. Significant differences occur in δD values of methylhopanol versus hopanol, and of unsaturated versus saturated fatty acids. These cannot be explained by the small structural differences between the molecules.

Isotopic fractionation in SRB grown autotrophically on CO_2 and H_2 is similar to that observed in phytoplankton cultures, indicating that carbon-metabolic pathways have little effect on the hydrogen isotopic composition of lipids. A systematic increase in δD of fatty acids of up to 75‰ is observed with increasing chain length of fatty acids. This increase could be due to reduced fractionation between NADPH and fatty acids during rapid biosynthesis of these molecules.

INTRODUCTION

Compound-specific measurements of hydrogen isotope ratios are potentially useful tools in both organic geochemical and paleoclimatic research (Xie *et al.*, 2000; Sauer *et al.*, 2001). Central to the interpretation of such data is an understanding of the source and variability of hydrogen-isotopic fractionation in organic compounds. A few studies have provided a rudimentary understanding of fractionation associated with photosynthesis in higher plants (Smith and Epstein, 1970; Ziegler *et al.*, 1976; Estep and Hoering, 1980; Sternberg *et al.*, 1986a; Yakir and DeNiro, 1990), in algal macrophytes (Sternberg *et al.*, 1986b), and in phytoplankton (Stiller and Nissenbaum, 1980; Estep and Hoering, 1981). Cellulose has received particular attention in these and other studies, primarily because of its relevance to paleoclimatology (Edwards, 1993). Interest in hydrogen-isotopic fractionation in lipids has been rejuvenated by the introduction of irm-GCMS techniques, which allow analysis of individual lipids and examination of isotopic fractionations at a new level of detail.

Despite these advances, virtually nothing is known about hydrogen-isotopic fractionation in bacterial metabolism. What little is known pertains to the isotopic composition of methane produced by bacteria (Whiticar *et al.*, 1986; Balabane *et al.*, 1987; Sugimoto and Wada, 1995; Waldron *et al.*, 1999). Unfortunately, methane is not directly preserved in the geologic record, and analyses of methane tell us little about isotopic fractionation associated with biomass from these organisms. Considering the important role bacteria play in biogeochemical cycles, any tool that allows further identification and understanding of bacterial contributions to the sedimentary record would be invaluable.

The lipids of certain bacteria are particularly interesting from a hydrogen-isotopic standpoint because of the involvement of exotic sources of hydrogen, such as H_2 and CH_4. Anaerobic fermentation can produce, and sulfate-reducing and methanogenic bacteria will eagerly consume, molecular H_2. Indeed, interspecies hydrogen transfer is a central metabolic process in virtually all anaerobic communities, serving as the pathway for transfer of reducing power between organisms (Belaich *et al.*, 1990). Both equilibrium and kinetic isotope effects generally lead to H_2 that is strongly de-

pleted in D relative to H_2O (*e.g.,* Luo *et al.*, 1991; Bottinga, 1969). It is possible, therefore, that the biomass of bacteria producing H_2 could become D-enriched, and that the biomass of those consuming H_2 could become D-depleted. If realized, such an isotopic directional arrow would be tremendously valuable to biologists and geochemists alike.

Methane also provides an isotopically unusual source of hydrogen. Strong depletion of D in both biogenic and thermogenic methane is well documented (Schoell, 1980; Whiticar *et al.*, 1986), and it is frequently possible to distinguish the multiple sources of methane on the basis of isotopic ratios. In the analogous case of carbon isotopes, organisms consuming CH_4 produce ^{13}C-depleted lipids which serve as diagnostic geochemical evidence for the presence of methane consumption (Hayes, 1993; Hinrichs *et al.*, 1999). Currently, it is unknown whether the strong depletion of D in methane is reflected by the δD values of lipids produced by methanotrophs.

A separate motivation for examining hydrogen-isotopic fractionations in bacteria is that the biochemical processes that control them are complicated. Although H_2O is ultimately the only source of hydrogen in higher plants, there are many intervening products and processes that affect the pathway from H_2O to lipid hydrogen. For example, organelles provide cellular compartments with potentially differing isotopic compositions. Carbohydrate storage products are formed that can exchange hydrogen isotopes with H_2O as they are reprocessed for growth. In contrast, the hydrogen biochemistry of prokaryotes is relatively simple: heterogeneity due to organelles and multicellular bodies is eliminated, the number and complexity of biochemical pathways is greatly reduced, and carbohydrate storage products are much less prevalent. Bacteria therefore provide an attractive point of entry for studying the fundamental processes that govern hydrogen-isotopic fractionation in lipids.

In this study we systematically examine D/H ratios in lipids produced by the aerobic methane-oxidizing bacterium *Methylococcus capsulatus* (strain Bath) and by four species of anaerobic sulfate-reducing bacteria (SRB). The major goal was to determine the magnitude and direction of isotopic fractionation in these two major types of bacterial metabolism, in order to test the hypothesis that δD measurements can positively identify lipids produced by these bacteria in a typical sedimentary environment. A secondary goal was to provide preliminary evidence regarding the

biochemical processes responsible for fractionation in bacterial lipids. *M. capsulatus* was therefore grown in multiple, parallel cultures where the D/H ratio of both CH_4 and H_2O were varied independently, allowing quantitative determination of the sources of lipid hydrogen in this organism. *M. capsulatus* was chosen because: 1) it grows easily and rapidly in laboratory culture, 2) detailed information on carbon-isotopic fractionations in its lipids is available, and 3) the relatively simple metabolism of this bacterium is particularly amenable to deciphering sources of lipid hydrogen within the organism.

The sulfate-reducing bacteria *Desulfobacterium autotrophicum*, *Desulfobacter hydrogenophilus*, *Desulfotomaculum acetoxidans*, and *Desulfovibrio desulfuricans* were previously grown to study carbon-isotopic fractionations in several genera that utilize different carbon-fixation pathways (K. Londry *et al.*, in press). We have measured δD of fatty acids in those same cultures to provide a preliminary perspective on isotopic fractionations in this important group of anaerobic bacteria. However, because the D/H ratio of hydrogen sources was not varied in these cultures, the sources of lipid hydrogen cannot be tracked at the same level of detail as in *M. capsulatus*.

EXPERIMENTAL

Methylococcus capsulatus

Culture techniques have been described by Jahnke (1992) and by Jahnke and Nichols (1986). Briefly, *M. capsulatus* was grown in water-jacketed flasks at 40°C, continuously bubbled with 100 mL/min of a mixture of CH_4 (50%), O_2 (9.6%), CO_2 (0.8%), and N_2 (40%). Growth medium was the mineral salts of Whittenbury and Dalton (1981) with 7.5 μM $CuSO_4$ added to inhibit expression of the soluble form of methane mono-oxygenase enzyme (sMMO). Two isotopically distinct supplies of CH_4 and H_2O were used for the experiments (Table 5-1). Deuterium-enriched CH_4 was prepared by mixing 0.0266 L-atm of CH_3D (Cambridge Isotope Labs, Andover, MA) with 340 L-atm of ultra-high-purity CH_4 (Scott Gas, Fremont, CA) in a high-pressure cylinder. Deuterium-enriched H_2O was prepared by mixing 300 μL of 99.5% D_2O (Cambridge Isotope Labs) with 20 L of distilled H_2O

Table 5-1. Summary of experimental conditions

Species	Expt.	H-source	δD (‰)	O.D.[a]	Cell density[b]
Methylococcus	I	CH_4	−150	0.273	70
capsulatus		H_2O	−87		
	II	CH_4	+111	0.230	66
		H_2O	−87		
	III	CH_4	+111	0.163	48
		H_2O	+104		
	IV	CH_4	−150	0.338	84
		H_2O	+104		
	V	CH_4	−150	0.195	37
		H_2O	+104		
	VI	CH_4	−150	0.401	400
		H_2O	−87		
Desulfobacter	VII, VIII	H_2	−210		
hydrogenophilus		H_2O	−84		
	IX,X	acetate	−95		
		H_2O	−84		
Desulfobacterium	XI,XII	H_2	−210		
autotrophicum		H_2O	−84		
	XIII, XIV	acetate	−95		
		H_2O	−84		
Desulfotomaculum	XV, XVI	H_2	−210		
acetoxidans		H_2O	−84		
	XVII, XVIII	acetate	−95		
		H_2O	−84		
Desulfovibrio	XIX, XX	H_2	−210		
desulfuricans		H_2O	−84		
		acetate	−95		
	XI, XII	lactate	−58		
		H_2O	−84		

[a] Optical density at harvest, measured at 420 nm.
[b] Cell density at harvest, mg dry biomass/L.

(δD = –87‰) in a glass carboy. The δD value of each CH_4 and H_2O source was determined at Indiana University by offline combustion (of CH_4), reduction to H_2 over U turnings, and measurement by dual-inlet isotope-ratio mass spectrometry following the method described by Schimmelmann *et al.* (1999).

Starter cultures used to inoculate each culture were prepared in non-enriched CH_4 and H_2O for all experiments, but comprised < 0.5% of the final harvested biomass. Cultures were harvested based on optical density measured at 420 nm using a Milton-Roy 401 spectrophotometer. Exponential phase cultures (I, II, III, V) were harvested at OD ≈ 0.2, and stationary phase cultures (IV, VI) were harvested at OD > 0.3 (Table 1). Culture VI was grown to a very high cell density of 400 mg/L. Harvested cells were immediately centrifuged then lyophilized.

Extraction and preparation of lipids is similar to that described by Summons *et al.* (1994). Briefly, Bligh and Dyer (1959) extraction followed by cold-acetone precipitation produced an acetone-soluble fraction (supernatant) and a phospholipid fraction (precipitate). Solid-phase extraction of the acetone-soluble lipids on amino-propyl stationary phase (Sessions *et al.*, 1999) produced two fractions: hydrocarbons + sterols eluted with 5 mL of 9:1 DCM/acetone, and fatty acids eluted with 8 mL of 4:1 DCM/formic acid. Fatty acids in this fraction are assumed to represent mostly free fatty acids, although may be derived in part from transesterification of diacyl- and triacyl-glycerols, or from cleavage of phospholipids during sample workup. 10% of the phospholipid fraction was set aside for analysis of fatty acids. Hopanol cleavage products were prepared from the remainder of the phospholipid fraction by periodate oxidation - $NaBH_4$ reduction (Rohmer *et al.*, 1984), then separated from fatty acids by solid-phase extraction.

Both acetone-soluble and phospholipid fatty acid fractions were derivatized as methyl esters by heating with CH_3OH/acetyl-chloride. The dimethylated derivative of phthalic acid was prepared in parallel with each group of samples in order to measure the δD value of H added by methylation. The δD of disodium phthalate was determined by offline combustion/reduction to be -97.0 ± 0.6‰, and the δD of methanol H added by derivatization was measured by difference to be -102 ± 3‰. Sterol and hopanol fractions were derivatized as acetyl esters by heating with acetic anhydride/ pyridine. The δD value of this acetate H was previously measured by offline combustion/reduction (Sauer *et al.*, 2001).

Individual lipids were identified by GCMS using a Hewlett Packard 5973 mass-selective detector and their abundance was quantified by GC/FID relative to an internal standard (pristane or epiandrosterone). Hydrogen isotope ratios were measured using a Finnigan-MAT Delta+XL connected to an HP 6890 gas chromatograph via the Finnigan GC-III thermal conversion interface. The H_3 factor for this instrument was measured daily by injecting pulses of H_2 gas with constant δD and peak heights varying over a 10-fold range, and was typically < 6 ppm mV^{-1} with a daily variability of about 0.1 ppm mV^{-1}. Mass-2 and -3 ion-current data were collected in 250-ms intervals, and corrected for H_3^+ contributions using the "pointwise" correction of Sessions *et al.* (2001a). Data were processed with Isodat NT software version 1.1 (Finnigan-MAT, Bremen). Considering the

range of peak-height and δD differences between sample and standard peaks, variability in the H_3 factor, and time constants associated with data collection and processing, the maximum systematic error expected due to H_3^+ correction for these samples is $< 0.9‰$.

Two types of isotopic standards were analyzed. A mixture of $C_{16} - C_{30}$ n-alkanes ("external standards"), with concentrations varying over a five-fold range (see details in Sessions *et al.*, 2001a), was analyzed after every third sample analysis. Between three and five n-alkanes ("internal standards") were also coinjected with each unknown sample at concentrations similar to those of the analytes. One of the coinjected compounds was used as the isotopic reference peak for each analysis (n-C_{18} for fatty acids, $\delta D = -55‰$; n-C_{32} for sterols and hopanols, $\delta D = -210‰$), while the remaining standards were used to assess accuracy.

Sulfate-Reducing Bacteria

Four strains of SRB were grown, all obtained from the American Type Culture Collection: *Desulfobacter hydrogenophilus*, *Desulfobacterium autotrophicum*, *Desulfotomaculum acetoxidans*, and *Desulfovibrio desulfuricans*. These cultures are the same as those described in Londry *et al.* (in press). *Desulfobacter, Desulfobacterium*, and *Desulfotomaculum* were all grown heterotrophically on acetate, and were grown autotrophically on H_2 plus CO_2. *Desulfovibrio* is an incomplete oxidizer, and will oxidize organic substrates to acetate that is then excreted. In addition, *Desulfovibrio* can use H_2 to reduce sulfate for energetic requirements, but cannot fix CO_2 so an organic carbon source must be supplied during lithotrophic growth. For these reasons, *Desulfovibrio* was grown heterotrophically on lactate, and lithotrophically on H_2 plus sulfate, but with acetate supplied as an organic carbon source.

Cultivation of these SRB is described in detail by Londry *et al.* (in press) and is summarized here. All experiments were batch cultures prepared anaerobically in 2.2-L sealed media bottles. Cultures were incubated at 30ºC with rotary shaking (100 rpm) in the dark. The SRB were grown in saltwater (*Desulfobacterium*, *Desulfobacter*) or freshwater (*Desulfotomaculum*, *Desulfovibrio*) mineral media containing 20 mM sulfate. Media was reduced with 0.6 mM sulfide and 20 mg/L dithionite just prior to innoculation. For heterotrophic experiments, 10 mM sodium acetate or so-

dium lactate was supplied (5 mM acetate for *Desulfotomaculum*, to reduce sulfide toxicity effects). The gas phase of each culture bottle consisted of 80/20 N_2/CO_2 (heterotrophic cultures) or 80/20 H_2/CO_2 (lithotrophic cultures). Lithotrophic cultures of *Desulfovibrio* were supplemented with 10 mM acetate as an organic carbon source. δD values of H_2O, H_2, acetate, and lactate supplied to the cultures were all measured at Indiana University by offline combustion/reduction and dual-inlet isotope-ratio mass spectrometry (Schimmelmann *et al.*, 1999).

Growth was monitored by consumption of substrates for heterotrophic cultures, and by headspace pressure decrease for lithotrophic cultures. Cultures were harvested by centrifugation as they entered stationary phase and were immediately lyophilized. Cells were examined microscopically following harvest to ensure that the cultures were axenic. Lipids were extracted using a modified Bligh and Dyer procedure (Jahnke *et al.*, 1992), followed by mild alkaline methanolysis to prepare the methyl-ester derivatives of phospholipid fatty acids. Fatty acid methyl esters (FAME's) were further purified by thin-layer chromatography, and individual FAME's were quantified by GC/FID. The positions of double bonds were assigned by comparison to published results.

D/H ratios of fatty acids were measured using the GC-pyrolysis-IRMS system assembled and described by Sessions *et al.* (2001b). Data were collected at 250-ms intervals using Isodat v7.1 (Finnigan-MAT) and corrected for contributions from H_3^+ utilizing the pointwise method of Sessions *et al.* (2001a). All data were processed using Microsoft Excel. The magnitude and variability of the H_3 factor for this instrument has been documented over the same time interval as the measurements reported here by Sessions *et al.* (2001b). Considering all factors, H_3^+-related errors for these samples are expected to be < 3.5‰.

Analysis of standards was similar to that for *M. capsulatus* lipids. The $C_{16}-C_{30}$ *n*-alkane external standard was analyzed after every three or four analyses of samples. Internal standards coinjected with samples were C_{14}, C_{16}, and $C_{24}-C_{28}$ *n*-alkanes. *n*-C_{16} and *n*-C_{28} alkanes were used as isotopic reference peaks.

Table 5-2. Precision and accuracy of δD measurements

	M. capsulatus			Sulfate-reducing bacteria		
	external standards[a]	internal standards	analytes	external standards[a]	internal standards	analytes
pooled standard deviation[b] (‰)	5.1	5.6	3.7	4.0	5.7	5.7
degrees of freedom	662	139	137	419	227	178
mean error (‰)	0.7	−0.9		0.1	−2.2	
RMS error[c] (‰)	4.9	8.5		3.9	8.8	

[a] The n-C_{16} – n-C_{30} alkane mixture described by Sessions *et al.* (2001a) was the external standard.

[b] $\sqrt{\sum d^2 / \sum (n-1)}$; d is the deviation of each measurement from the mean value of a set of replicates, (n - 1) is the number of degrees of freedom for that set of replicates, both summed over all available sets of replicates.

[c] $\sqrt{\sum d^2 / n}$; d is the deviation of each measurement from the true value, n is the number of measurements

RESULTS AND DISCUSSION

D/H ratios in lipids from *M. capsulatus* and from SRB were measured using different analytical systems. Accordingly, we separate the two sets of results for the purpose of assessing precision and accuracy. Statistics calculated for external and internal standards and for sample analytes are provided in Table 5-2. The arithmetic mean error for all standards, both external and internal, was between -2.2 and $+0.7$‰.

The root-mean-square (RMS) accuracy of external standards for *M. capsulatus* was 4.9‰, while for internal standards it was 8.5‰. This decrease in accuracy, with no substantial decrease in precision, is due primarily to systematic offsets in two of the internal standards. The C_{30} n-alkane internal standard coinjected with sterol and hopanol fractions produced a mean error of -11.0 ± 5.1‰ ($n = 42$), while n-C_{23} coinjected with phospholipid fractions produced a mean error of $+13.7 \pm 3.3$‰ ($n = 18$). The other six coinjected n-alkanes revealed no systematic errors, so the cause of errors in n-C_{23} and n-C_{30} is likely to be coelution of other peaks with the standard compounds, or fractionation of the standard compounds during preparation or handling. Considering all these factors, the accuracy of

δD measurements for *M. capsulatus* probably approaches 5‰, though it is possible that systematic errors as large as 14‰ exist for specific analytes.

A similar situation was encountered for analyses of SRB lipids. The RMS accuracy of external standards was 3.9‰, while for internal standards was 8.8‰. The 13:0 FAME internal standard produced a mean error of -20 ± 9‰. If this result is discounted, the other five internal standards were measured with an RMS accuracy of 5.3‰. As with *M. capsulatus*, we conclude that the accuracy of δD measurements for SRB lipids probably approaches 5‰, though larger systematic errors may exist for specific analytes.

The precision of sample analyses, as measured by the pooled standard deviation, was 3.7‰ for *M. capsulatus* and 5.7‰ for SRB, despite the similarities in accuracy for the two sets of measurements. The fact that precision of sample measurements from *M. capsulatus* greatly exceeds that for corresponding standards probably reflects the difference between short-term and long-term precision. These results emphasize that while impressive precision may be obtained for individual compounds analyzed repeatedly under identical conditions, long-term accuracy in hydrogen isotopic measurements is significantly more difficult to achieve.

Table 5-3. Lipid concentrations obtained from *M. capsulatus* cultures

Lipid	Culture					
	I	II	III	IV	V	VI
14:0 fatty acid (AS[a])	2.2[b]	0.10	0.14	2.8	0.10	1.2
14:0 fatty acid (PL[a])	0.56	2.1	2.0	0.49	1.5	3.8
16:1 fatty acid[c] (AS)	25	1.8	2.8	37	2.0	9.1
16:1 fatty acid[c] (PL)	9.1	29	31	5.8	26	18
16:0 fatty acid (AS)	21	1.8	2.5	29	2.3	7.9
16:0 fatty acid (PL)	12	30	31	10	29	30
squalene	3.5	1.6	1.1	1.4	0.79	0.56
4α-methyl-5α-cholest-8(14)-en-3β-ol	3.8	1.4	1.4	1.7	1.1	2.5
diplopterol +	3.0	1.5	1.4	1.1	1.0	0.51
4α-methyl-5α-cholest-8(14),24-dien-3β-ol						
4,4-dimethyl-5α-cholest-8(14)-en-3β-ol	5.4	2.3	2.1	2.5	1.7	1.2
4,4-dimethyl-5α-cholest-8(14),24-dien-3β-ol	0.14	0.23	0.89	0.11	0.22	0.049
hopan-30-ol	2.1	2.3	3.6	4.3	12	3.1
3β-methylhopan-30-ol	3.8	3.0	4.0	6.5	12	13

[a] AS = acetone-soluble fraction, PL = phospholipid fraction.
[b] Units for all values are μg lipid / mg dry biomass.
[c] Mixture of up to 4 positional isomers.

Table 5-4. δD values of *M. capsulatus* lipids

Lipid	Culture					
	I	II	III	IV	V	VI
14:0 fatty acid (AS[a])	−157[b]			−16		−157
14:0 fatty acid (PL[a])					−17	−177
16:1 fatty acid[c] (AS)	−172	−95	41	−59	−43	−169
16:1 fatty acid[c] (PL)	−171	−94	33	−50	−33	−172
16:0 fatty acid (AS)	−122	−55	88	−19	−4	−146
16:0 fatty acid (PL)	−130	−53	89	−3	23	−138
squalene	−258	−208	−103	−162	−142	−251
4α-methyl-5α-cholest-8(14)-en-3β-ol + diplopterol	−255	−199	−92	−162	−149	−258
4α-methyl-5α-cholest-8(14),24-dien-3β-ol			−87			
4,4-dimethyl-5α-cholest-8(14)-en-3β-ol	−250	−188	−75	−152	−135	−256
4,4-dimethyl-5α-cholest-8(14),24-dien-3β-ol			−81			
hopan-30-ol	−256	−209	−99	−162	−160	−245
3β-methylhopan-30-ol	−231	−168	−45	−132	−126	−233
CH_4[d]	−150	111	111	−150	−150	−150
H_2O[d]	−87	−87	104	104	104	−87

[a] AS = acetone-soluble fraction, PL = phospholipid fraction.
[b] All values are means from 3 or more analyses, and have been corrected for hydrogen added by derivatizing agents.
[c] Mixture of up to 4 positional isomers.
[d] Values repeated from Table 5-1.

Methylococcus capsulatus

Concentrations of extracted lipids in *M. capsulatus* are summarized in Table 5-3, and δD values measured for those lipids are summarized in Table 5-4. In general, fatty acids were about ten-fold more abundant in the phospholipid fraction than in the acetone-soluble fraction. The increase in acetone-soluble fatty acids and proportionate decrease in phospholipids in cultures I and IV probably represent hydrolysis of the phospholipids during extraction. The 16:0 and 16:1 fatty acids were obtained from both acetone-soluble and phospholipid fractions of every experiment in sufficient quantity for isotopic analysis. The 14:0 fatty acid was present in all cultures, but was sufficiently abundant for isotopic analysis only in cultures I, IV, V, and VI. *M. capsulatus* produces up to four positional isomers of 16:1 fatty acids (Δ^8, Δ^9, Δ^{10}, and Δ^{11}; Jahnke and Diggs, 1989) which were not chromatographically separated in our analyses, so composite values are reported in Tables 5-3 and 5-4 for all 16:1 isomers.

M. capsulatus is unique in producing sterols via the oxygen-dependent cyclization of squalene, as well as hopanols via oxygen-independent cyclization. *M. capsulatus* produces two abundant

sterols: 4α-methyl-5α(H)-cholest-8(14)-en-3β-ol, and 4,4-dimethyl-5α-cholest-8(14)-en-3β-ol (Summons *et al.*, 1994). The $\Delta^{8(14),24}$ diunsaturated analogs of these two sterols are also produced in lower abundance. Quantities of the diunsaturated sterols were sufficient for isotopic analysis only in culture III. Squalene and diploptene were also abundant in the acetone-soluble fraction. In GCMS analyses using a DB-5ms analytical column (J&W Scientific), diploptene coeluted with 4-methylcholestadienol. In irmGCMS analyses using an HP-1 analytical column (Agilent Technologies) diploptene coeluted with 4-methylcholestenol, and a single combined δD value is reported for these compounds in Table 5-4. Diploptene was present at roughly the same abundance as 4-methylcholestenol in all cultures. Hopan-30-ol and 3-methylhopan-30-ol were abundant in the periodate cleavage products of bacteriohopanepolyol. Smaller amounts of C_{31} hopanol and methylhopanol were also present, but sufficient quantities were not available for isotopic measurement.

Although cultures of *M. capsulatus* were not replicated, comparison of cultures harvested during exponential and stationary phase indicates that the reproducibility of δD values between cultures was within ± 20‰ (2σ). Values of δD in both fatty acids and triterpenols responded strongly to changes in δD of either methane or water. In general, lipids were depleted in D relative to water but D-enriched relative to methane. Cultures in which δD of methane was enriched relative to that of water, a situation almost never encountered in nature, are an exception to this pattern. Because there are two hydrogen sources in these cultures, developing a quantitative description of the fractionation between CH_4, H_2O, and lipids first requires knowledge of the proportion of lipid hydrogen derived from each source.

Hydrogen sources for lipids. Lipid hydrogen in *M. capsulatus* can derive from CH_4 or from H_2O. Allowing for fractionation associated with utilization of each hydrogen source, the hydrogen isotopic composition of a particular lipid will be described by

$$\delta D_l = f_m\left(\delta D_m + \varepsilon_{l/m}\right) + \left(1 - f_m\right)\left(\delta D_w + \varepsilon_{l/w}\right) \qquad (1)$$

where the subscripts *l*, *m*, and *w* indicate lipid, methane, and water, respectively, and f_m is the fraction of hydrogen derived from methane. Values of epsilon, defined as

$\varepsilon_{a/b} \equiv 1000\left[\left(\delta D_a + 1000\right)/\left(\delta D_b + 1000\right) - 1\right],$ represent the isotopic fractionations between hydrogen sources (water or methane) and lipid hydrogen. In this formulation, ε represents the net fractionation resulting from many individual isotope effects, including those due to substrate assimilation, biosynthetic fractionations, exchange, and perhaps others. Many of these individual effects may change with varying growth conditions, but at present such a level of detail cannot be discerned. Note also that $\varepsilon_{l/w}$ and $\varepsilon_{l/m}$ can have different values for each lipid.

The terms in equation 1 can be expanded and rearranged to yield

$$\delta D_l = f_m \delta D_m + (1 - f_m)\delta D_w + f_m \varepsilon_{l/m} + (1 - f_m)\varepsilon_{l/w} \tag{2}$$

The values of δD_m and δD_w were varied in our cultures, while f_m, $\varepsilon_{l/m}$, and $\varepsilon_{l/w}$ are properties of the bacteria and cannot easily be manipulated. Since growth conditions were identical between cultures, we assume that the values of f_m, $\varepsilon_{l/m}$, and $\varepsilon_{l/w}$ were constant for a given lipid in all cultures. The last two terms in equation 2 are therefore constant, giving:

$$\delta D_l = f_m \delta D_m + (1 - f_m)\delta D_w + \Delta_l \tag{3}$$

where $\Delta_l = f_m \varepsilon_{l/m} + (1 - f_m)\varepsilon_{l/w}$ and represents the weighted-average isotopic fractionation between lipids and hydrogen sources.

Our approach to solving equation 3 was to use a numerical minimization of errors for the six cultures, as follows. Values of δD were independent of growth phase (see below), so all six cultures were treated equally in our analysis. For each compound, a unique set of values for f_m and Δ_l was first assumed. The predicted value for δD_l in each culture was then calculated using equation 3, with appropriate values for δD_m and δD_w obtained from Table 5-1. Comparing the predicted values of δD_l to the measured values of δD_l, we calculated the sum of squared errors ($= \sum_{n=1}^{6}\left[\left(\delta_{n,m} - \delta_{n,p}\right)^2\right]$, where the subscripts m and p represent measured and predicted δD values, summed over all six cultures) and recorded that value. By systematically varying the values of f_m and Δ_l across a wide range, we obtained unique values for f_m and Δ_l that correspond to the minimum sum of squared errors.

Table 5-5. Fraction of lipid H derived from methane (f_m) and average hydrogen isotopic fractionation (Δ_l)

Lipid	f_m	Δ_l (‰)	$r^{2\,a}$
squalene	0.29	−175	.983
4-methyl sterol + diplopterol	0.32	−171	.994
4,4-dimethyl sterol	0.32	−162	.992
hopanol	0.31	−175	.985
3-methyl hopanol	0.34	−140	.994
16:1 fatty acid (AS)	0.33	−68	.993
16:1 fatty acid (PL)	0.30	−68	.995
16:0 fatty acid (AS)	0.33	−28	.985
16:0 fatty acid (PL)	0.29	−23	.991

[a] Correlation coefficient between measured δD values and those predicted using equation 3.

The resulting values for f_m and Δ_l associated with each lipid are summarized in Table 5-5, along with the correlation coefficient (r^2) for comparison of predicted versus measured δD_l values. The value of f_m was surprisingly constant at 0.314 ± 0.017 across the entire suite of compounds examined, while Δ_l varied from a maximum of –23‰ in fatty acids to a minimum of –175‰ in triterpenols. Values of r^2 were greater than 0.98 in every case, indicating that all six cultures are fit very well by equation 3 using a single set of values for f_m and Δ_l. The parameter Δ_l combines information about isotopic fractionation of both hydrogen sources ($\varepsilon_{l/m}$ and $\varepsilon_{l/w}$). Unfortunately, because both $\varepsilon_{l/m}$ and $\varepsilon_{l/w}$ remain constant, we cannot uniquely solve for either variable. Instead, the equation $\Delta_l = f_m(\varepsilon_{l/m})$ + $(1 - f_m)(\varepsilon_{l/w})$ provides a functional relationship between $\varepsilon_{l/m}$ and $\varepsilon_{l/w}$. If the value of one variable is known the other can be calculated. To independently obtain unique values for $\varepsilon_{l/m}$ and $\varepsilon_{l/w}$, the value of f_m for a particular lipid would have to vary between cultures while $\varepsilon_{l/m}$ and $\varepsilon_{l/w}$ remained constant. Since f_m is dependent on the organism rather than conditions of growth, this is not possible.

Hydrogen-isotopic fractionation in M. capsulatus. In photoautotrophs, where H_2O represents the only source for organic hydrogen, the value of $\varepsilon_{l/w}$ can be measured directly. In higher plants and in the few photosynthetic algae examined to date, $\varepsilon_{l/w}$ has a mean value of approximately –150‰ for fatty acids and –225‰ for triterpenols (Sauer *et al.*, 2001; Sessions *et al.*, 1999; Estep and Hoering, 1980). In *M. capsulatus*, Δ_l represents the weighted average of both $\varepsilon_{l/w}$ and $\varepsilon_{l/m}$. Values of Δ_l in *M. capsulatus* fatty acids are 75 – 100‰ smaller (less negative) than corresponding values of $\varepsilon_{l/w}$ in
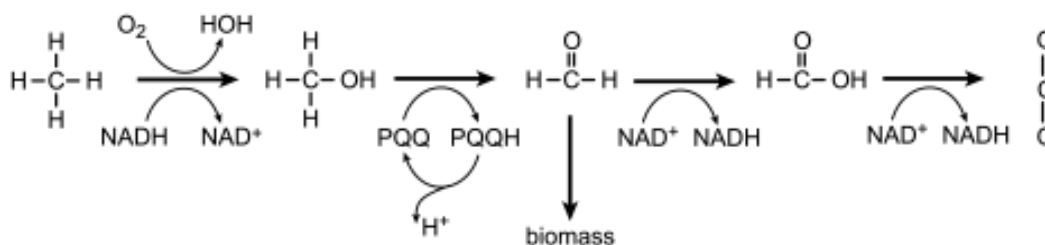
Figure 5-1. The oxidation of CH_4 to CO_2 in *M. capsulatus* (after Anthony, 1982). An intermolecular kinetic isotope effect leads to methane entering the pathway that is depleted in D relative to supplied methane. An intramolecular isotope effect leads to methanol that is enriched in D relative to methane entering the pathway. PQQ is the prosthetic group of methanol dehydrogenase, and transfers only electrons from methanol to electron-transport chains.

photoautotrophs. If we assume that $\varepsilon_{l/w}$ for fatty acids in *M. capsulatus* is –150‰, as in plants, then $\varepsilon_{l/m}$ for fatty acids must be close to +150‰, *i.e.,* hydrogen derived from methane is D-enriched relative to the methane source. Similarly, if we assume that $\varepsilon_{l/w}$ for isoprenoid lipids in *M. capsulatus* is –225‰, then $\varepsilon_{l/m}$ must be close to +20‰.

Studies of the oxidation of methane by the soluble form of methane monooxygenase (sMMO) indicate the presence of both intermolecular and intramolecular isotope effects (Figure 5-1; Nesheim and Lipscomb, 1996; Wilkins *et al.*, 1994). The magnitude of the intermolecular isotope effect was estimated as 1.75 from the comparison of the reaction velocities of CH_4 and CD_4 (Wilkins *et al.* (1994). Accordingly, methane entering the oxidation pathway will be depleted in D relative to the supplied methane. The magnitude of the intramolecular isotope effect was estimated at 1.29 (Wilkins *et al.*, 1994), indicating that H is preferentially removed from methane relative to D, producing methanol that is enriched in D relative to the oxidized methane. Although it has not been studied, a similar intramolecular isotope effect is likely present during the oxidation of methanol to formaldehyde. The directions of these isotope effects counteract each other with respect to the hydrogen-isotopic composition of formaldehyde, the compound that is assimilated into biomass (Anthony, 1982). On the other hand, water resulting from the oxidation of methane should be strongly depleted in D relative to the supplied methane as a result of both intermolecular and intramolecular isotope effects. Our estimates of $\varepsilon_{l/m}$ for *M. capsulatus* lipids indicate a small enrichment in D
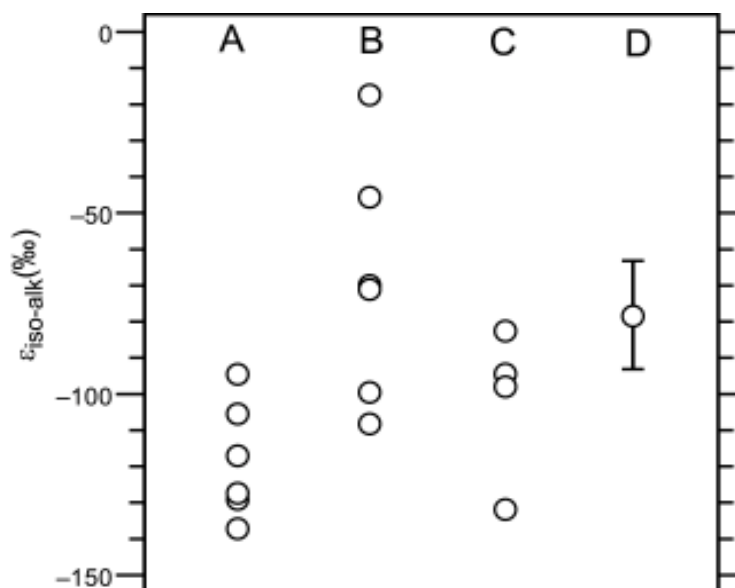
Figure 5-2. Hydrogen isotopic fractionation between isoprenoid and *n*-alkyl lipids. Except for group D, each point represents the fractionation (ε) between the mean δD values for *n*-alkyl lipids and isoprenoid lipids in a single plant or culture. Marker for group D indicates the mean and 1σ range for *n*-alkyl and isoprenoid lipids extracted from lake sediments. Group A — current *M. capsulatus* experiments; B — aquatic higher plants, brown algae, diatoms, dinoflagellates (Sessions *et al.,* 1999); C — terrestrial and aquatic higher plants (Estep and Hoering, 1980); D — extractable lipids in Great Pond sediments (Sauer *et al.,* 2001).

during the incorporation of methane hydrogen, and thus suggest that some methane hydrogen is incorporated into lipids via formaldehyde enriched in D by intramolecular fractionations.

The average isotopic fractionation between isoprenoid and *n*-alkyl lipids ($\varepsilon_{iso/alk}$) within a culture of *M. capsulatus* is -119 ± 16‰ (Figure 5-2). By comparison, values of $\varepsilon_{iso/alk}$ for sterols and fatty acids in individual plants and algae range from -18 to -132‰, with a mean of -82‰ (Sessions *et al.*, 1999; Estep and Hoering, 1980). The average isotopic fractionation between *n*-alkanes and plant sterols extracted from Great Pond sediments was -78 ± 15‰ (Sauer *et al.*, 2001). Several explanations have been suggested for the hydrogen isotopic differences between *n*-alkyl and isoprenoid lipids, including fractionation in biosynthetic pathways, differences in time or location of biosynthesis, and differences in the amount of hydrogen derived from NADPH versus substrates (Estep and Hoering, 1980; Sessions *et al.*, 1999).

Two pathways for the biosynthesis of isopentenyl pyrophosphate (IPP), the precursor building block of all isoprenoid lipids, have been described: the mevalonic acid (MVA) pathway, and the more recently discovered deoxyxylulose-phosphate (DXP) pathway (described in further detail below). The distribution of these two pathways has been well established in higher plants (Lichtenthaler *et al.*, 1999), where the MVA pathway is used to produce cytosolic isoprenoid compounds such as sterols and pentacyclic triterpenols, and the DXP pathway is used to synthesize plastidic isoprenoids, including phytol and carotenoids. In two higher plants and a dinoflagellate examined by Sessions *et al.* (1999), phytol was consistently depleted relative to sterols by 50–100‰. They suggested that difference might be due to characteristic fractionations of the MVA and DXP pathways. The isoprenoid pathway used by *M. capsulatus* is unknown, but nearly all other Proteobacteria that have been examined carry genes for enzymes of the DXP pathway exclusively (Lange *et al.*, 2000). If it is confirmed that *M. capsulatus* uses the DXP pathway, then our observation that $\varepsilon_{iso/alk}$ in *M. capsulatus* is similar to that in many plants would imply that there is no difference in D/H fractionation between the two pathways.

Hydrogen pathways in biosynthesis. The value of f_m represents the fraction of lipid hydrogen derived from methane, and is virtually constant across all compounds at $31.4 \pm 1.7\%$ (Table 5-5). To quantitatively discuss the significance of this result, it is first necessary to consider the pathways through which hydrogen flows from CH_4 and H_2O to lipids. During lipid biosynthesis, there are three immediate sources for organic hydrogen: C-bound hydrogen in biosynthetic precursors, hydrogen added during reduction and hydrogenation by NADPH, and hydrogen that exchanges with or is obtained from cellular water during biosynthesis (Figure 5-3; Sessions *et al.*, 1999). There are also three different biosynthetic pathways which must potentially be considered: synthesis of *n*-alkyl lipids from acetate, and synthesis of isoprenoid lipids by either the MVA or DXP pathways. Details about the importance of each hydrogen source vary with the particular biosynthetic pathway, so we begin by briefly summarizing those pathways.

Fatty acid synthesis in both eukaryotes and bacteria proceeds similarly (Figure 5-4), with the head-to-tail linkage of acetyl-ACP units to form a chain that grows in 2-carbon increments (Wakil *et al.*, 1983). Following the addition of acetate to the chain, the carboxyl carbon of the previous ac-
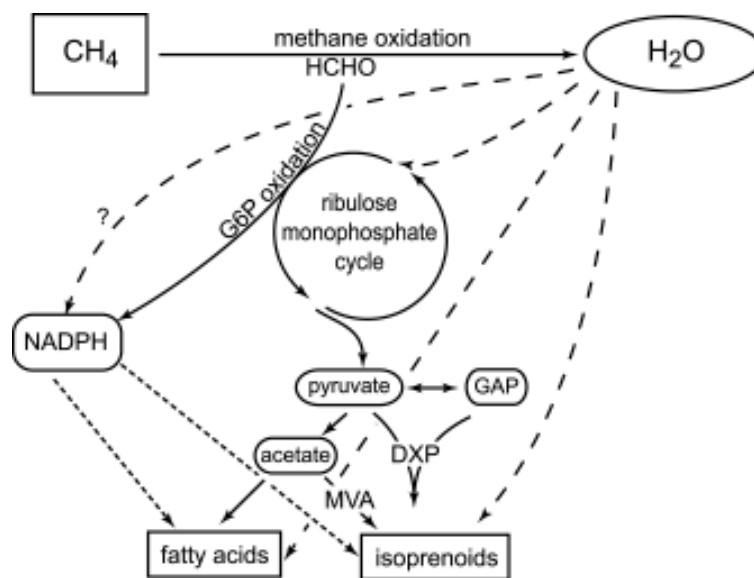
Figure 5-3. Generalized flow of hydrogen in *M. capsulatus* metabolism. Arrows indicate reactions of hydrogen, rather than carbon, so for example CH_4 is oxidized to H_2O. Carbon from methane is incorporated into biomass by the RuMP cycle, but hydrogen from methane is not. Solid lines indicate carbon-bound hydrogen carried on organic substrates; dotted lines indicate hydrogen carried by NADPH; dashed lines indicate hydrogen in water. It is expected that either the MVA or DXP pathway, but not both, operates in *M. capsulatus*. G6P is glucose-6-phosphate, GAP is glyceraldehyde-3-phosphate.
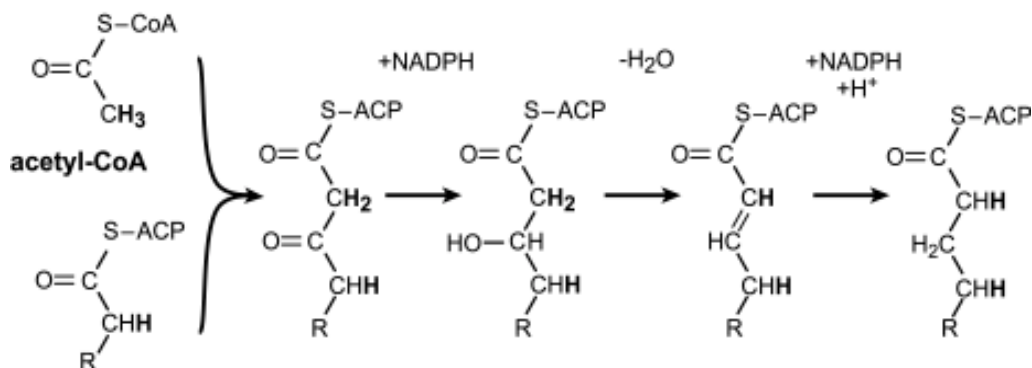

Figure 5-4. Sources of hydrogen during fatty acid biosynthesis (after White, 1995). Hydrogen shown in bold is inherited from methyl groups of acetate. Note that the initial condensation of acetyl-CoA with the fatty acid chain occurs in several steps that do not affect hydrogen budgets and have been omitted. ACP is acyl carrier protein, CoA is coenzyme-A.

etate is reduced to an alcohol by addition of H$^-$ from NADPH. Dehydration then removes the hydroxyl group and one hydrogen from the adjacent methylene (former methyl) group. Addition of a second H$^-$ from NADPH hydrogenates the double bond, with the final H$^+$ probably obtained from water. The net result of this process is that roughly one-quarter of lipid hydrogen is inherited from the methyl group of acetate, one-quarter is obtained directly from water, and one-half is supplied by NADPH. The extent of hydrogen exchange accompanying this process is currently unknown. Up to 75% of C-bound hydrogen is potentially subject to exchange with water via keto-enol tautomerization, although the importance of this exchange probably depends on whether intermediate molecules remain bound to enzymes. In *E. coli* for example, the fatty acid biosynthetic enzymes exist as separate enzymes in the cytosol, while in eukaryotes the enzymes exist as a single complex (White, 1995).

The isoprenoid biosynthetic pathways in *M. capsulatus* have not been studied. Both pathways are therefore summarized below and in Figure 5-5. In the MVA pathway, two acetyl-CoA molecules are condensed to form acetoacetyl-CoA, and a third acetyl-CoA is then added to form the 6-carbon compound 3-hydroxy-3-methylglutaryl-CoA. Two NADPH molecules reduce C-1, a former carboxyl carbon, to the level of methylene. Finally, concerted loss of the carboxyl carbon at C-6 and the hydroxyl group at C-3 results in the fully reduced product IPP, in which 7 out of 9 hydrogens are inherited directly from the methyl groups of acetate and the remaining two are from NADPH.

The DXP pathway begins with the condensation of glyceraldehyde phosphate (GAP) and pyruvate (Figure 5-5; Schwender *et al.*, 1996). During this condensation, the carboxyl carbon of pyruvate is lost, resulting in the 5-carbon intermediate 1-deoxyxylulose phosphate (DXP). A carbon-skeletal rearrangement produces 2-methylerythrose-phosphate, which is then reduced to 2-methylerythritol-phosphate. A series of unknown steps, which must involve two reductions and one dehydration, then lead to IPP. This pathway has only recently been recognized, and the identities of the reducing cofactors have not been confirmed, but are assumed to be NADPH. Considering what is known, 3 of 9 hydrogens in IPP are inherited directly from the methyl group of pyruvate, and 2 to 4 are inherited directly from GAP. The remaining hydrogens (2 – 4) are supplied either by a reductant, presumably NADPH, or by water.
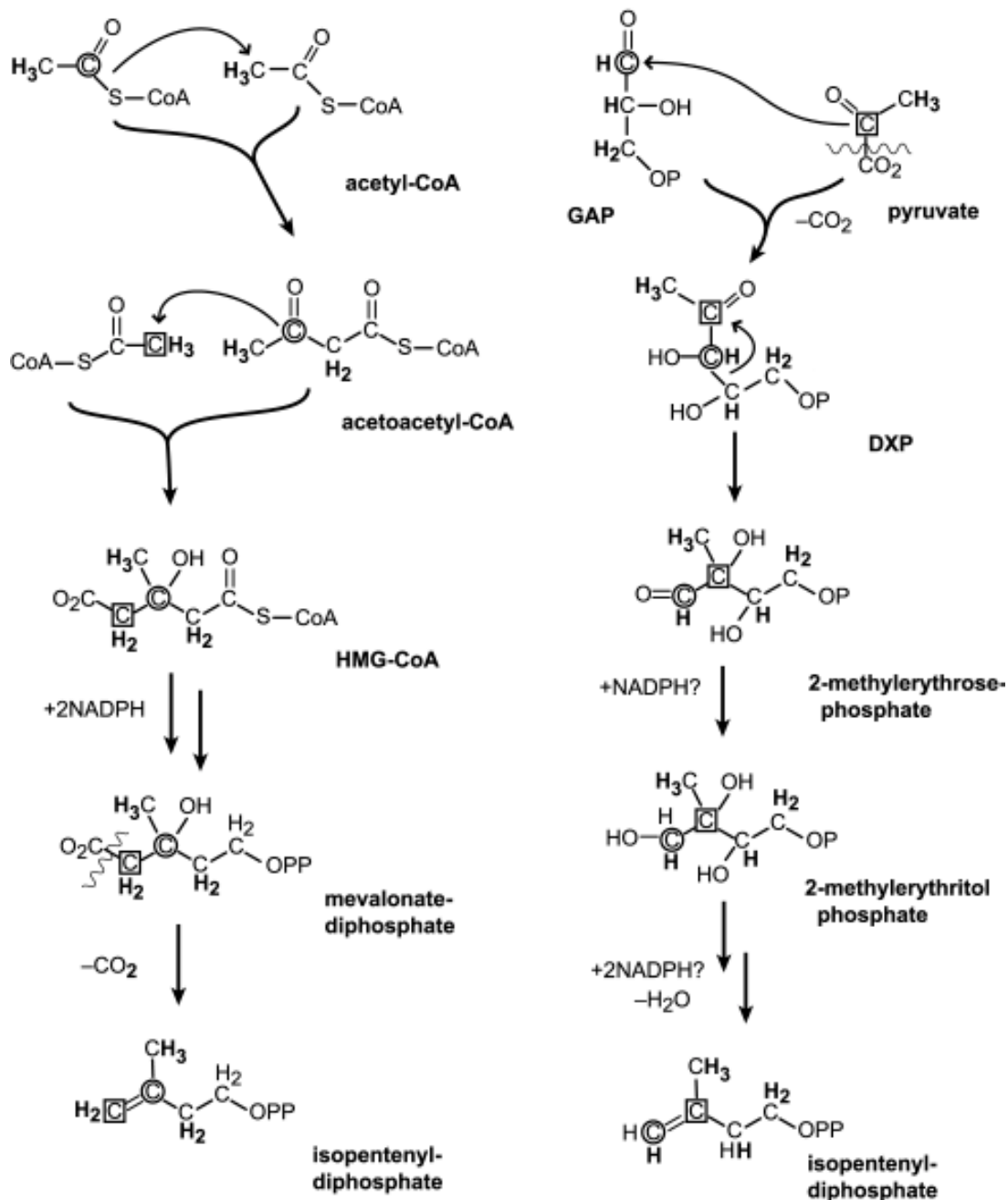
Figure 5-5. Sources of hydrogen during MVA (left) and DXP (right) pathways of isoprenoid bio-synthesis (after Lange *et al.*, 2000). Hydrogen shown in bold is inherited from organic substrates. Circles and boxes around carbon atoms are present for identification. Abbreviations: HMG, 3-hydroxy-3-methylglutarate; GAP, glyceraldehyde-3-phosphate; DXP, 1-deoxy-D-xylulose-5-phosphate. Two arrows indicate multiple steps that have been condensed in this illustration.
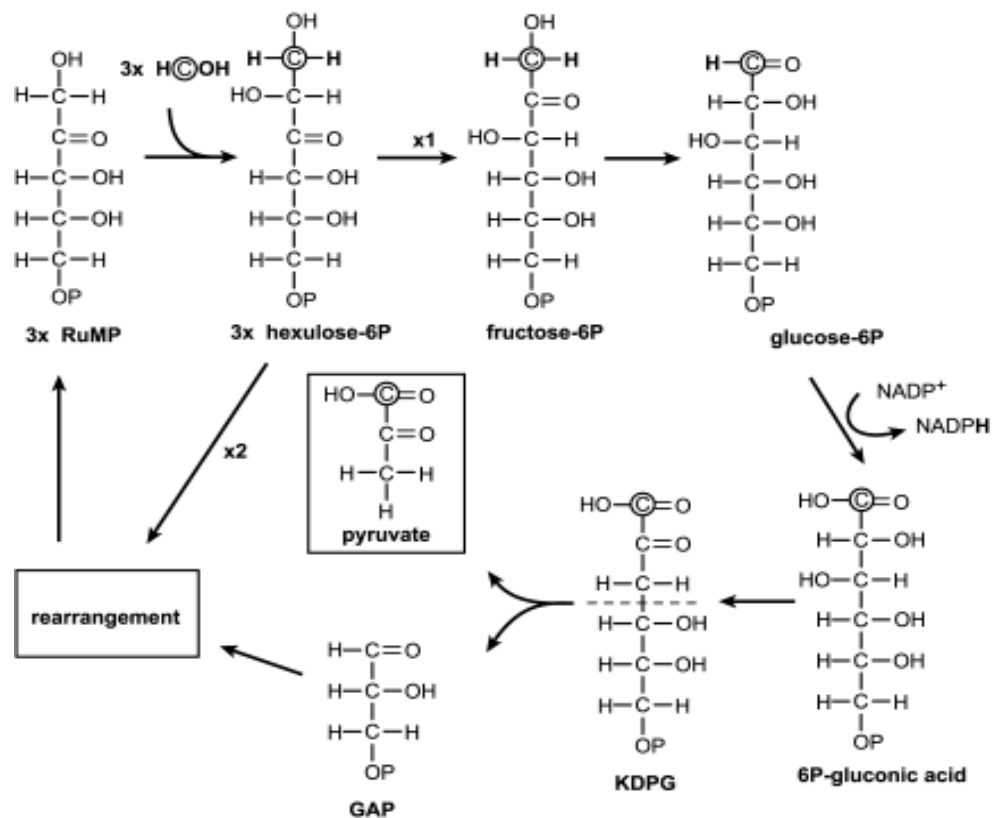
Figure 5-6. RuMP cycle for assimilation of carbon in *M. capsulatus* (after Anthony, 1982). Abbreviations: RuMP, ribulose-5-phosphate; KDPG, 2-keto-3-deoxy-6-phosphogluconate; GAP, glyceraldehyde-3-phosphate. Hydrogen shown in bold is that inherited from methane.

To make the connection between these immediate sources of hydrogen (NADPH, organic substrates) and the ultimate sources of hydrogen (CH_4 and H_2O), it is necessary to trace in turn the sources of hydrogen to NADPH and to organic substrates. In *M. capsulatus*, carbon is assimilated through the ribulose-monophosphate (RuMP) cycle (Figure 5-6). Carbon enters the pathway as formaldehyde, and is condensed with the 5-carbon sugar ribulose-5-phosphate (Anthony, 1982). A series of isomerizations produces glucose-6-phosphate, which is then oxidized (yielding NADPH) to 6-phosphogluconate. The carbon inherited from formaldehyde is C-1, the carboxyl group of gluconate, so no hydrogen is transferred directly (*i.e.*, with the C-H bond remaining intact) from methane to biomass. It is possible that methane hydrogen is transferred from C-1 of hexulose-6P to other carbon positions during isomerization reactions, but for now we assume this is not the case.

In most eukaryotes and eubacteria that have been examined, the roles of NADH and NADPH are clearly separated between catabolic and anabolic processes, respectively (White, 1995). In some methanotrophs, though not in *M. capsulatus* specifically, cytochromes in electron-transport chains have been shown to use both NADH and NADPH as substrates (Anthony, 1982). In these bacteria, it is possible that NADH and NADPH are interchangeable, so both sources of reducing power must be considered. Major sources of NADH are the oxidation of formaldehyde to formate, and the oxidation of formate to CO_2, as part of the methane oxidation pathway (Figure 5-1). H^- transferred to NAD^+ in these reactions is derived from methane. A major source of NADPH is the oxidation of glucose-6-phosphate during the RuMP cycle of carbon assimilation (Figure 5-6). H^- transferred to $NADP^+$ from glucose-6-phosphate is also inherited from methane. Unfortunately, there is little information about alternative sources of NADPH, such as the pentose-phosphate pathway, in *M. capsulatus*. We can only conclude that both NADH and NADPH provide *potential* pathways for transferring hydrogen from methane to lipids.

With these biochemical details in hand, we now turn to the significance of $f_m = 0.31$ in *M. capsulatus* lipids. Except for water produced by the oxidation of methane, NADH and NADPH represent the only immediate sources for lipid H that contain methane-derived hydrogen. All other immediate sources (exchange, uptake of H^+, organic substrates) supply water-derived hydrogen. The proportion of NADPH hydrogen deriving from CH_4 versus H_2O is not known, but is assumed to be constant for all lipids. In fatty acids, ~50% of hydrogen comes from NADPH. In isoprenoid lipids, this proportion is ~22% (MVA pathway) or ~33% (DXP pathway). Regardless of which isoprenoid pathway is used, isoprenoid lipids and fatty acids obtain different proportions of their hydrogen from NADPH. If NADPH was the only source of methane-derived hydrogen, different values of f_m should arise for these two lipid classes. Since they do not, alternative explanations must be considered.

One possible source of confusion is that the proportions of lipid hydrogen attributed to each immediate source could be incorrect due to exchange of C-bound hydrogen with water. If hydrogen supplied to a lipid by NADPH were subsequently replaced by exchange, the fraction of lipid hydrogen derived ultimately from methane would drop. For example, if one-third of hydrogen in a fatty

acid exchanged with water, only ~33% of hydrogen in the resulting molecule would be due to NADPH. This is not only identical to the proportion expected for the DXP pathway of isoprenoid biosynthesis, but would be consistent with all methane-derived hydrogen flowing to lipids via NADPH obtained from the RuMP cycle. Other combinations of these processes are possible, but all require more extensive exchange in fatty acids than in isoprenoids in order to explain a constant value of f_m.

Such a balancing of processes to produce a constant value of f_m in all lipids is certainly possible, but would seem to require considerable coincidence. A different explanation is that the catabolic oxidation of methane supplies ~31% of cellular water in *M. capsulatus*. Subsequent biosynthesis and exchange then results in essentially all hydrogen reservoirs (lipids, water, carbohydrates, NADPH, etc.) containing ~31% methane-derived hydrogen. Growth-yield calculations (Anthony, 1982) indicate the oxidation of no more than ~1 g of CH_4 in each 5-L culture, so the culture medium could not contain an appreciable amount of methane-derived water. Water continuously diffuses through cell membranes, and the amount of cellular water derived from methane should be very sensitive to the rate at which methane is oxidized. The value of f_m might then be expected to differ in cultures harvested in different phases of growth, but this is not observed in our experiments. Below we present evidence that, once synthesized, lipids in *M. capsulatus* do not turn over. The isotopic composition of lipids from cells in stationary phase should therefore reflect hydrogen budgets prevailing during growth, so a change in f_m as growth slowed might not be reflected in the δD values of lipids. On the other hand, as noted above the slight D enrichment accompanying incorporation of methane H suggests that the incorporation is via formaldehyde rather than water.

In summary, there are still many uncertainties about the pathways that convert CH_4 and H_2O into lipid hydrogen, and we cannot explain why all *M. capsulatus* lipids derive one-third of their hydrogen from methane. Although the specific biochemical pathways present in *M. capsulatus* are rather unique, the fundamental processes involved in the transfer of hydrogen to lipids are common to all organisms. Predictions about sources of hydrogen based on the known details of biosynthetic pathways do not satisfactorily explain our data. Alternative explanations include a significant role for exchange during lipid biosynthesis, or the supply of 31% of cellular water from methane oxida-

tion. Both alternatives have significant implications for our understanding of D/H fractionation in other, more complex organisms.

Values of δD in native methanotroph lipids. Using the data in Table 5-5, it is possible to describe the δD value of methanotrophic lipids as a simple function of the δD values of methane and water. Averaging data from the five isoprenoid lipids and four *n*-alkyl lipids in Table 5-5 produces the following approximate relationships:

$$\delta D_{n\text{-alkyl}} = 0.31 \cdot \delta D_{\text{methane}} + 0.69 \cdot \delta D_{\text{water}} - 47 \qquad (4)$$

$$\delta D_{\text{isoprenoid}} = 0.32 \cdot \delta D_{\text{methane}} + 0.68 \cdot \delta D_{\text{water}} - 165 \qquad (5)$$

These equations can then be used to make general predictions about δD values of methanotrophic lipids in natural environments, with the caveat that they were derived under constant, nutrient-replete growth conditions. Given typical values for seawater $\delta D = 0‰$ and thermogenic "dry" methane $\delta D = -150‰$ (Schoell, 1980), equations 4 and 5 predict δD values for methanotroph fatty acids of $-93‰$, and for isoprenoid lipids of $-213‰$. These values, especially for fatty acids, are D-enriched relative to those expected in marine plants (*e.g.*, Sessions *et al.*, 1999). However, δD values of thermogenic methane as low as $-250‰$ have been reported (Schoell, 1980), and δD values for biogenic methane as low as $-300‰$ are known (Whiticar *et al.*, 1986). Using $\delta D_{\text{methane}} = -300‰$, equations 4 and 5 predict δD values for methanotroph fatty acids and isoprenoid lipids of $-140‰$ and $-261‰$, respectively. These values are indistinguishable from those expected for marine plants, and we conclude that methanotroph lipids in the sedimentary record will be difficult to identify solely on the basis of D/H ratios. On the other hand, a third of lipid hydrogen in these organisms is derived from methane. When methanotroph lipids can be identified by their structure or carbon isotopic composition, δD values may then provide some indication about the source of CH_4 consumed.

D/H fractionation in triterpenol biosynthesis. The 30-carbon skeleton of hopan-30-ol derives from that of squalene, the precursor of all triterpenols (Figure 5-7). In the four cultures harvested during exponential growth, δD values of hopan-30-ol and squalene were identical. This suggests
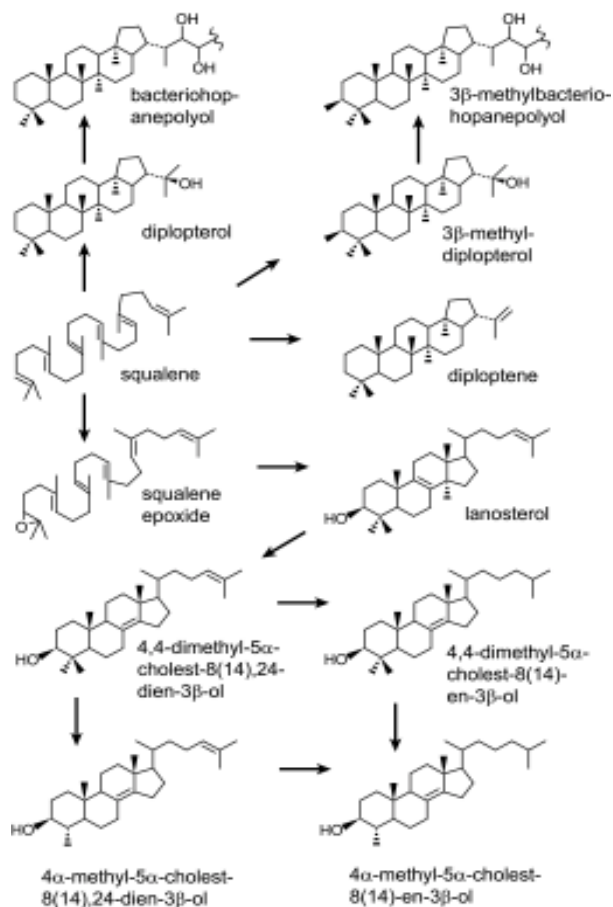
Figure 5-7. Proposed pathways for sterol and hopanol biosynthesis in *M. capsulatus* (after Summons *et al.*, 1994).

that little or no hydrogen isotopic fractionation is associated with the branching of squalene between sterol and hopanol biosynthetic pathways. To facilitate comparison of sterols and hopanols between cultures in which δD values varied widely, we therefore normalized δD values of all triterpenols to those of squalene from the same culture (Figure 5-8)

A significant D enrichment, averaging 32‰, was measured in 3-methylhopan-30-ol relative to both hopan-30-ol and squalene (Figure 5-8). A similar *carbon* isotope fractionation of 5.7‰ was measured by Summons *et al.* (1994) for cultures in Cu-enriched media, in which 3-methylhopanol was ^{13}C-enriched relative to coexisting hopanol. Jahnke *et al.* (1999) also reported $\delta^{13}C$ differences between C_{30} hopanol and 3-methyhopanol of 2 – 6‰. Squalene is converted to 3-methyldiplopterol,
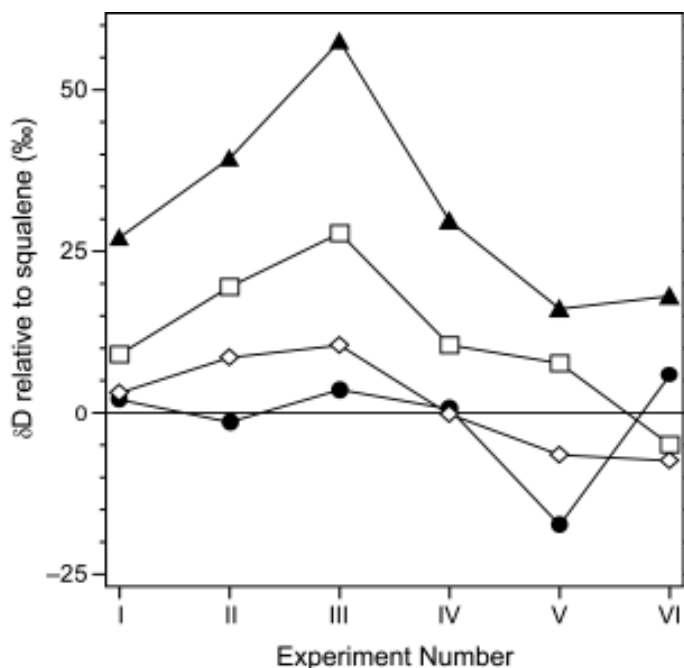
Figure 5-8. Hydrogen isotopic compositions of *M. capsulatus* triterpenols: hopan-30-ol (solid circles), 3-methylhopan-30-ol (solid triangles), 4-methylcholest-8(14)-enol (open diamonds), and 4,4-dimethylcholest-8(14)-enol (open squares). All δD values are relative to that of squalene from the same culture.

the precursor of 3-methylhopanoids, by the intact transfer of a methyl group from S-adenosoyl-methionine (Summons *et al.*, 1994). This methyl group represents only ~6% of hydrogen and ~3% of carbon in the methylhopanol, so the observed isotopic shifts would seem to require that the methyl group has δD ~500‰ enriched and $\delta^{13}C$ ~200‰ enriched relative to the parent hopanol. As noted by Summons *et al.* (1994), such an enrichment seems unlikely. It is possible that an isotope effect is associated with the distribution of squalene between the two hopanol end products, al-though the δD values of hopan-30-ol and squalene are similar. Additional exchange of H with H_2O could also explain the hydrogen isotopic enrichment of 3-methylhopanol, but not the carbon isoto-pic enrichment. Differences in the timing of biosynthesis of the two hopanoid end products may be responsible, as suggested by Summons *et al.* (1994), but δD values for cultures harvested in differ-ent phases of growth are equivalent. Our results seem to provide no further insight into this puzzle, but add support to the suggestion that some fundamental difference in the biosynthesis of these two products may be involved.

Comparison of δD values for the monoene versus diene sterols in Culture III indicates that there is no significant shift in δD associated with hydrogenation of the Δ^{24} double bond (Table 5-4). Presumably this hydrogenation is the result of H⁻ supplied by NADPH, and H⁺ supplied by water. The average δD of these two hydrogens must therefore be close to the average δD for lipid hydrogen, although the measurement is not particularly sensitive because the added hydrogen represents only ~4% of total lipid hydrogen.

D/H fractionation in fatty acid synthesis. Hydrogen isotopic compositions of fatty acids obtained from acetone-soluble and phospholipid fractions are compared in Figure 5-9. The average difference in δD of equivalent lipids (*e.g.*, 16:0 fatty acid) between the two fractions was 3 ± 12‰. There is, accordingly, no systematic difference between these two functionally defined classes. A pronounced isotopic fractionation was measured between the saturated and monounsaturated C_{16} fatty acids (Figure 5-9). Considering both acetone-soluble and phospholipid fractions, the average
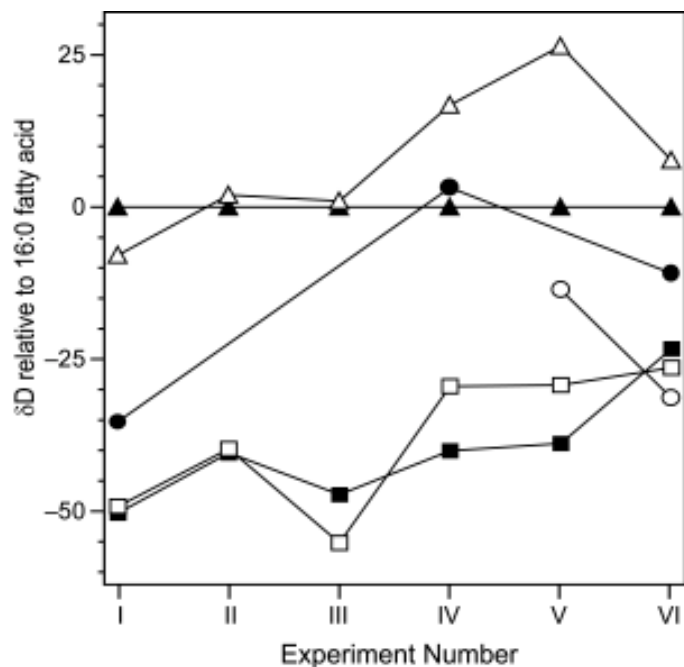

Figure 5-9. Hydrogen isotopic compositions of *M. capsulatus* fatty acids: 14:0 (circles), 16:1 (squares), and 16:0 (triangles). Filled symbols represent fatty acids from the acetone-soluble fraction, open symbols represent those from the phospholipid fraction. All δD values are relative to that of 16:0 fatty acid from the acetone-soluble fraction of the same culture.

difference is $43 \pm 9‰$, with 16:0 enriched in D relative to 16:1. δD values for saturated C_{14} fatty acids fall between those of the 16:0 and 16:1 fatty acids. *M. capsulatus* is known to synthesize unsaturated fatty acids via the anaerobic mechanism (Jahnke and Diggs, 1989), in which the carbon-carbon double bond created by dehydration (see Figure 5-4) is preserved during continued chain elongation. The net difference between hydrogen in 16:0 and 16:1 fatty acids is therefore the two hydrogens added during one double-bond hydrogenation. For these two hydrogen atoms alone to explain the isotopic difference would require that they be enriched in D by 667‰ relative to the 16:1 fatty acid. By comparison, hydrogenation of the Δ^{24} position in sterols does not produce any measurable change in δD.

Given the similarities between the two fatty acids, the most plausible explanation is that there is a more fundamental difference in the biosynthesis of the two compounds. For example, their synthesis may be mediated by different isozymes or cofactors, with consequent differences in associated fractionation. The two fatty acids may be synthesized preferentially at different times in the cell's growth, although both appear to derive 32% of their hydrogen from methane. Alternately, the compounds may be synthesized from separate, isotopically distinct pools of substrates (either acetate, NADPH, or both).

Isotope fractionation and growth rate. Hydrogen isotopic compositions of lipids did not vary significantly between cultures harvested during exponential growth versus stationary phase (compare cultures I and VI, and IV and V in Table 5-4). Summons *et al.* (1994) observed that carbon isotope fractionation decreased systematically with increasing cell density in their cultures. They attributed this decrease to a shift in the form of methane monooxygenase enzyme utilized to metabolize CH_4. During exponential growth, only the particulate form of the enzyme (pMMO) is expressed while, in stationary phase, both particulate and soluble forms of the enzyme are produced. Cultures grown using a Cu-enriched growth medium, which inhibits production of sMMO, showed no change in carbon isotopic fractionation from exponential to stationary phase. The alternate hypothesis is that changes in methane uptake or diffusion with increasing cell density lead to changes in fractionation. The lack of any variation in δD values with cell density in our cultures, which also used Cu-enriched media, supports the former explanation.

Yakir and DeNiro (1990) showed that, during heterotrophic processing of carbohydrates in plants, transformations of carbohydrate carbon skeletons led to the exchange of C-bound hydrogen in carbohydrates with cellular water, even though the net inventory of carbohydrate hydrogen did not change. Associated isotopic fractionations led to a strong increase in δD of carbohydrates during this processing. Yakir (1992) accordingly argued that δD of plant carbohydrates should be correlated with metabolic status. During periods of low photosynthetic activity, the utilization and reprocessing of existing biochemical stores should increase, leading to a net increase in δD. Sessions *et al.* (1999) found indirect evidence that this situation is also true in lipids from higher plants. Sterols from dormant plants were D-enriched relative to actively-growing cultures by 50 to 100‰, whereas fatty acids were enriched in D by 0 to 30‰.

The lack of D enrichment in *M. capsulatus* lipids from exponential to stationary phase is in contrast to the available data for higher plants. Tritium- and radiocarbon-labeling experiments with *E. coli* have shown that, although significant turnover of membrane phospholipids does occur, this process involves the transfer of intact fatty acids between different head groups (Cronan and Vagelos, 1972). The fatty acids themselves appear highly resistant to degradation by the host organism, despite the fact that *E. coli* possesses an active β-oxidation system for degrading fatty acids. Based on our D/H data, and by analogy with *E. coli*, we speculate that this lack of turnover of membrane lipids may be a general feature of bacteria.

Sulfate-Reducing Bacteria

Fatty acids were the only lipids recovered from the SRB in sufficient abundance for isotopic measurements. The distribution of fatty acids varied widely between species (Table 5-6), and included several unusual structures such as 10-methyl 16:0 and cyclopropyl fatty acids with 17 or 19 carbon atoms. Representative abundances from heterotrophic cultures are given in Table 5-6. The distribution of fatty acids in lithotrophic cultures was similar. Values of δD for the fatty acids are summarized in Tables 5-7 and 5-8 and in Figure 5-10. Where several fatty acids appear beside a single ID in Table 5-6, a single composite δD value is reported in Tables 5-7 and 5-8 due to incomplete resolution of closely-related compounds.

Table 5-6. Identities and relative abundance of recovered SRB fatty acids from heterotrophic cultures

ID	*Desulfovibrio desulfuricans* compound	%[a]	*Desulfotomaculum acetoxidans* compound	%[a]	*Desulfobacter hydrogenophilus* compound	%[a]	*Desulfobacterium autotrophicum* compounds	%[a]
n14					14:0	5.7	14:0	5.6
i15	iso-15:0[b]	17.9			iso-15:0[b]	3.8	iso-15:0[b]	3.5
n16	16:1ω7	7.6	16:1ω9	3.5	16:1ω9	11.8	16:1ω9	8.8
	16:0	16.0	16:1ω7	24.0	16:0	41.8	16:1ω7	1.2
			16:1ω5	1.8			16:0	41.6
			16:0	27.0				
i17	iso-17:1ω7[b]	27.5			10-methyl 16:0	7.1	10-methyl 16:0	7.9
	iso-17:0[b]	32.6					iso-17:0[b]	0.7
	17:0	0.3						
c17					cyclopropyl-17:0[b]	27.9	cyclopropyl-17:0[b]	28.1
n18	18:1ω7	0.5	18:1ω9	1.2	18:1ω9	1.2	18:1ω7	1.7
	18:0	0.6	18:1ω7	40.8				
			18:1ω5	0.5				
			18:0	1.4				
c19					cyclopropyl-19:0[b]	0.7	cyclopropyl-19:0[b]	1.0

[a] Abundance is given as % of lipids recovered for that culture.
[b] Position of methyl or cyclopropyl substituent was not determined.

Table 5-7. Values of δD for fatty acids in sulfate-reducing bacteria grown lithotrophically on $CO_2 + H_2$

	Culture							
	Desulfobacter		*Desulfobacterium*		*Desulfotomaculum*		*Desulfovibrio*[a]	
ID[b]	VII	VIII	XI	XII	XV	XVI	XIX	XX
n14				-359[c]				
i15				-349			-244	-268
n16	-326	-303	-324	-345	-281	-299	-270	-282
i17	-311		-293	-321			-252	-274
c17	-296	-278	-286	-313				
n18				-288	-268	-294	-246	-258
c19	-280		-281	-296				
abundance-weighted mean[d]:	-310	-292	-303	-331	-273	-296	-259	-276

[a] Acetate was supplied to *Desulfovibrio* as an organic carbon source.
[b] Where multiple lipids are listed under one ID in Table 5-6, they have been combined for measurement of a single δD value.
[c] All δD values have been corrected for hydrogen added by derivatization as methyl esters.
[d] H_2 peak areas were used as the weighting factors.

Table 5-8. Values of δD for fatty acids in sulfate-reducing bacteria grown heterotrophically on either lactate (*Desulfovibrio*) or acetate (all others)

ID[a]	Culture							
	Desulfobacter		*Desulfobacterium*		*Desulfotomaculum*		*Desulfovibrio*	
	VII	VIII	XI	XII	XV	XVI	XIX	XX
n14	-278[b]	-272	-287	-255				
i15	-300	-291	-305	-271			-275	-268
n16	-255	-256	-256	-254	-246	-248	-309	-309
i17	-242	-232	-232	-229			-281	-283
c17	-217	-217	-213	-214				
n18	-222	-215	-213	-216	-247	-253	-271	-277
c19	-181	-188	-177					
abundance-weighted mean[c]:	-245	-241	-244	-240	-246	-251	-288	-287

[a] Where multiple lipids are listed under one ID in table 5-6, they have been combined for measurement of a single δD value.
[b] All δD values have been corrected for hydrogen added by derivatization as methyl esters.
[c] H_2 peak areas were used as the weighting factors.

The absolute difference in δD for individual fatty acids between replicate cultures (*e.g.*, n16 in cultures VII and VIII) averaged 29‰ for cultures grown under autotrophic conditions, and 7‰ for those grown under heterotrophic conditions. The reasons for this substantial difference in reproducibility are not known, but the data suggest that the magnitude of hydrogen-isotopic fractionation in SRB during autotrophic growth is sensitive to growth conditions.

The isotopic compositions of different fatty acids varied by up to 120‰ within individual cultures, and were correlated with fatty acid carbon number. To facilitate comparison of average hydrogen isotopic compositions between cultures, weighted-average δD values were calculated using H_2 peak areas (data not shown) for each fatty acid as weighting factors. Isotopic compositions of fatty acids were similar for cultures of *Desulfobacter*, *Desulfobacterium*, and *Desulfotomaculum*, but were different in *Desulfovibrio* (Figure 5-10). For example, the isotopic fractionation between lipids and lactate averaged –244‰ in *Desulfovibrio*, while the fractionation between lipids and acetate ranged from –160 to –172‰ in the other SRB. Based on these patterns, as well as differences in growth conditions, the data for *Desulfovibrio* are discussed separately from the other three SRB below.

D/H fractionation during autotrophic growth. As for *M. capsulatus*, there are two potential sources of hydrogen during autotrophic growth of SRB: H_2 and H_2O. In the case of SRB, however, the
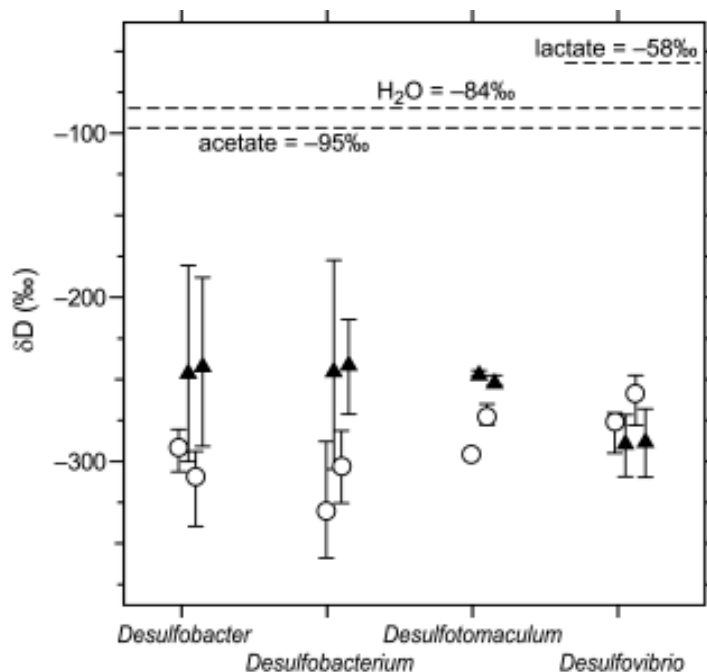
Figure 5-10. Hydrogen isotopic compositions of SRB fatty acids during heterotrophic (filled symbols) and lithotrophic(open symbols) growth. Plotted values are abundance-weighted means, error bars indicate the range of values for all fatty acids. δD values of growth water and organic substrates are indicated by dashed lines.

isotopic compositions of hydrogen sources were not varied, so their individual contributions to lipid hydrogen cannot be distinguished from the available data. When SRB grow autotrophically on H_2 plus CO_2, hydrogenase enzymes located in the periplasmic space oxidize H_2 to H_2O and transfer a pair of electrons across the cell membrane to reduce sulfate (see Fauque *et al.*, 1988, and Hatchikian *et al.*, 1990 for recent reviews). This separation of electrons from protons, termed "vectorial electron transport" (Odom and Peck, 1981), generates a membrane potential that can be used for ATP synthesis. Apparently, H_2 serves only as a source of reducing power, not hydrogen, to the SRB. Although this scheme represents the general case, exceptions are possible. For example, Malki *et al.* (1995, 1997) have identified a cytoplasmic hydrogenase from *Desulfovibrio fructosovorans* that can use H_2 to reduce $NADP^+$ to NADPH *in vitro*. This raises the possibility that H_2 is used directly as a source of reducing power and hydrogen for biosynthesis. Here we assume that the SRB do not incorporate any hydrogen from H_2 into biomass, and so H_2O is the only source of lipid H during autotrophic growth.
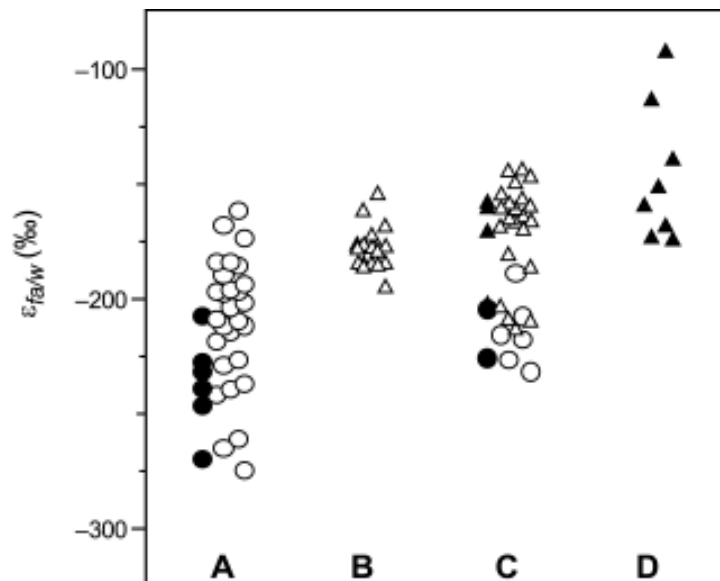
Figure 5-11. Comparison of hydrogen isotopic fractionation between *n*-alkyl lipids and growth water for various organisms. Circles represent bacteria or phytoplankton, triangles represent higher plants. Solid symbols are averages for an entire plant or culture, open symbols are values for specific lipids. Group A - fatty acids in current SRB autotrophic experiments; B - *n*-alkanes extracted from Great Pond sediments, Sauer *et al.* (2001) C - fatty acids and *n*-alkanes in aquatic higher plants, brown algae, diatoms, dinoflagellates, Sessions *et al.* (1999). D - bulk fatty acids in emergent aquatic plants, Estep and Hoering (1980).

When H_2O is the only hydrogen source, the measured isotopic fractionation between fatty acids and water is equal to $\varepsilon_{l/w}$. Average values of $\varepsilon_{l/w}$ calculated from weighted-mean δD values for the SRB during autotrophic growth are –237‰ (*Desulfobacter*), –254‰ (*Desulfobacterium*), and –219‰ (*Desulfotomaculum*). Values for $\varepsilon_{l/w}$ in SRB are compared to those obtained for higher plants and algae in Figure 5-11. Data from Estep and Hoering (1980) were produced by offline combustion/ reduction measurements, and so represent average values for a bulk fatty acid fraction from each plant. Data from Sauer *et al.* (2001) are the δD values of *n*-alkanes extracted from core-top sediments in Great Pond. Those *n*-alkanes are thought to represent inputs from nearby terrestrial plants. Pentacyclic triterpenols, also products of higher plants, are enriched in D relative to dinosterol, an unambiguous phytoplanktonic product, by an average of 47‰ in Great Pond. To account for this difference, presumably due to D enrichment of plant leaf water by evapotranspiration, a correction of –47‰ was applied to the Great Pond *n*-alkanes in Figure 5-11.

Values of $\varepsilon_{l/w}$ for individal fatty acids in SRB cover a wide range of more than 100‰ (Figure 5-11). Although the magnitude of this range is similar to that reported by Sessions *et al.* (1999) for plants, values of $\varepsilon_{l/w}$ for the SRB are up to 100‰ more negative than comparable values in plants. However, the average values for the SRB do overlap with those obtained by Sessions *et al.* for cultures of *Isochrysis galbana*, a haptophyte, and *Alexandrium fundeyense*, a dinoflagellate.

Several conclusions can be drawn from Figure 5-11. First, the similarity of $\varepsilon_{l/w}$ between SRB and phytoplankton cultures supports our earlier assumption that H_2 is not a significant source for lipid hydrogen. Although the δD value of H_2 used in these experiments (–210‰) is quite similar to that of the SRB fatty acids, H_2 in the cultures was only partially consumed. A large isotope effect, favoring reaction of H_2 over HD, is expected in the dissociation of H_2 by hydrogenase enzymes. Any hydrogen supplied to cells by oxidation of H_2 should be strongly depleted in D. If weighted-mean δD values are considered, the most negative value of $\varepsilon_{l/w}$ in SRB was –254‰ (the average for cultures XI and XII), only ~25‰ more negative than values observed for *Alexandrium* by Sessions *et al.* (1999). While this similarity does not eliminate the possibility that H_2 contributes to lipid hydrogen, it suggests that the significance of this pathway is negligible.

Second, there appears to be a consistent difference in $\varepsilon_{l/w}$ between cultures of unicellular organisms on one hand, and multicellular organisms collected from natural habitats on the other. These differences would be consistent with hydrogen exchange accompanying carbohydrate reprocessing in plants, but not in microbes. The differences might also be due to variations in growth rate, the physical size of the organisms, or other factors. An important question remaining to be answered is whether this discrepancy reflects differences between microbes and plants, or between cultures and natural habitats.

Third, the similarity of $\varepsilon_{l/w}$ between SRB and phytoplankton is striking when the fundamental biochemical differences between the organisms are considered. Both *Isochrysis* and *Alexandrium* use the Calvin-Benson cycle to fix carbon. In contrast, *Desulfobacterium* and *Desulfotomaculum* use carbon monoxide dehydrogenase to fix carbon via the acetyl-CoA pathway (Schauder *et al.*, 1989; Spormann and Thauer, 1988), while *Desulfobacter* uses a reductive citric acid cycle (Schauder *et al.*, 1987). The relative consistency of $\varepsilon_{l/w}$ in organisms with such diverse metabolic pathways

supports our earlier suggestion that the intact transfer of carbon-bound hydrogen through biosynthetic pathways is only a minor contributor to the final hydrogen inventory in lipids.

A common denominator between phytoplankton and bacteria which might explain their equivalent values of $\varepsilon_{l/w}$ is the use of NADPH as a reductant during biosynthesis. Estep and Hoering (1980, 1981) first hypothesized that the large depletion of D in lipids relative to growth water in plants is due primarily to a parallel depletion in NADPH. Luo *et al.* (1991) further noted that a strong depletion of D in NADPH relative to water could be explained by the greater acidity of protium versus deuterium. H_2O has a pKa of 14.0, while D_2O has a pKa of 14.9, indicating that, proportionately, H^+ will be nearly three times more abundant in solution than D^+. This mechanism implies physical-chemical, rather than biochemical, control over the depletion of organic-H relative to water. Our observation that hydrogen-isotopic fractionation between fatty acids and water is nearly constant in several diverse microorganisms is consistent with both of these hypotheses.

D/H fractionation during heterotrophic growth. There are two likely sources of lipid H during heterotrophic sulfate reduction: water and organic substrates. Again, the relative contributions of the two sources cannot be determined from our experimental data. However, sources of hydrogen vary between lithotrophic and heterotrophic modes of growth, so comparison of fractionations during those two modes of growth yields some insight.

Desulfovibrio represents the simplest case, because it was grown on organic C sources in all cultures. The average isotopic fractionation between fatty acids and organic substrate was –191‰ when grown lithotrophically on H_2 plus acetate, and –244‰ when grown heterotrophically on lactate. Anabolic processes in these two modes of growth should be the same, yet the change in fractionation appears to have biochemical origins. Several explanations are possible. First, fractionation of organic substrates during uptake by cells is likely, and it is conceivable that such fractionation might differ by the observed amount (~50‰) for acetate and lactate. Second, lactate from the medium is oxidized to acetate during heterotrophic growth. The acetate is then either used for biosynthesis or excreted. Isotope effects at this branchpoint may result in fractionation of the acetate used for biosynthesis.

A third possibility is that δD of hydrogen supplied by NADPH differs between the two cultures. A depletion of D in NADPH of 65‰ from lithotrophy to heterotrophy is required to explain the observed results, assuming that 50% of fatty acid hydrogen is supplied by NADPH. Such a difference might be related to the shift in energy sources, although few details about how NADPH is produced in SRB are available.

A scheme for energy conservation during heterotrophic sulfate reduction that involves cycling of molecular hydrogen across the cell membrane was proposed by Odom and Peck (1981). They suggested that, in *Desulfovibrio vulgaris*, reducing power from organic substrates is used to produce H_2 in the cytoplasm. The H_2 diffuses through the membrane to the periplasm where it is reoxidized and can be coupled to generation of a membrane potential. This process would produce a continuous, unidirectional flow of H_2 from the cytoplasm to the periplasm. If the H_2 were depleted in D relative to cellular water, the net transfer of H_2 could result in enrichment of D in the cytoplasm. In our cultures of *Desulfovibrio*, the opposite pattern is observed: fatty acids are more D-*depleted* when lactate is the energy source than when exogenous H_2 is the energy source. This result does not disprove hydrogen cycling in *Desulfovibrio desulfuricans*, but does indicate that large D enrichments due to hydrogen cycling do not exist.

Fatty acid δD values from the other three SRB increase from approximately –300‰ during autotrophic growth to –245‰ during heterotrophic growth on acetate. The water used in the two sets of cultures was identical, so it appears likely that some acetate hydrogen is incorporated into lipids. The δD value of acetate supplied to the cultures (–95‰) was very similar to that of the water (–84‰). The difference in δD between autotrophic and heterotrophic cultures also implies that the fractionation between acetate hydrogen and lipids is smaller than that between water and lipids.

More detailed analysis of δD data from heterotrophic experiments is complicated by uncertainties about pathways linking the ultimate sources of hydrogen to SRB with the immediate sources of hydrogen to lipids. In particular, it is unknown whether hydrogen carried by NADPH is derived from organic substrates, *e.g.* using the pentose-phosphate pathway, or from water by some other process. Attempts to calculate the fractionation associated with each hydrogen source require assuming δD values for one or more pools of hydrogen, and the results of such calculations are very
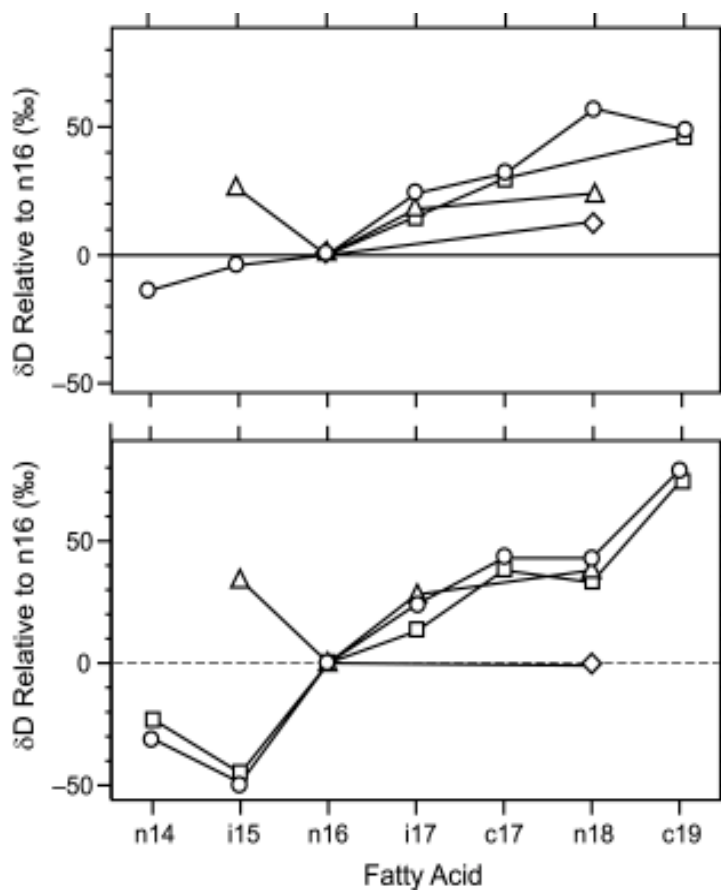
Figure 5-12. Hydrogen isotopic compositions of fatty acids produced by SRBs during lithotrophic (upper panel) and heterotrophic (lower panel) growth. Circles = *Desulfobacterium*, squares = *Desulfobacter*, triangles = *Desulfovibrio*, diamonds = *Desulfotomaculum*. Plotted δD values are relative to n16 fatty acids from the same culture.

sensitive to the starting assumptions. More sophisticated experiments are required to distinguish fractionation in each of the hydrogen sources.

Fatty acid chain length. Fatty acids from all four species of SRB, in both lithotrophic and heterotrophic cultures, exhibit a large and systematic increase in δD with chain length (Figure 5-12). This increase spans roughly 60‰ in autotrophic cultures, and over 100‰ in heterotrophic cultures. The increases are very similar between different SRB cultures with the same mode of

growth (*i.e.*, lithotrophic or heterotrophic). Exceptions to this pattern include the branched 15:0 fatty acid in *Desulfovibrio* and the C_{18} fatty acids in *Desulfotomaculum*. Similar trends of increasing δD value with greater chain length have also been tentatively identified in fatty acids from higher plants by Sessions *et al.* (1999).

Such a large and consistent enrichment of D might plausibly result from analytical artifacts, but several observations argue against this possibility. First, homologous *n*-alkanes covering a wide range in vapor pressure have been extracted and measured with the same analytical system without any observable fractionation (Session *et al.*, 1999). Second, δD values of the 13:0 FAME internal standard were measured accurately in every sample. Third, the pattern of enrichment is highly reproducible between replicate cultures, but differs significantly between heterotrophic and lithotrophic cultures. It seems likely that the observed δD trends represent a biochemical process.

The enrichment of D in longer-chain fatty acids is probably not due to differences in the isotopic composition of acetate used to initiate the fatty acid chain versus that used to extend the chain. The two types of acetate are carried via separate enzymes, so the possibility exists. Still, the difference in δD between C_{14} and C_{19} fatty acids is up to 100‰, and would require that the terminal acetate group be depleted relative to chain-elongation acetate by well over 500‰. Alternatively, the pattern of enrichment is consistent with a normal isotope effect during the hydrogenation of a nascent fatty acid by NADPH. A normal isotope effect would result in H^- that is transferred to the lipid being depleted in D relative to the remaining pool of NADPH. If the pool of NADPH is small, and fatty acid synthesis is rapid compared to the rate at which NADPH is replenished, the pool of remaining NADPH will become D-enriched as NADPH is consumed. As a fatty acid grows, progressively more D-enriched NADPH will be utilized, and the average D/H ratio of the fatty acid will increase. This hypothesis implies that the initial (*n*-alkyl) end of the fatty acid should be depleted in D relative to the terminal (carboxyl) end.

CONCLUSIONS

We have measured hydrogen isotopic fractionation in cultures of the aerobic, methanotrophic bacterium *Methylcoccus capsulatus* and in cultures of the anaerobic, sulfate-reducing bacteria (SRB) *Desulfobacter hydrogenophilus, Desulfobacterium autotrophicum, Desulfotomaculum acetoxidans,* and *Desulfovibrio desulfuricans*. In *M. capsulatus*, we calculate that $31 \pm 2\%$ of all lipid hydrogen is derived from methane. This is apparently true for both *n*-alkyl and isoprenoid lipids, and for cultures in both exponential- and stationary-phase growth. The pathways by which hydrogen is transferred from methane to lipids are not known. Possibilities include the transfer of methane hydrogen to lipids via NADPH, and water derived from methane oxidation.

Our measurements of isotopic fractionation in *M. capsulatus* show that, if fractionation between water and lipids is similar to that in plants, then a small, inverse isotope effect is associated with the assimilation of methane hydrogen into biomass. This agrees with *in vitro* studies of methane monooxygenase that have measured both intermolecular and intramolecular isotope effects. These effects push the D/H ratio of methane-oxidation products in opposite directions, resulting in a small net fractionation. In natural settings, where δD of methane is typically depleted in D by 200 – 300‰ relative to water, the δD value of methanotroph lipids will be between that of water and methane, and will not be distinguishable from δD of plant lipids. D/H fractionation between isoprenoid and *n*-alkyl lipids is indistinguishable from that in phytoplankton cultures, suggesting that fractionation by the MVA and DXP pathways of isoprenoid biosynthesis are equivalent.

Significant differences in δD of 3-methylhopan-30-ol versus hopan-30-ol, and 16:0 versus 16:1 fatty acids were observed. These differences are consistent across all cultures, and cannot easily be attributed to differences in the isotopic composition of hydrogen that was added or lost. In the case of hopanols, equivalent carbon isotopic differences have also been reported. We propose that these differences reflect some separation in the biosynthesis of these homologous molecules, such as the timing, the pool of resources utilized, or the mediating enzymes.

SRB were grown autotrophically on $H_2 + CO_2$, and heterotrophically on acetate or lactate. Hydrogen isotopic fractionation between water and fatty acids in autotrophic cultures averaged –237‰,

and is indistinguishable from that in photosynthetic organisms. This similarity, despite the use of fundamentally differing pathways for assimilation of carbon, suggests that organic substrates contribute little to the hydrogen isotopic composition of lipids. More importantly, it emphasizes that the hydrogen isotopic composition of lipids reflects different processes and controls than does the carbon isotopic composition. Coupled measurements of the two isotopic systems should provide complementary, rather than duplicative, information about biochemical processes.

REFERENCES CITED

Anthony, C. (1982) *The Biochemistry of Methylotrophs*. Academic Press, London.

Balabane, M., Galimov, E., Hermann, M., and Letolle, R. (1987) Hydrogen and carbon isotope fractionation during experimental production of bacterial methane. *Organic Geochemistry* **11**, 115–119.

Belaich, J.-P., Bruschi, M., and Garcia, J.-L. (1990) *Microbiology and Biochemistry of Strict Anaerobes Involved in Interspecies Hydrogen Transfer*. Plenum Press, New York.

Bligh, E. G. and Dyer, W. J. (1959) A rapid method of total lipid extraction and purification. *Canadian Journal of Biochemistry and Physiology* **37**, 911–917.

Bottinga, Y. (1969) Calculated fractionation factors for carbon and hydrogen isotope exchange in the system calcite-CO_2-graphite-methane-hydrogen and water vapour. *Geochimica et Cosmochimica Acta* **33**, 49–64.

Cronan, J.E. and Vagelos, P.R. (1972) Metabolism and function of the membrane phospholipids of Escherichia coli. *Biochimica et Biophysica Acta* **265**, 25–60.

Edwards, T. W. D. (1993) Interpreting past climate from stable isotopes in continental organic matter. In *Climate Change in Continental Isotopic Records*, Vol. 78 (ed. P. K. Swart, K. C. Lohmann, J. McKenzie, and S. Savin), pp. 333–341. American Geophysical Union, San Francisco.

Estep, M. F. and Hoering, T. C. (1980) Biogeochemistry of the stable hydrogen isotopes. *Geochimica et Cosmochimica Acta* **44**, 1197–1206.

Estep, M. F. and Hoering, T. C. (1981) Stable hydrogen isotope fractionations during autotrophic and mixotrophic growth of microalgae. *Plant Physiology* **67**, 474–477.

Fauque, G., Peck, H. D. J., *et al.* (1988) The three classes of hydrogenases from sulfate-reducing bacteria of the genus *Desulfovibrio*. *FEMS Microbiology Reviews* **54**, 299–344.

Hatchikian, E. C., Fernandez, V. M., and Cammack, R. (1990) The hydrogenases of sulfate-reducing bacteria: Physiological, biochemical, and catalytic aspects. In *Microbiology and biochemistry of strict anaerobes*

involved in interspecies hydrogen transfer, FEMS Symposium No. 54 (ed. J. P. Belaich, M. Bruschi, and J.-L. Garcia), pp. 53–73. Plenum Press, New York.

Hayes J. M. (1993) Global methanotrophy at the Archean-Proterozoic transition. In *Early Life on Earth* (ed. S. Bengtsen). Proceedings of Nobel Symposium 84.

Hinrichs, K.-U., Hayes, J. M., Sylva, S. P., Brewer, P. G., and DeLong, E. F. (1999) Methane-consuming archaebacteria in marine sediments. *Nature* **398**, 802–805.

Jahnke, L. L., Summons, R. E., Hope, J. M., and DesMarais, D. J. (1999) Carbon isotopic fractionation in lipids from methanotrophic bacteria II: The effects of physiology and environmental parameters on the biosynthesis and isotopic signatures of biomarkers. *Geochimica et Cosmochimica Acta* **63**, 79–93.

Jahnke, L. (1992) The effects of growth temperature on the methyl sterol and phospholipid fatty acid composition of *Methylococcus capsulatus* (Bath). *FEMS Microbiology Letters* 93, 209–212.

Jahnke, L. L. and Diggs, K. (1989) Evidence for the synthesis of the multi-positional isomers of monounsaturated fatty acid in *Methylococcus capsulatus* by the anaerobic pathway. *FEMS Micriobiology Letters* **58**, 183–188.

Jahnke, L.L. and Nichols, P.D. (1986) Methyl sterol and cyclopropane fatty acid composition of *Methylococcus capsulatus* grown at low oxygen tensions. *Journal of Bacteriology* **167**, 238-242.

Lange, B. M., Rujan, T., Martin, W., and Croteau, R. (2000) Isoprenoid biosynthesis: The evolution of two ancient and distinct pathways across genomes. *Proceedings of the National Academy of Science* **97**, 13172–13177.

Lichtenthaler, H. K. (1999) The 1-deoxy-D-xylulose-5-phosphate pathway of isoprenoid biosynthesis in plants. *Annual Reviews of Plant Physiology* **50**, 47–65.

Luo, Y.-H., Sternberg, L., Suda, S., Kumazawa, S., and Mitsui, A. (1991) Extremely low D/H ratios of photoproduced hydrogen by cyanobacteria. *Plant and Cell Physiology* **32**, 897–900.

Malki, S., De Luca, G., *et al.* (1997) Physiological characteristics and growth behavior of single and double hydrogenase mutants of *Desulfovibrio* fructosovorans. *Archives of Microbiology* **167**, 38–45.

Malki,S., Saimmaime, I., deLuca, G., Rousset, M., Dermoun, Z., and Belaich, J.-P. (1995) Characterization of an operon encoding an NADP-reducing hydrogenase in *Desulfovibrio fructosovorans*. *Journal of Bacteriology* **177**, 2628–2636.

Nesheim, J. C. and Lipscomb, J. D. (1996) Large kinetic isotope effects in methane oxidation catalyzed by methane monooxygenase: Evidence for C-H bond cleavage in a reaction cycle intermediate. *Biochemistry* **35**, 10240–10247.

Odom, J. M. and Peck, H. D., Jr. (1981) Hydrogen cycling as a general mechanism for energy coupling in the sulfate-reducing bacteria, *Desulfovibrio* sp. *FEMS Microbiology Letters* **12**, 47–50.

Rohmer, M., Bouvier, P. and Ourisson, G. (1984) Distribution of hopanoid triterpenes in prokaryotes. *Journal of General Microbiology* **130**, 1137-1150.

Sauer, P. E., Eglinton, T. I., Hayes, J. M., Schimmelmann, A., and Sessions, A. L. (2001) Compound-specific D/H ratios of lipid biomarkers from sediments as a proxy for environmental and climatic conditions. *Geochimica et Cosmochimica Acta* **65**, 213–222.

Schauder, R., Preub, A., Jetten, M. and Fuchs, G. (1989) Oxidative and reductive acetyl CoA/carbon monoxide dehydrogenase pathway in *Desulfobacterium autotrophicum*. *Archives of Microbiology* **151**, 84-89.

Schauder, R., Widdel, F. and Fuchs, G. (1987) Carbon assimilation pathways in sulfate-reducing bacteria II. Enzymes of a reductive citric acid cycle in the autotrophic *Desulfobacter hydrogenophilus*. *Archives of Microbiology* **148**, 218-225.

Schimmelmann, A., Lewan, M.D. and Wintsch, R.P. (1999) D/H ratios of kerogen, bitument, oil, and water in hydrous pyrolysis of source rocks containing kerogen types I, II, IIS, and III. *Geochimica et Cosmochimica Acta* **63**, 3751-3766.

Schoell, M. (1980) The hydrogen and carbon isotopic composition of methane from natural gases of various origins. *Geochimica et Cosmochimica Acta* **44**, 649–661.

Schwender, J., Seemann, M., Lichtenthaler, H. K., and Rohmer, M. (1996) Biosynthesis of isoprenoids (carotenoids, sterols, prenyl side-chains of chlorophylls and plastoquinone) via a novel pyruvate/glyceraldehyde 3-phosphate non-mevalonate pathway in the green alga *Scenedesmus obliquus*. *Biochemical Journal* **316**, 73–80.

Sessions, A. L., Burgoyne, T. W., and Hayes, J. M. (2001a) Correction of H_3^+ contributions in hydrogen isotope-ratio-monitoring mass spectrometry. *Analytical Chemistry* **73**, 192–199.

Sessions, A. L., Burgoyne, T. W., and Hayes, J. M. (2001b) Determination of the H_3^+ factor in hydrogen isotope-ratio-monitoring mass spectrometry. *Analytical Chemistry* **73**, 200–207.

Sessions, A. L., Burgoyne, T. W., Schimmelmann, A., and Hayes, J. M. (1999) Fractionation of hydrogen isotopes in lipid biosynthesis. *Organic Geochemistry* **30**, 1193–1200.

Smith, B. N. and Epstein, S. (1970) Biogeochemistry of the stable isotopes of hydrogen and carbon in salt marsh biota. *Plant Physiology* **46**, 738–742.

Sporrmann and Thauer, R. (1988) Anaerobic acetate oxidation to CO_2 by *Desulfotomaculum acetoxidans*. *Archives of Microbiology* **150**, 374-380.

Sternberg, L. d. S. L., DeNiro, M. J., and Johnson, H. B. (1986a) Oxygen and hydrogen isotope ratios of water from photosynthetic tissues of CAM and C3 plants. *Plant Physiology* **82**, 428–431.

Sternberg, L. d. S. L., DeNiro, M. J., and Ajie, H. O. (1986b) Isotopic relationships between saponifiable lipids and cellulose nitrate prepared from red, brown, and green algae. *Planta* **169**, 320–324.

Stiller, M. and Nissenbaum, A. (1980) Variations of stable hydrogen isotopes in plankton from a freshwater lake. *Geochimica et Cosmochimica Acta* **44**, 1099–1101.

Sugimoto, A. and Wada, E. (1995) Hydrogen isotopic composition of bacterial methane: CO_2/H_2 reduction and acetate fermentation. *Geochimica et Cosmochimica Acta* **59**, 1329–1337.

Summons, R. E., Jahnke, L. L., and Roksandic, Z. (1994) Carbon isotopic fractionation in lipids from methanotrophic bacteria: Relevance for interpretation of the geochemical record of biomarkers. *Geochimica et Cosmochimica Acta* **58**, 2853–2863.

Wakil, S. J., Stoops, J. K., and Joshi, V. C. (1983) Fatty acid synthesis and its regulation. *Annual Reviews of Biochemistry* **52**, 537–579.

Waldron, S., Lansdown, J. M., Scott, E. M., Fallick, A. E., and Hall, A. J. (1999) The global influence of the hydrogen isotope composition of water on that of bacteriogenic methane from shallow freshwater environments. *Geochimica et Cosmochimica Acta* **63**, 2237–2245.

White, D. (1995) *The physiology and biochemistry of prokaryotes.* Oxford University Press, New York.

Whiticar, M. J., Faber, E., and Schoell, M. (1986) Biogenic methane formation in marine and freshwater environments: CO_2 reduction vs. acetate fermentation — Isotope evidence. *Geochimica et Cosmochimica Acta* **50**, 693–709.

Whittenbury, R. and Dalton, H. (1981) The methylotrophic bacteria. In *The Prokaryotes* (ed. M. P. Starr, H. Stolp, H. G. Truper, A. Balows, and H. G. Schlegel), pp. 894–902. Springer-Verlag, Berlin.

Wilkins, P. C., Dalton, H., Samuel, C. J., and Green, J. (1994) Further evidence for multiple pathways in soluble methane-monooxygenase-catalysed oxidations from the measurement of deuterium kinetic isotope effects. *European Journal of Biochemistry* **226**, 555–560.

Xie, S., Nott, C. J., Avsejs, L. A., Volders, F., Maddy, D., Chambers, F. M., Gledhill, A., Carter, J. F., and Evershed, R. P. (2000) Palaeoclimate records in compound-specific δD values of a lipid biomarker in ombrotrophic peat. *Organic Geochemistry* **31**, 1053–1057.

Yakir, D. (1992) Variations in the natural abundance of oxygen-18 and deuterium in plant carbohydrates. *Plant, Cell, and Environment* **15**, 1005–1020.

Yakir, D. and DeNiro, M. J. (1990) Oxygen and hydrogen isotope fractionation during cellulose metabolism in *Lemna gibba* L. *Plant Physiology* **93**, 325–332.

Ziegler, H., Osmond, C. B., Stickler, W., and Trimborn, P. (1976) Hydrogen isotope discrimination in higher plants: Correlation with photosynthetic pathway and environment. *Planta* **128**, 82–92.